Science of Climate Change

Volume 1.2
2021

https://scienceofclimatechange.org

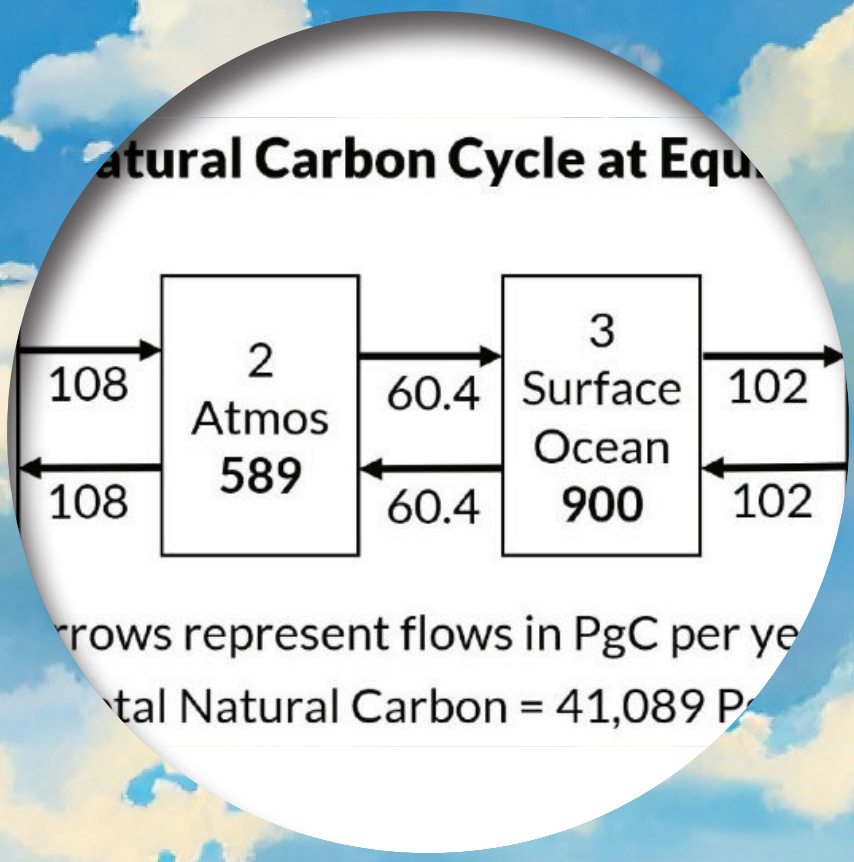

Published by: Klimarealistene (Org. no. 995 314 592)

ISSN 2703-9080 (print) ISNN 2703-9072 (online)

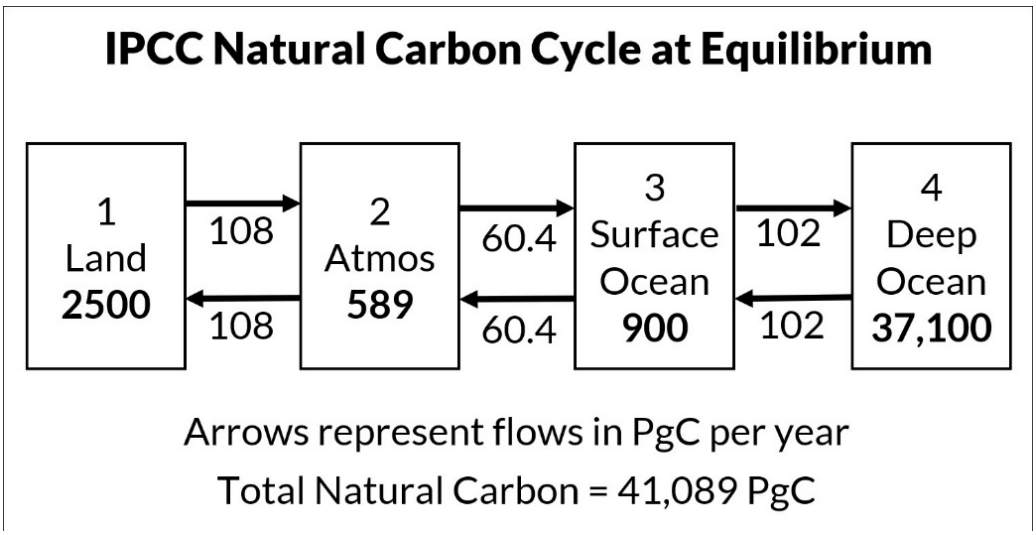

Levels and flows for IPCC's (2013) natural carbon cycle. The boxes represent the reservoirs and arrows represent the flows between the reservoirs.

From article by Edwin X Berry: T*he impact of Human CO_2 on Atmospheric CO_2,*
Figure 2, page 220.

SCIENCE OF CLIMATE CHANGE

Volume 1.2

December 2021

ISSN 2703-9072

Klimarealistene, P.O. Box 33, 3901 Porsgrunn, Norway

Table of Content

Page

Editorial

After the launch of the first volume journal in August 2021 we got several good articles to publish in the second volume. Many of us worked really hard to finish this volume at the end of the year. In fact, we had decided that each volume should be between 100 and 150 pages, and we had an overflow which could be published in volume 2.1.

Due to a heavy workload the previous editor was not able to finish the job. I was assigned editor Oct 24, 2022, with the task of finishing the editing of the Journal and move all the articles to a new website with Open Access. I have received good web expertise from the Norwegian Climate Realists, so the job should be done in a few weeks. This is the first of 4 volumes we have articles for.

Most of the articles in this volume discuss the question what controls the amount of CO_2 in our atmosphere. Is it from natural sources or the use of fossil fuel? And how much is from anthropogenic sources? In the review process I invited IPCC experts on the carbon cycle. To busy. I also asked the responsible for the Bern model to review the Ed Berry paper. They never answered.

As gift from the cradle of science we publish a paper by Christopher Moncton of Brenchley: *The application of Classical simplicity to present-day mathematical problems*. He shows that not only mathematical problems, but problems related to climate change and COVID can be easily solved by classical simplicity.

Good reading

Jan-Erik Solheim
Editor

The articles are first published here: www.scienceofclimatechange.org

Correspondence to
harde@hsu-hh.de

Vol. 1.2 (2021)
pp. 177-196

Control of Atmospheric CO_2 Part I:

Relation of Carbon 14 to the Removal of CO_2

Murry Salby[1], Hermann Harde[2]

[1]Ex Macquarie University, Sydney, Australia

[2]Helmut-Schmidt-University, Hamburg, Germany

Abstract

An in-depth analysis is performed on the record of atmospheric $^{14}CO_2$, an isotopic tracer of CO_2 that was perturbed by nuclear testing. In addition to long-term behaviour, we examine short-term changes that have been largely ignored. It pays to look closely. Those changes reveal the underlying mechanisms responsible for the observed decline of atmospheric $^{14}CO_2$ and, thereby, for removal of overall CO_2. They represent effective absorption that is considerably faster than appears in the average decline of $^{14}CO_2$, initially and then later in its long-term decline. The average decline of $^{14}CO_2$ is slowed initially by periodic re-enrichment from the stratosphere, which offsets direct absorption at the Earth's surface. Eventually, however, its decline is slowed by re-emission of absorbed $^{14}CO_2$ from the Earth's surface, which likewise offsets direct absorption. With CO_2 absorption revealed by the record of nuclear-perturbed ^{14}C, fundamental principles are then shown to reproduce the observed evolution of $^{14}CO_2$, on long as well as short time scales. Applying the same considerations to anthropogenic emission of CO_2 recovers effective absorption that is an order of magnitude faster than operates on $^{14}CO_2$. The difference follows from magnified disequilibrium between the atmosphere and the Earth's surface, a state which, unlike for perturbed $^{14}CO_2$, is maintained by continuous anthropogenic emission. Supported by fundamental principles, the observed behavior of $^{14}CO_2$ provides an upper bound on the anthropogenic perturbation of atmospheric CO_2. It represents only a few percent of the observed increase.

Keywords: Carbon cycle; carbon 14 decay; CO_2 absorption time.

Submitted 2021-09-10, Accepted 2021-10-24. https://doi.org/10.53234/SCC202112/30

1. Introduction

Carbon in the atmosphere is represented almost entirely by CO_2, with methane being a distant second. Its observed evolution, inclusive of its annual cycle, has recently been reproduced in numerical simulations (Harde and Salby 2021). In both, the abundance of atmospheric CO_2 is controlled by a competition between two opposing influences: Introduction of CO_2, through emission at the Earth's surface, and removal of CO_2, through absorption at the Earth's surface. This competition governs time-mean CO_2, which is determined by mean emission and absorption. It also governs changes of CO_2, which follow from perturbations to mean emission and absorption.

In each of these components of CO_2 behavior, absorption figures centrally. By opposing emission, absorption determines if and how fast CO_2 grows, as well as the magnitude of its perturbation, for example, by anthropogenic emission. Yet, actual observations of CO_2 absorption are

scarce. Observations of global absorption, the property which regulates the overall abundance of CO_2, are nonexistent. The impact of global absorption on atmospheric CO_2, however, is represented in carbon 14, an isotope of atmospheric carbon that has been observed in the troposphere since the 1950s (CDIAC 2017).

Atmospheric CO_2 is comprised chiefly of the stable isotope, carbon 12. A minute fraction of CO_2 molecules, however, is comprised of the meta-stable isotope carbon 14, which has a radioactive half life of 5730 years. On time scales of relevance, the operation of $^{14}CO_2$ is virtually identical to that of the preponderance of carbon dioxide molecules, $^{12}CO_2$. Dynamical, chemical, and thermodynamic processes acting on those two isotopes of CO_2 (including those in the biosphere) are, for practical considerations, indistinguishable.

This feature makes carbon 14 a tracer of atmospheric CO_2. Once CO_2 is introduced into the atmosphere, whatever influence is experienced by one isotope is experienced by the other. Owing to this property and its artificial enrichment by nuclear testing, ^{14}C is central to estimates of CO_2 absorption, which vary widely[1]. Absorption, in turn, is essential to understanding changes of atmospheric CO_2.

Among the properties that have been applied to infer absorption of atmospheric CO_2, $^{14}CO_2$ is unique. It is the only property whose observation not only represents CO_2 directly but represents it in the atmosphere. Accordingly, atmospheric $^{14}CO_2$ provides an unrivalled means through which to understand key mechanisms underpinning the evolution of atmospheric CO_2.

During the 1950s and early 1960s, atmospheric testing of nuclear devices sharply enriched ^{14}C in the stratosphere. Through the atmospheric circulation, ^{14}C-enriched air in the stratosphere was subsequently transferred into the troposphere. By 1963, when the Nuclear Test Ban Treaty (NTBT) was implemented, tropospheric ^{14}C had increased by nearly 100%. The NTBT virtually eliminated the anomalous nuclear source of ^{14}C, leaving its perturbation of ^{14}C to decline through absorption and overall ^{14}C to return to its unperturbed equilibrium abundance. Represented in the decline of ^{14}C is the removal of all CO_2, through its absorption at the Earth's surface.

Here, we perform an in-depth analysis on the record of atmospheric ^{14}C, to better understand how CO_2 is removed from the atmosphere. In addition to long-term behavior, we examine short-term changes that have been largely ignored. Those changes reveal the underlying mechanisms responsible for the observed evolution of $^{14}CO_2$ and, thereby, for removal of overall CO_2. Fundamental principles, jointly with CO_2 absorption revealed by the record of perturbed ^{14}C, are then shown to reproduce the observed evolution of ^{14}C. Applying the same considerations to anthropogenic emission recovers the effective rate at which anthropogenic CO_2 is removed from the atmosphere. Together with fundamental principles, it provides an upper bound on the anthropogenic perturbation of atmospheric CO_2.

2. Observed Evolution

2.1 Records of Atmospheric Carbon 14

Atmospheric ^{14}C was observed through surface measurements. There are two long continuous records: one in the Northern Hemisphere (NH) and one in the Southern Hemisphere (SH). Both are archived (CDIAC 2017). The record from Vermunt Austria (Fig. 1a: Magenta) evidences a pronounced increase shortly before the NTBT in 1963. It is followed by a long-term decline that continued to the end of the Vermunt record in 1983. The record from Wellington New Zealand (Aqua) also evidences the pronounced increase, but mitigated and lagged from the NH increase by 1-2 years. By 1970, ^{14}C in the SH converged to ^{14}C in the NH. Both then underwent a long-

[1] An overview is presented in Segalstad (1998) and, more recently, in Harde and Salby (2021).

term decline that continued to the end of the Wellington record in 1993.

The records in Fig. 1a are of anomalous carbon 14, $\Delta^{14}C$, in percent. $\Delta^{14}C$ describes the fractional deviation of ^{14}C from a reference concentration, further normalized by the concentration of ^{12}C (see, e.g., Levin et al. 2010; Stenstrom et al. 2011). In practice, however, the definition of $\Delta^{14}C$ varies widely, depending upon the choice of reference concentration (ibid). Further complicating $\Delta^{14}C$ is its normalization by ^{12}C, which increased during the modern era.

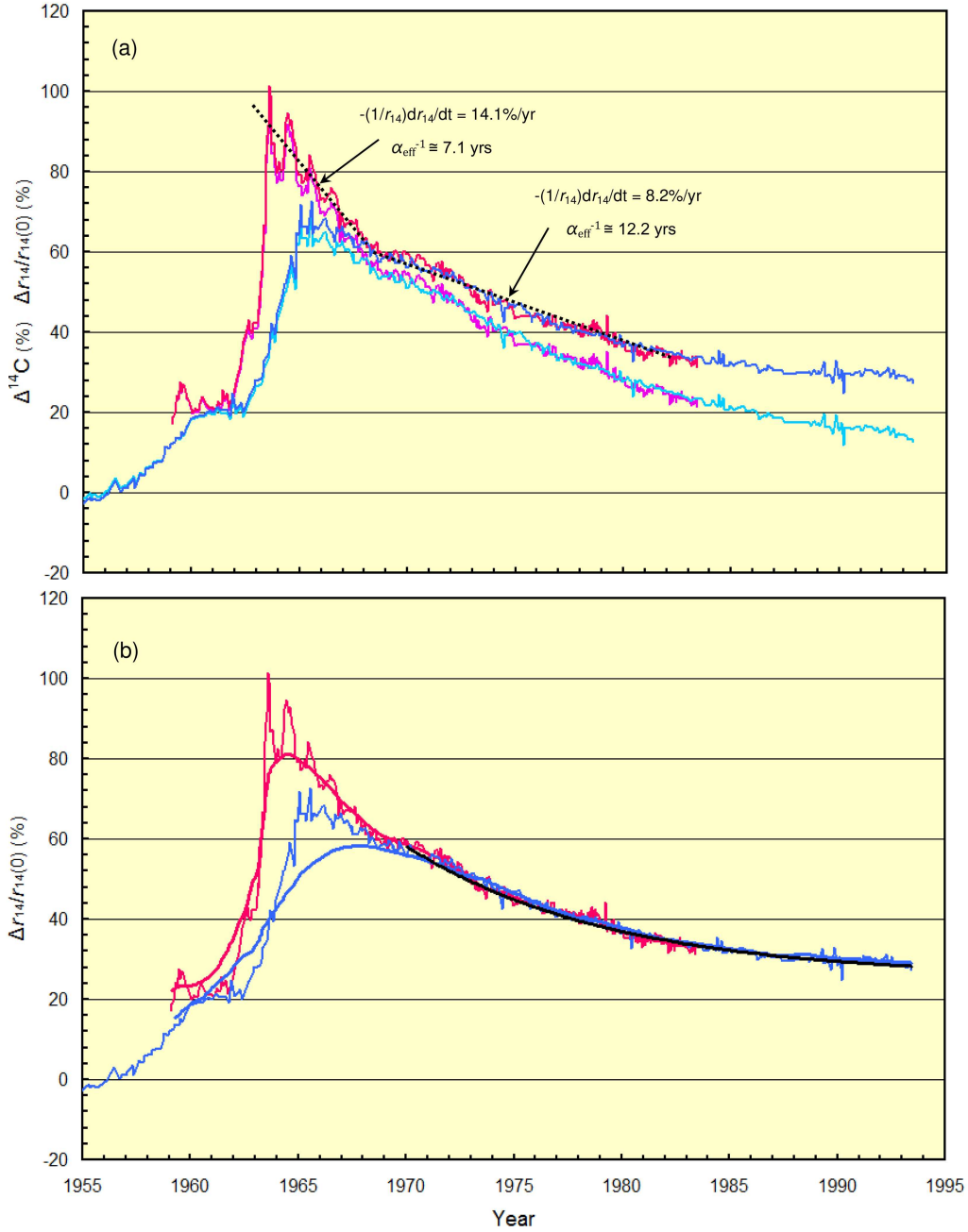

Figure 1: (a) Anomalous carbon 14, $\Delta^{14}C$, in percent observed at Vermunt Austria (Magenta) and at Wellington NZ (Aqua), along with anomalous carbon 14 mixing ratio (normalized), Δr_{14}, in percent at Vermunt (Red) and Wellington (Blue). (b) As in (a) for anomalous carbon 14 mixing ratio, along with those records low pass filtered to periods longer than 5 yrs. Superimposed is a pure exponential decline corresponding to an absorption time of 9.5 yrs (Black).

The property relevant to absorption of atmospheric ^{14}C is its volume mixing ratio, r_{14}, which is equivalent to the molar fraction of $^{14}CO_2$ to overall air molecules. Unlike $\Delta^{14}C$, r_{14} is conserved:

Its value is preserved in individual bodies of air. r_{14} changes only through emission and absorption at the Earth's surface. It follows from $\Delta^{14}C$ by removing the normalization with respect to ^{12}C .

Plotted in Fig. 2 is the increase of $^{12}CO_2$ mixing ratio in ppmv, $r = r_{12}$ (Green), exclusive of its mean annual cycle. Observed at Mauna Loa (CDIAC 2017), r closely tracks an exponential evolution,

$$\Delta r = 43 \cdot \left(e^{0.0196 \cdot t} - 1 \right), \tag{1.1}$$

which is superimposed (Black). The fractional change of ^{14}C mixing ratio then becomes

$$\frac{\Delta r_{14}}{r_{14}(0)} = \left(\Delta^{14}C + 100 \right) \frac{r}{r(0)} - 100, \tag{1.2}$$

where $r(0)$ and $r_{14}(0)$ are values at the onset of Mauna Loa measurements in 1959 and $r/r(0)$ compensates for the normalization of $^{14}CO_2$ by ^{12}C.

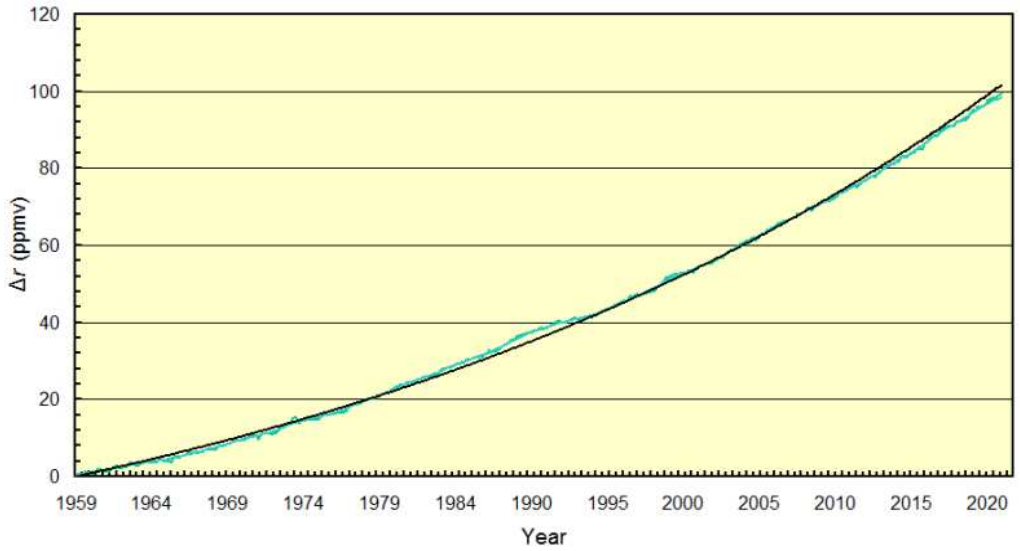

Figure 2: Increase of CO_2 mixing ratio in ppmv observed at Mauna Loa (Green), exclusive of its annual cycle, along with pure exponential increase (Black).

Superimposed in Fig. 1a is the percentage change of ^{14}C mixing ratio, in the records from Vermunt (Red) and Wellington (Blue). r_{14} evolves similar to $\Delta^{14}C$, but declines more gradually. It also approaches a new equilibrium level, about 25% higher than that adopted before the era of nuclear testing. The higher equilibrium level is well accounted for by an observed increase of neutron activity in the stratosphere, which provides the natural source of ^{14}C (Harde and Salby 2021).

Notice that, at Vermunt (where the nuclear surge was most evident), r_{14} declines steeply in the first half dozen years following the NTBT. Decreasing towards the local equilibrium at 14.1%/yr (dotted), the steep decline corresponds to an effective absorption rate of α_{eff} = (5-10 yrs)$^{-1}$. After a distinct bend in the record around 1970, r_{14} thereafter declines slower. At 8.2%/yr, the decline then corresponds to an effective absorption rate of α_{eff} = (10-20 yrs)$^{-1}$. This change in ^{14}C decline reflects a change in the underlying mechanics of CO_2 absorption, as will become evident shortly.

Plotted in Fig. 1b is the long-term evolution of r_{14} , which follows by low-pass filtering the raw records (bold). The long-term decline at Vermunt (Red), as well as at Wellington after the records have converged (Blue), closely track an exponential decline towards the new equilibrium level:

$$\frac{\Delta r_{14}}{r_{14}(0)} = 25.5 + (90 - 25.5)\, e^{-0.105\cdot(t-t_0)}, \tag{2}$$

which is superimposed (Black). The nearly-exponential decline which prevails then reflects an effective absorption rate of $\alpha_{\text{eff}} = 0.105$ yrs^{-1} and an absorption time of ~ 9.5 yrs.

2.2 Effective Absorption

As the mixing ratio of ^{14}C is conserved, its perturbation from local equilibrium, r'_{14}, satisfies the conservation law

$$\frac{dr'_{14}}{dt} = E'_{14} - \alpha_{\text{eff}}\, r'_{14}, \tag{3}$$

where E'_{14} is the perturbing emission and α_{eff} is the effective rate at which ^{14}C is absorbed from the atmosphere - both at the Earth's surface. Implicit in α_{eff} is re-emission of carbon from the Earth's surface, after it has been removed through direct absorption. By offsetting absorption, re-emission reduces α_{eff} from the rate of direct absorption, α.

After implementation of the NTBT, the nuclear perturbation in emission was mostly eliminated. The perturbing source of ^{14}C then vanished. With $E'_{14} = 0$, the effective absorption rate then follows from the conservation law:

$$\alpha_{\text{eff}} = -\frac{1}{r'_{14}}\frac{dr'_{14}}{dt}. \tag{4}$$

Plotted in Fig. 3 is the effective absorption rate inherent to the long-term decline in Fig. 1b, which prevails after the steeper decline during the first half dozen years. Superimposed is the effective absorption rate implicit in the pure exponential decline (Black), which is nearly constant: $\alpha \cong 0.105$ yrs^{-1}. At Vermunt (Red), the absorption rate varies gradually about a mean of $\langle\alpha\rangle = \sim 0.12$ yrs^{-1}, corresponding to an average absorption time of ~ 8 yrs. From early in the Vermunt record, absorption gradually accelerates, eventually slowing after 1980, shortly before the end of the Vermunt record. A similar variation is evident in the absorption rate inherent to the Wellington record (Blue), but slightly reduced and lagged with respect to the Vermunt record. At both sites, effective absorption is consistent with that of the nearly-exponential decline obeyed by r_{14} (Fig 1b: Black).

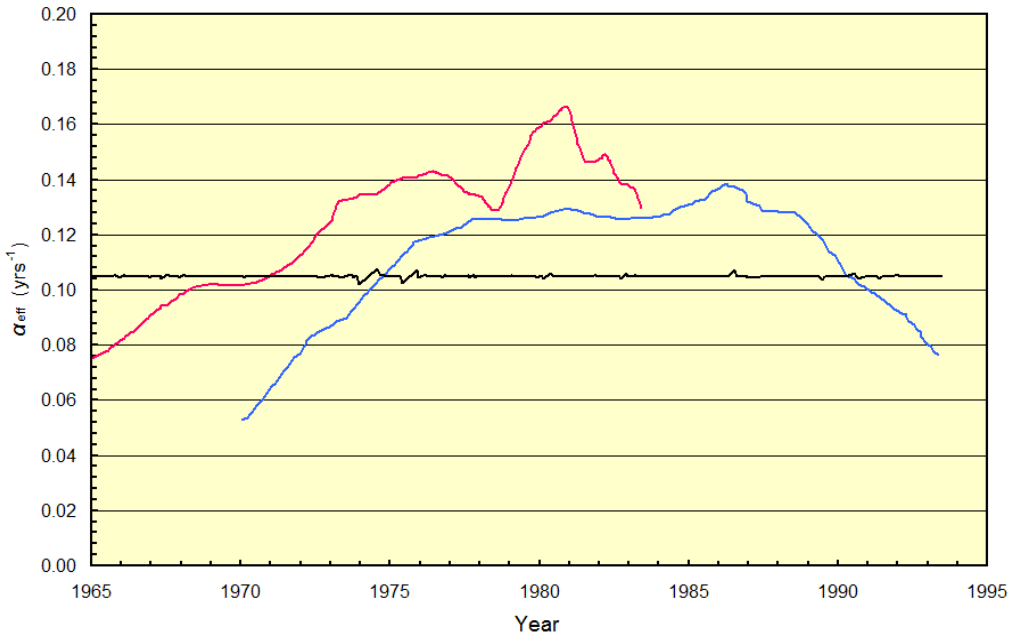

Figure 3: Effective absorption rate evaluated from the low-pass filtered record of ^{14}C at Vermunt (Red) and at Wellington (Blue). Superimposed is the absorption rate evaluated in the same manner from the pure exponential in Fig. 1b (Black).

3. Detailed Analysis of Absorption

The key to understanding ^{14}C and its relationship to absorption of CO_2 is what is often discarded: short-term fluctuations that punctuate initial years of the ^{14}C record (Fig. 1a). Usually filtered out, those fluctuations appear annually, reflecting dynamics of the seasonal cycle.

Close inspection of the initial years (Fig. 4) reveals that each annual perturbation is comprised of an abrupt increase, almost a step enrichment of ^{14}C, followed by sharp decline.

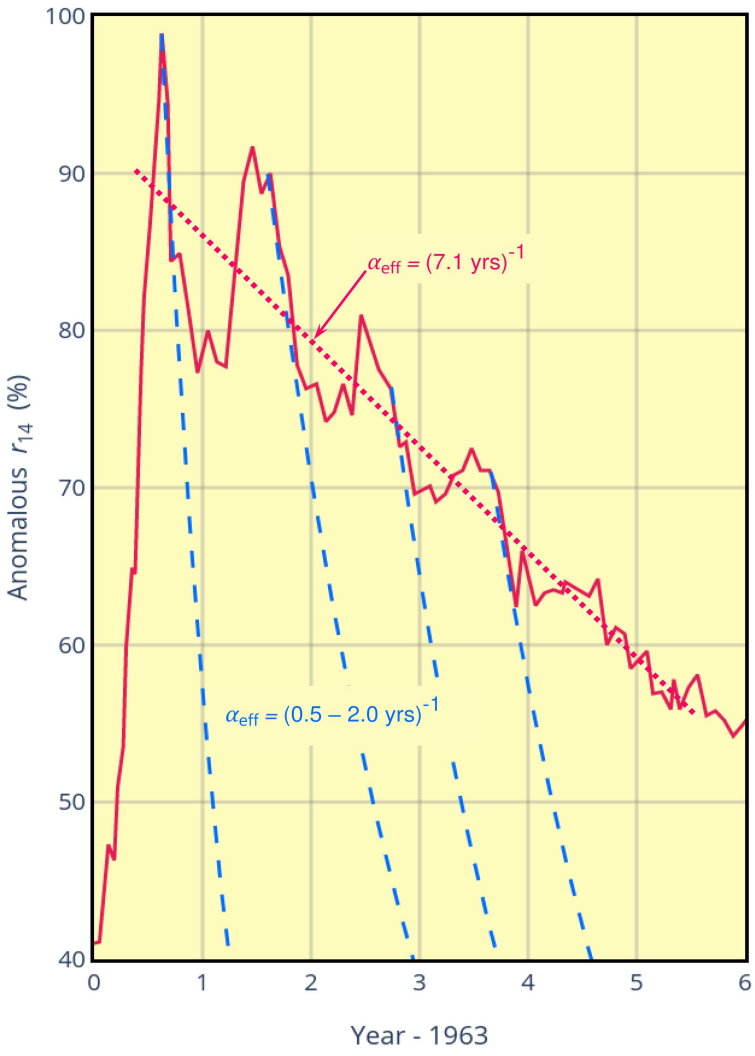

Figure 4: Anomalous ^{14}C mixing ratio observed at Vermunt during initial years after the Nuclear Test Ban Treaty (Red), along with the mean decline (dotted). Superimposed is exponential decline following each annual re-enrichment from the stratosphere (Blue).

The annual enrichments of tropospheric ^{14}C reflect the Brewer-Dobson circulation (BDC) of the stratosphere, a gradual overturning of air between the equator and poles (see, for example, Holton 2004; Salby 2012). This stratospheric circulation is coupled to the troposphere through exchanges of air: downward transport over the poles, compensated over the equator by upward transport. The BDC is strongest in the winter hemisphere, especially during boreal winter. It intensifies each year during late winter and spring.[2]

The intensified BDC transports ^{14}C-rich stratospheric air downward into the Arctic troposphere. Compensating it in the tropics is upward transport into stratosphere of ^{14}C-lean tropospheric air. Through annual injections of stratospheric air, the initial decline of tropospheric ^{14}C after 1963 was interrupted (Fig. 4) - temporarily reversed by successive re-enrichments from the stratosphere. Offsetting absorption of ^{14}C, those re-enrichments had the effect of turning back the clock on absorption - by repeatedly re-enriching tropospheric ^{14}C. Simultaneously, the compensating upward flow of tropospheric air acted to dilute ^{14}C in the stratosphere.

[2] The BDC intensifies during stratospheric warmings. Forced by planetary waves, stratospheric warmings develop sporadically during winter and each year during late winter and spring in the stratospheric final warming.

Each step in enrichment lasted just a couple of months. After each, tropospheric ^{14}C declined, with the rate of decline gradually weakening in successive years. The declines following annual re-enrichments track exponential declines - but with absorption rates of (0.5 - 2.0 yrs)$^{-1}$, superimposed in Fig. 4 (Blue). Unopposed by stratospheric re-enrichment, the exponential declines then reveal the actual absorption of ^{14}C. Absorption during those intervals was an order of magnitude faster than is reflected in the average decline in Fig 1a (dotted), as well as the long-term decline that prevails later.

Each sharp decline persists for half a year, until being interrupted by re-enrichment during the next annual cycle. This duration is much longer than the time for anomalous ^{14}C to be dispersed and diluted over the Northern Hemisphere - which is accomplished in only a couple of weeks. Mixing of ^{14}C is illustrated by the global distribution of water vapor, which experiences the same large-scale dispersion and can be animated from satellite observations: https://tinyurl.com/H2O-Animation. Anomalous H_2O is seen to be dispersed hemispherically in a matter of only days. The sharp declines following annual enrichments of ^{14}C (Fig. 4) persist much longer, reflecting its absorption at the Earth's surface.

The rapid removal of ^{14}C early in the record is borne out in the instantaneous absorption rate during intervals immediately following the stratospheric enrichments (Fig. 5). Following the first injection of stratospheric air, the effective absorption rate (4) approaches 3.0 yrs^{-1}. Corresponding to an absorption time of only months, the rapid removal of ^{14}C then occurs when re-emission of perturbation carbon that has been absorbed at the Earth's surface is still weak. The rate of effective absorption, α_{eff}, is then closest to the rate of direct absorption, α. Following subsequent enrichments, α_{eff} swings between 1.0 yrs^{-1} (an absorption time of 1 yr) and $\alpha < 0.25$ yrs^{-1} (absorption times longer than 4 yrs).

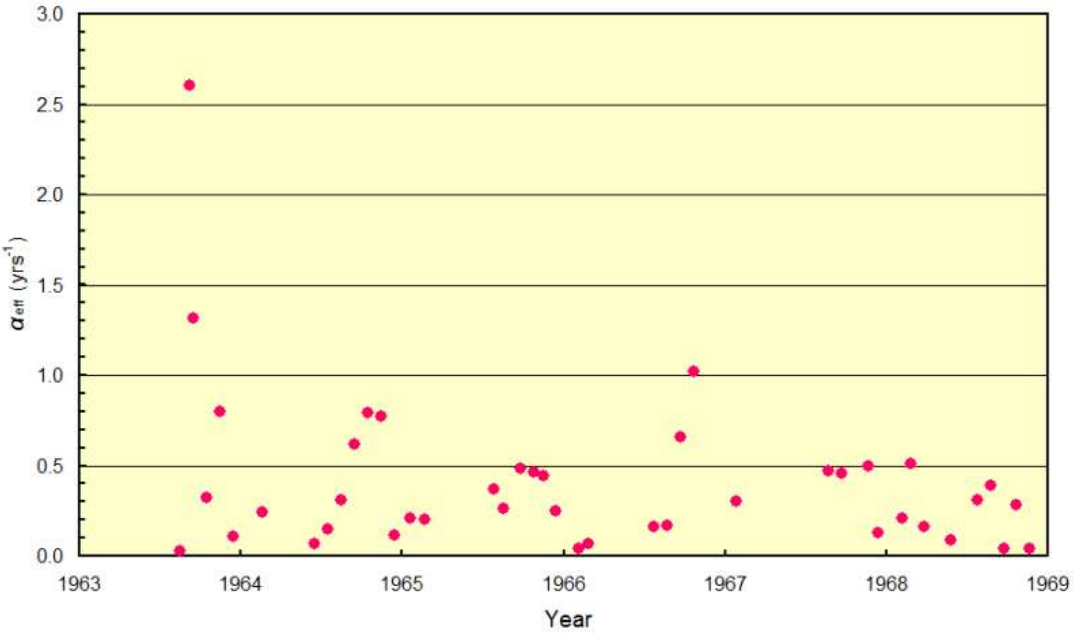

Figure 5: Instantaneous absorption rate following annual re-enrichments from the stratosphere.

Notice: While absorption develops after each annual re-enrichment, the pace of absorption gradually slows. After half a dozen re-enrichments, peak α_{eff} in Fig. 5 has declined from almost 3.0 yrs^{-1} to slower than 0.5 yrs^{-1}. The slowing of effective absorption reflects an increasing role of re-emission of absorbed carbon, which offsets its direct absorption.

Injections of ^{14}C-rich stratospheric air and compensating returns of ^{14}C-lean tropospheric air gradually weakened the contrast of ^{14}C between the stratosphere and troposphere. After half a dozen such exchanges, the contrast was weakened sufficiently for subsequent annual re-enrich-

ments to sink into the interannual noise (Fig. 1). Thereafter, ^{14}C declined without interruption.

Following the distinct bend in the average decline of ^{14}C (Fig. 1a), the absorption time became distinctly longer, 10-20 yrs. This slowing of absorption reflects the intensification of the second opposing influence: re-emission from the Earth's surface. Of anomalous ^{14}C that was absorbed at the Earth's surface, not all of it remained there. A fraction of absorbed ^{14}C was re-emitted back into the atmosphere. The reversed transfer offsets direct absorption of ^{14}C, slowing its net or effective absorption.

4. Theoretical Treatment of Absorption

To develop a comprehensive treatment of carbon transfer, evaluations of CO_2 absorption have relied upon estimates of carbon reservoirs at and beneath the Earth's surface (e.g., IPCC 2013). Extraneous to the atmosphere, those global carbon abundances are grossly under-observed and, hence, largely guesswork. Transfers between them are even more uncertain. Such uncertainty is averted here by focusing upon perturbations that originate in the atmosphere, where carbon is well observed. Their evolution can be evaluated through interaction with the Earth's surface, which observed behavior shows is determined autonomously by the atmosphere (Harde and Salby 2021). The system governing atmospheric perturbations is then free of arbitrary parameters associated with extraneous carbon reservoirs, which are largely unknown.

To understand the mechanics behind the observed evolution of ^{14}C, we consider the response to impulsive emission in a 3-volume system: a stratosphere, a troposphere, and a surface layer that is characteristic of the ocean mixed layer and the uppermost layer of land, surface layers that exchange carbon with the troposphere (Fig. 6).

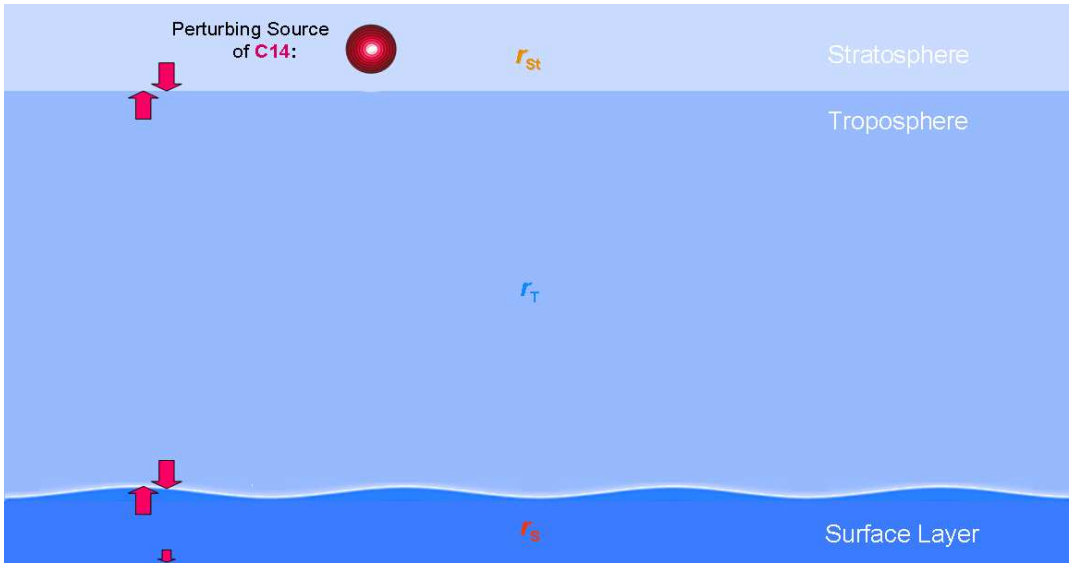

Figure 6: Three-volume system which follows from the 3-dimensional continuity equation that governs atmospheric carbon, comprised of a stratosphere, a troposphere, and a surface layer characteristic of the ocean mixed layer and uppermost layer of land, with mixing ratios, respectively, r_{St}, r_T, *and* r_S.

The respective mixing ratios of ^{14}C are r_{St}, r_T, and r_S, where r here is understood to refer to ^{14}C. The 3-volume system follows rigorously by integrating the 3D continuity equation, the basis of the conservation law (3), over the individual volumes. The resulting discrete system provides a realistic description of mean CO_2 in those subsystems and exchanges between them - because of the disparate time scales of transport in the individual volumes. In the troposphere, CO_2 is homogenized hemispherically in only a couple of weeks (Sec. 3). In the stratosphere and surface layer, the same transport operates on time scales that are two orders of magnitude longer. Rela-

tive to those time scales, CO_2 in the troposphere (at least in an individual hemisphere) may therefore be regarded as adjusting uniformly and instantly to its supply from the stratosphere and removal by the surface layer.

The three volumes interact through transfers of carbon. In addition to exchanging carbon with the troposphere, the surface layer loses carbon through transfer to depths sufficiently great for carbon to be sequestered from the troposphere. In ocean, this corresponds to entrainment from the mixed layer into the deep ocean, where transport operates on the time scale of centuries to millennia. In land, it corresponds to percolation to depths greater than a few tens of cm, where CO_2 is no longer emitted through soil respiration (e.g., Fang and Montcrief 2005; Maier et al. 2020).

Consider now an incremental transfer of carbon mass $dm_{\mathrm{St}}^{\mathrm{C}}$ from the stratosphere to the troposphere:

$$dm_{\mathrm{T}}^{\mathrm{C}} = -dm_{\mathrm{St}}^{\mathrm{C}}. \tag{5}$$

The induced change of tropospheric mixing ratio is

$$dr_{\mathrm{T}} = \frac{dm_{\mathrm{T}}^{\mathrm{C}}}{m_{\mathrm{T}}} = -\frac{dm_{\mathrm{St}}^{\mathrm{C}}}{m_{\mathrm{T}}} \tag{6.1}$$

$$= -\frac{m_{\mathrm{St}} dr_{\mathrm{St}}}{m_{\mathrm{T}}} \tag{6.2}$$

$$= -\frac{1}{\delta_{\mathrm{St}}} dr_{\mathrm{St}}\,, \tag{6.3}$$

where m_{T} and m_{St} are the total masses of the troposphere and stratosphere, respectively,

and

$$\delta_{\mathrm{St}} = \frac{m_{\mathrm{T}}}{m_{\mathrm{St}}} \tag{6.4}$$

is the ratio of tropospheric mass to stratospheric mass. Letting $\xi\, dt$ denote the fractional decrease of stratospheric mixing ratio in time dt then gives

$$dr_{\mathrm{T}} = \frac{1}{\delta_{\mathrm{St}}} \xi\, r_{\mathrm{St}}\, dt, \tag{7.1}$$

where a decrease of ^{14}C in the stratosphere ($\xi > 0$) is accompanied by an increase in the troposphere. Analogous treatment for an incremental transfer from the troposphere to the stratosphere gives the respective change of stratospheric mixing ratio

$$dr_{\mathrm{St}} = \delta_{\mathrm{St}}\, \kappa\, r_{\mathrm{T}}\, dt, \tag{7.2}$$

where $\kappa\, dt$ denotes the respective fractional decrease of tropospheric mixing ratio.

With (7), conservation of carbon mass in the stratosphere is expressed by

$$\frac{dr_{\mathrm{St}}}{dt} = -\xi\, r_{\mathrm{St}} + \delta_{\mathrm{St}}\, \kappa\, r_{\mathrm{T}}. \tag{8}$$

Now, in equilibrium, $r_{\mathrm{T}} = r_{\mathrm{St}}$ and $dr_{St}/dt = 0$. Then (8) reduces to

$$\xi = \delta_{\mathrm{St}}\, \kappa\,. \tag{9.1}$$

Since ξ and κ are constant, (9.1) must hold in general. The conservation law for stratospheric ^{14}C (8) then becomes

$$\frac{dr_{St}}{dt} = -\delta_{St}\,\kappa\,(r_{St} - r_T)\cdot \tag{9.2}$$

^{14}C is seen to evolve according to its contrast between the stratosphere and troposphere, κ serving as the exchange coefficient between the two volumes.

Proceeding along similar lines for transfers between the troposphere and surface layer leads to the conservation laws governing carbon in all three volumes:

$$\frac{dr_{St}}{dt} = -\delta_{St}\,\kappa\,(r_{St} - r_T) + \gamma_{St} \tag{10.1}$$

$$\frac{dr_T}{dt} = -\kappa\,(r_T - r_{St}) - \alpha\,(r_T - r_S) + \gamma_T \tag{10.2}$$

$$\frac{dr_S}{dt} = -\delta_S\,\alpha\,(r_S - r_T) - \eta\, r_S + \gamma_S\,, \tag{10.3}$$

where

$$\delta_S = \frac{m_T}{m_S}, \tag{10.4}$$

α serves as the exchange coefficient between the troposphere and surface layer, γ_i represent emission in the individual volumes, and η is the rate at which carbon is lost through sequestration beneath the surface layer[3].

Equations (10) express conservation of carbon in terms of mixing ratio, the relative abundance of ^{14}C in the individual volumes. Multiplying across by the respective masses, as embodied in (6.4) and (10.4), expresses conservation in terms of the absolute abundance of ^{14}C in the individual volumes. It can be shown that, absent internal sources and discharge into the sub-surface volume, total ^{14}C in the three volumes is conserved.

The conservation laws (10) represent fundamental constraints on carbon. These physical laws govern total carbon, as well as perturbations introduced by anomalous emission. They form a coupled system of 1st-order ordinary differential equations. For specified coefficients, the system can be integrated through eigenanalysis. As representative, $\delta_{St} = 10$ corresponds to stratospheric mass above 100 mbar, $\delta_S = 0.10$ to a mixed layer depth of 100 m, $\alpha = 6.0$ yrs^{-1} to a time scale for direct absorption of months (Fig. 5), $\kappa = 0.2$ yrs^{-1} to the time for transfer of stratospheric carbon to the troposphere of 5 yrs (Fig. 1a), and $\eta = 0.105$ yrs^{-1} to the time scale of sequestration beneath the surface layer of 9.5 yrs.

4.1 Absorption of Anomalous ^{14}C

The governing system is now integrated with $\gamma_{St} = \gamma_T = \gamma_S = 0$, from an initially unperturbed troposphere and surface layer, $r_T(0) = r_S(0) = 0$, but from an initial stratospheric perturbation (introduced by impulsive emission) of $r_{St}(0) = 2600\%$.[4] Displayed in Fig. 7 is the normalized response of ^{14}C in the stratosphere (Yellow). From its initial perturbation, r_{St} declines sharply. Attending its decline is a sharp increase of ^{14}C in the troposphere (Blue), as ^{14}C is transferred down from the stratosphere.

---

[3] α represents the rate of direct absorption - not to be confused with the rate of effective absorption, α_{eff}, in (3).

[4] Note: Because tropospheric mass is an order of magnitude greater than that of the stratosphere, the minimum stratospheric perturbation that could increase tropospheric ^{14}C by 100% would be 1000%. The presence of absorption requires it to be even greater.

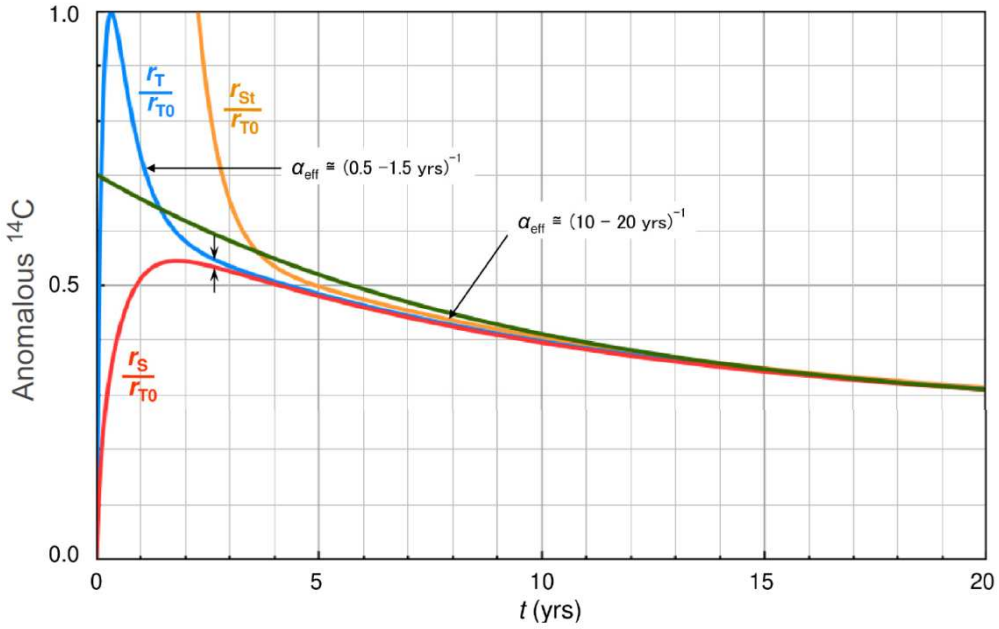

Figure 7: Normalized response of ^{14}C in the 3-volume system (Fig. 6) to impulsive emission in the stratosphere: Response in the stratosphere (Yellow), in the troposphere (Blue), and in the surface layer (Red). Superimposed is the pure exponential decline in Fig. 1b with an effective absorption rate of $\alpha_{eff} = 0.105$ yrs-1 (Green).

After attaining a maximum, r_T also declines sharply, with an effective absorption rate (4) of $\alpha_{eff} = (0.5 - 1.5\ \text{yrs})^{-1}$. Following a distinct bend in its evolution, r_T then declines more gradually, with an effective absorption rate of $\alpha_{eff} = (10 - 20\ \text{yrs})^{-1}$.

The distinct change of absorption time can be understood from ^{14}C in the surface layer, which is superimposed in Fig. 7 (Red). As the surface layer absorbs ^{14}C, r_S increases at the expense of r_T, which decreases. Eventually, the two volumes approach equilibrium, with r_S attaining a maximum nearly equal to r_T - at the bend in its evolution. Contrast between the troposphere and surface layer, reflected in the separation of r_T and r_S (arrows), has then become small. Under these conditions, re-emission from the surface layer nearly cancels direct absorption from the troposphere. Net transfer of carbon between the volumes, represented by $-\alpha\cdot(r_T - r_S)$ in (10.2), is then limited. Thereafter, ^{14}C in all three volumes decline in quasi-equilibrium with one another, r_{St} , r_T, and r_S remaining comparable. For reference, also superimposed in Fig. 7 is the pure exponential decline in Fig. 1b, with an effective absorption rate of $\alpha_{eff} = 0.105\ \text{yrs}^{-1}$ (Green). After attaining quasi-equilibrium, ^{14}C in all three volumes track the pure exponential decline.

Re-emission into the troposphere of absorbed ^{14}C depends on ^{14}C in the surface layer. Consider the conservation law governing tropospheric ^{14}C. After sufficient ^{14}C in the stratosphere has been transferred into the troposphere, those two volumes approach equilibrium, making $\kappa\,(r_T - r_{St}) << \alpha\,(r_T - r_S)$. The balance (10.2) then reduces to

$$\begin{aligned}\frac{dr_T}{dt} &\cong -\alpha\,(r_T - r_S)\\ &= -\alpha\,(1-\beta)\cdot r_T\\ &= -\alpha_{eff}\,r_T\end{aligned} \qquad (11.1)$$

where

$$\alpha_{eff} = \alpha\,(1-\beta) \qquad (11.2)$$

is recognized as the effective absorption rate, with

$$\beta = \frac{r_S}{r_T} \tag{11.3}$$

representing the fractional re-emission: In (11.1), βr_T is the fraction of ^{14}C that is absorbed by the surface layer which is re-emitted into the troposphere.

As is evident in Fig. 7, the bend in r_T marks when ^{14}C in the surface layer has become comparable to ^{14}C in the troposphere. Fractional re-emission (11.3), plotted in Fig. 8 (Green), then approaches unity. Much of the direct absorption thereafter is offset by re-emission, which returns to the troposphere the fraction β of ^{14}C that was removed through absorption. Through this offset, re-emission sharply slows the effective absorption rate (11.2), which is superimposed in Fig. 8 (Purple). Although α_{eff} is initially very fast, comparable to α, within as short as a year after the peak in tropospheric ^{14}C, re-emission from the surface layer has intensified, slowing α_{eff} to only a fraction of the initial absorption rate (cf. Fig. 5). Following the bend in r_T, α_{eff} approaches a limiting value of ~ 0.1 yrs^{-1}.

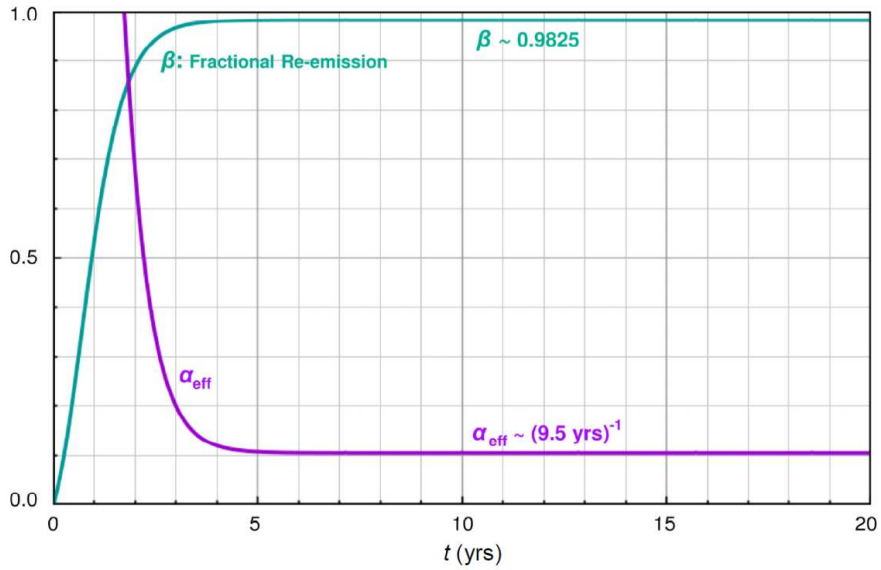

Figure 8: In the presence of impulsive emission in the stratosphere (Fig. 7): Fractional re-emission of perturbed ^{14}C from the surface layer (Green) and effective absorption rate (Purple).

The observed evolution in Fig. 1a follows, not from a single transfer from the stratosphere of enriched ^{14}C, but from a succession of brief annual injections, when the BDC intensifies. Restricting the stratospheric exchange coefficient $\kappa > 0$ in (10) to late winter and spring serves as a stratospheric valve, which throttles the transfer of ^{14}C into the troposphere. Cycling the stratospheric valve annually leads to the evolution of tropospheric ^{14}C plotted in Fig. 9 (solid). The calculated evolution reproduces salient features of the observed evolution (Fig. 1a). A sharp initial decline is interrupted by successive re-enrichments from the stratosphere. Each acts to turn back the clock on the decline of tropospheric ^{14}C - by (*i*) enriching r_T, reversing its removal through absorption and (*ii*) driving the troposphere back out of equilibrium with the surface layer (thereby reducing $r_S/r_T = \beta$), which weakens re-emission (Fig. 8) and, hence, its offset of direct

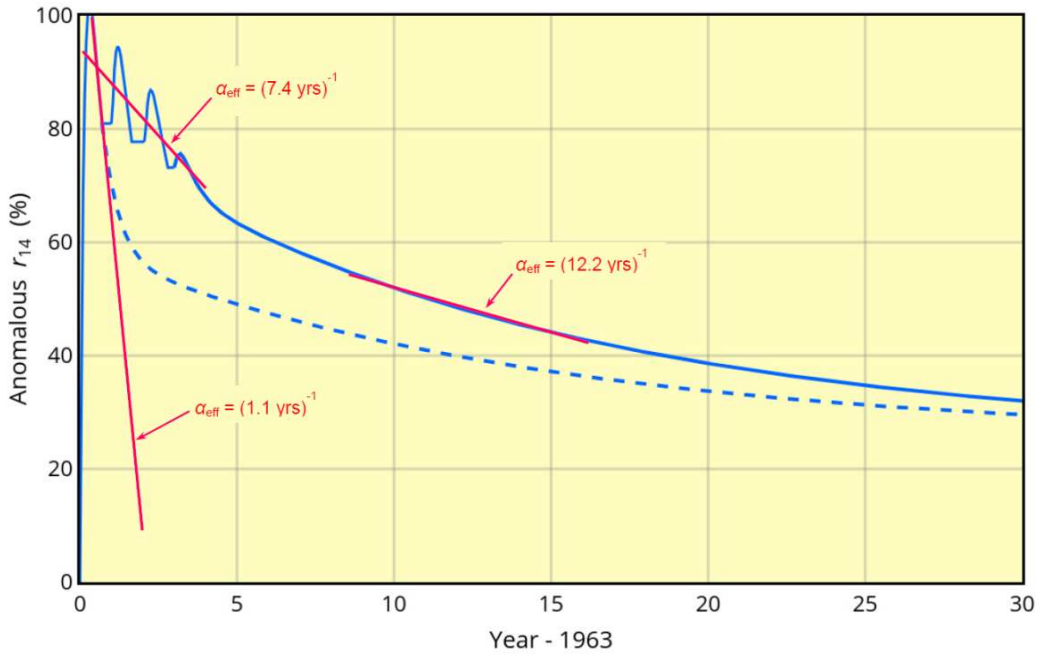

Figure 9: Evolution of tropospheric $^{14}C(r_T)$ calculated by cyclically restricting the stratospheric exchange coefficient to late winter and spring (Solid). Superimposed is the evolution when exchange between the stratosphere and troposphere is not limited (Dashed).

absorption (11.2).[5]

Each annual re-enrichment in Fig. 9 magnifies of the disequilibrium between the troposphere and surface. The effective absorption rate then increases sharply (Fig. 10). Successive enhancements of α_{eff}, however, gradually weaken, as r_{14} at the surface incrementally approaches r_{14} in the troposphere. The latter, in turn, intensifies re-emission, which offsets direct absorption of ^{14}C. Similar evolution is evident in the observed record (Fig. 5), but in the presence of intra-annual noise.

Jointly, the successive re-enrichments dramatically slow the initial decline of ^{14}C from what would exist in the absence of those re-enrichments. The average decline in Fig. 9 during the initial phase of the calculated evolution is 13.5%/yr. It corresponds to effective absorption of $\alpha_{eff} = (7.4 \text{ yrs})^{-1}$; cf. Fig. 1a. After a bend in the evolution, ^{14}C declines slower, at 8.2%/yr. Effective absorption has then slowed to only about half of the initial average rate: $\alpha_{eff} = (12.2 \text{ yrs})^{-1}$.

The average decline should not be confused with direct absorption, which is much faster - faster even than the initial average decline. Superimposed in Fig. 9 is the evolution that would occur in the absence of re-enrichments (dashed). During its initial phase, which in the full evolution is interrupted by successive re-enrichments, ^{14}C declines at of 91.2%/yr. The steep decline then corresponds to an effective absorption rate of $\alpha_{eff} = (1.1 \text{ yrs})^{-1}$.

[5] In relation to the sharp initial decline of observed ^{14}C (Figs 4 and 5), two features are noteworthy: (1) Peak r_T is reached more than a year after the nuclear perturbation has begun to amplify in 1962 (Fig. 1a) and, thus, induced re-emission back into the troposphere. (2) The stratosphere then is still enriched relative to the troposphere, as is evident from subsequent annual enrichments of the troposphere. The latter invalidates the limiting decline (11), wherein transport from the stratosphere is neglected. Both features (re-emission from the surface and continued enrichment from the stratosphere) offset direct absorption of tropospheric ^{14}C. It follows that even the fastest observed rate of decline is but a lower bound on the actual rate of direct absorption.

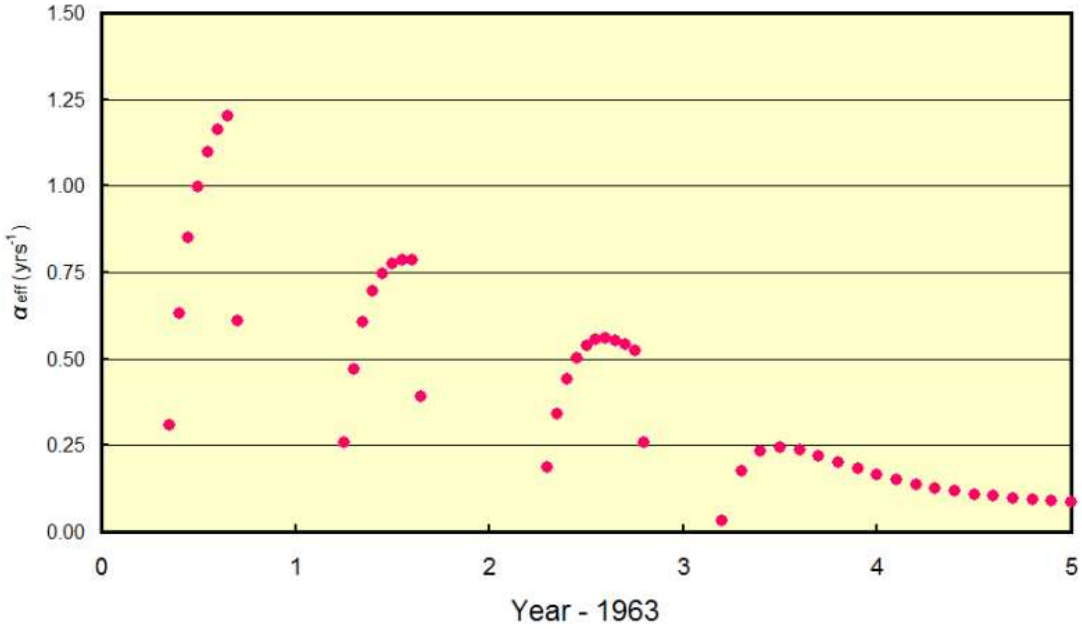

Figure 10: Effective absorption rate associated with the evolution of r_{14} in Fig. 9, following smoothing that discriminates to periods longer than half a year.

4.2 Absorption of Anthropogenic Carbon

The foregoing features apply to anomalous $^{14}CO_2$, which was emitted impulsively - only initially through nuclear testing. We turn now to anthropogenic CO_2, which is emitted continuously. The same 3-volume system is now perturbed by continuous emission in the troposphere, with $r_{St}(0) = r_T(0) = r_S(0) = 0$ and $\gamma_{St} = \gamma_S = 0$, but with $\gamma_T = 0.62 \cdot \Delta E_A$ which, with the increase of anthropogenic emission since 1960 ($\Delta E_A = 3.5$ ppmv/yr $\cong 7.3$ GtC/yr), gives forcing representative of anthropogenic emission during its 20th-century increase.[6]

Under these conditions, r_T increases monotonically (Fig. 11). Dragged along are r_{St} and r_S, but lagged behind r_T. Anthropogenic CO_2 therefore increases steadily in all three volumes. In each, however, CO_2 approaches a limiting value. That value corresponds to the *equilibrium level* of CO_2: for the troposphere, the value of r_T wherein the rate at which CO_2 is removed through absorption is exactly balanced by the rate at which it is introduced through emission.

In the stratosphere, CO_2 is neither emitted nor absorbed. Within about a decade, it comes into equilibrium with the troposphere: $r_{St} \sim r_T$. The surface layer, on the other hand, never does. In the presence of continuous emission, r_S lags significantly behind r_T, maintaining the contrast between the troposphere and surface layer (arrows); cf. Fig. 7. The exaggerated lag results from the continuous re-supply of CO_2 in the troposphere. By enriching r_T over r_S , the latter continually restores the initial disequilibrium between the troposphere and the surface layer. Thereby, the lag reduces fractional re-emission, plotted in Fig. 12 (Green), from what exists in the presence of impulsive emission (cf. Fig. 8). Since β is reduced, direct absorption is offset less by re-emission (11.2) - less than occurred in the presence of impulsive emission of ^{14}C, which did not continually re-supply r_T. The effective absorption rate, superimposed in Fig. 12 (Purple), is therefore faster than under the conditions of ^{14}C (Fig. 8). An order of magnitude faster, α_{eff} now approaches a limiting value of 0.90 yrs^{-1}. It is noteworthy that, independently, strong coherence between observed CO_2 and its thermally-induced component reveals a removal time of anthropogenic CO_2 of order a year (Salby and Harde 2021).

---

[6] Note: Unlike r_T, β and α_{eff} are independent of the magnitude of γ_T (11).

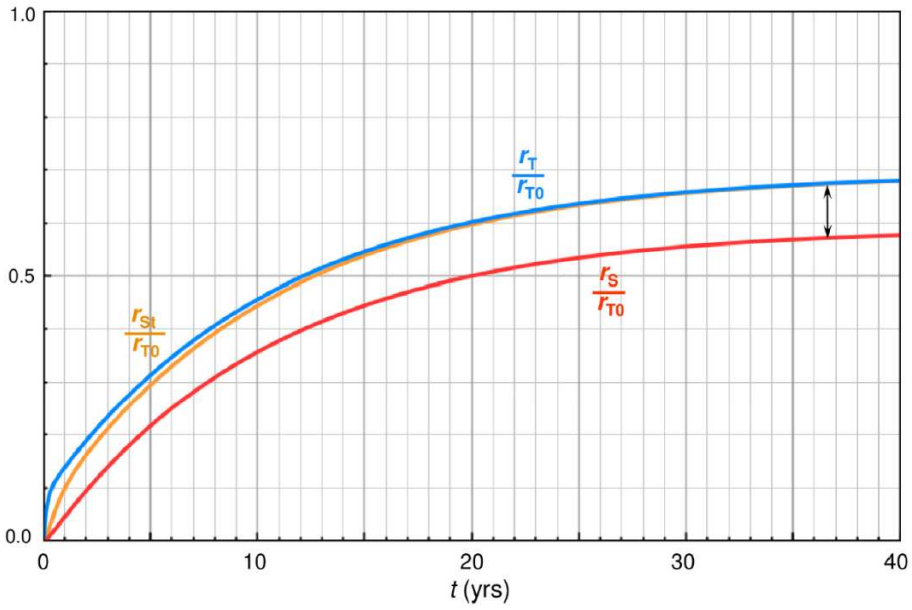

Figure 11: As in Fig. 7, but for continuous emission in the troposphere that is constant, representative of anthropogenic emission during the last half century ($r_{T0} = \Delta E_A/\alpha_0$; $\alpha_0 = 1.0\ yrs^{-1}$).

In the presence of anthropogenic emission, the counterpart of (11.1) is

$$\frac{dr_A}{dt} = -\alpha_{eff}\, r_A + E_A\ , \tag{12}$$

where $r_T = r_A$ denotes the anthropogenic perturbation of tropospheric CO_2. Under conditions of equilibrium, the left-hand side of (12) vanishes. The equilibrium level of anthropogenic CO_2 is therefore:

$$r_A^{Eq} = \frac{E_A}{\alpha_{eff}}\ . \tag{13}$$

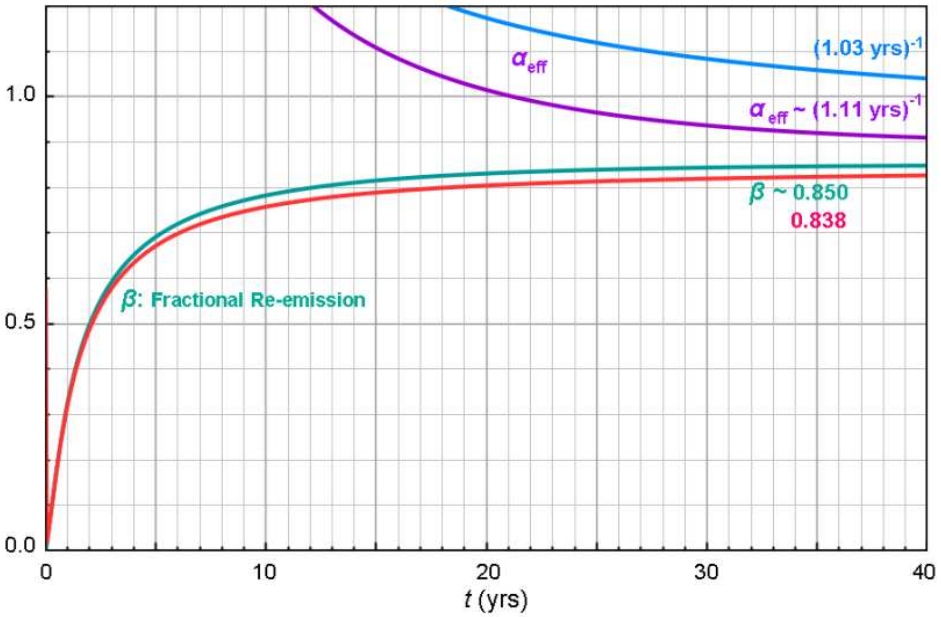

Figure 12: As in Fig. 8, but for anthropogenic emission that is constant (Fig. 11): Fractional re-emission from the surface layer (Green) and effective absorption rate (Purple). Superimposed is the response for anthropogenic emission that increases at 5%/yr (Fig. 13):Fractional re-emission from the surface layer (Red) and effective absorption rate (Blue).

Emission prescribed in this integration is representative of mean anthropogenic emission over the latter half of the 20th century: E_A = 2.2 ppmv/yr (4.6 GtC/yr). With α_{eff} equal to its limiting value (Fig. 12), this continuous perturbation to emission induces an equilibrium level of anthropogenic CO_2 of $r_A^{Eq} \cong 2.4$ ppmv. The latter corresponds to the limiting perturbation of CO_2 to which r_T asymptotically approaches in Fig. 11. It represents only about 2% of the observed increase of atmospheric CO_2 during the last century (~ 100 ppmv).

Finally, instead of constant anthropogenic emission, the 3-volume system is now integrated with E_A increasing at 5%/yr, representative of the recorded increase. As shown in Fig. 13, r_{St}, r_T, and r_S again increase monotonically. However, with E_A steadily increasing, they no longer approach a limiting value - because quasi equilibrium is never achieved (cf. Fig. 11). Instead, the equilibrium level of CO_2, to which the mixing ratios gravitate, slowly drifts higher, mirroring the upward drift of E_A.

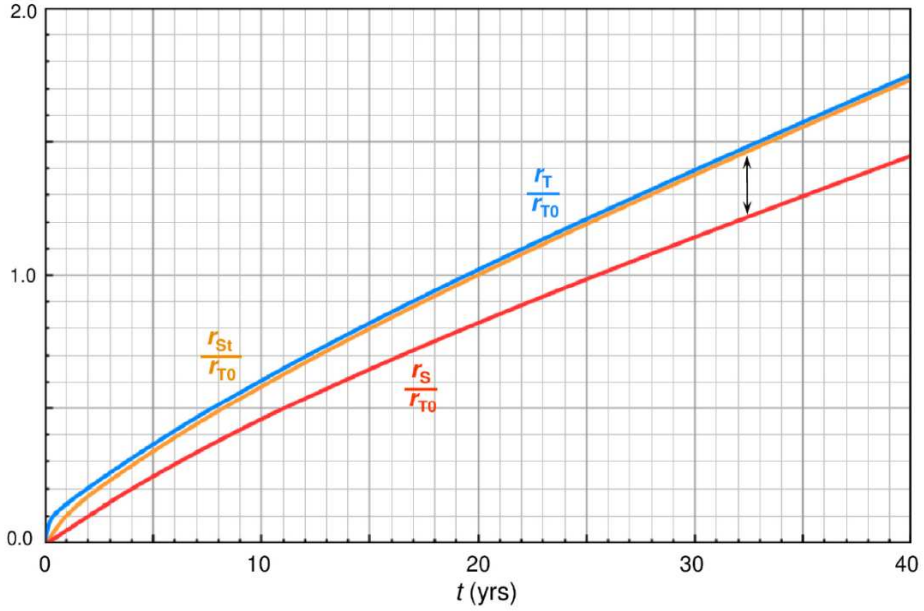

Figure 13: As in Fig. 11, but for anthropogenic emission that increases at 5%/yr.

Despite this difference, the salient features of re-emission and its influence on effective absorption that operate in the presence of E_A = const also operate here. Remaining is the separation between r_T and r_S (arrows), which measures the disequilibrium between the troposphere and surface layer. Consequently, fractional re-emission from the surface layer, which is superimposed in Fig. 12 (Red), remains weak. In fact, β is even weaker than it is in the presence of constant anthropogenic emission (Green). So too then is its offset of direct absorption in α_{eff}, which is also superimposed in Fig. 12 (Blue). Consequently, effective absorption is now even faster than it is in the presence of constant anthropogenic emission (Purple), approaching a limiting value of $\alpha_{eff} = 0.97$ yrs^{-1}.

It is noteworthy that the two evolutions considered, the nuclear perturbation of ^{14}C in Fig. 8 and the anthropogenic perturbation of CO_2 in Fig. 12, follow from the same 3-volume system. What differs between the integrations is how the system is perturbed. For perturbing emission that is impulsive, as applies to nuclear emission of ^{14}C, the separation (lag) between r_T and r_S in Fig. 7 narrows, eventually becoming small. The troposphere and surface layer then lapse into quasi equilibrium, with fractional re-emission ($\beta = r_T/r_S$) approaching unity (Fig. 8). In that limiting state, direct absorption experiences a large offset, sharply reducing effective absorption (11.2).

For perturbing emission that is continuous, as applies to anthropogenic emission of CO_2, this limiting state is never achieved. Continuous emission may be regarded as a succession of pulses, analogous to successive re-enrichments of ^{14}C from the stratosphere (Figs 7, 8). An individ-

ual pulse of emission in the troposphere introduces an incremental increase of r_T. Before that perturbation of tropospheric CO_2 can evolve beyond the preliminary regime of disequilibrium (when r_T and r_S in Fig. 7 are widely separated), its approach to quasi equilibrium is interrupted by the next pulse in emission. The incremental increase of r_T it introduces again widens the separation between r_T and r_S, driving the troposphere back out of equilibrium with the surface layer. Thereby, the successor pulse reverses the intensification of fractional re-emission (Fig. 8), along with its offset of direct absorption (11.2). In Fig. 7, this corresponds to the instantaneous separation between r_T and r_S (arrows) being driven backward, from right to left, restoring the contrast between the troposphere and the surface layer. The restored contrast limits fractional re-emission and its offset of direct absorption that would otherwise weaken effective absorption (Fig. 8). By maintaining the separation of r_T and r_S (Fig. 11), continuous emission in the troposphere prevents β from approaching unity, leaving α_{eff} fast (Fig. 12).

5. Implications

Effective absorption of atmospheric CO_2 depends upon its re-emission from the Earth's surface, which offsets direct absorption. This dependence distinguishes the absorption of $^{14}CO_2$, which was perturbed impulsively by nuclear testing, from the absorption of anthropogenic CO_2, which is perturbed continuously by fossil fuel emission. Unlike impulsive emission of $^{14}CO_2$, continuous anthropogenic emission maintains the disequilibrium between the atmosphere and the Earth's surface. Thereby, it inhibits the offset of direct absorption by re-emission from the Earth's surface, resulting in faster effective absorption of anthropogenic CO_2.

The evolution in Figs 8 and 12 also indicates that re-emission and, hence, its weakening of α_{eff} depend upon time scale. Fluctuations of emission operating on time scales of only a couple year will introduce anomalous CO_2 that falls within the short-time regime in Fig. 12, before re-emission can intensify and offset direct absorption. Such perturbations will therefore experience effective absorption that is fast, comparable to direct absorption. On the other hand, emission that varies slowly or is invariant will introduce anomalous CO_2 that falls within the long-time regime in Fig. 12, when re-emission has intensified and offset direct absorption. Such perturbations will therefore experience effective absorption that is slow, operating at only a fraction of the pace of direct absorption.

In the presence of anthropogenic emission, the actual value of r_A can never exceed its instantaneous equilibrium level, r_A^{Eq} - because once the equilibrium level is reached, CO_2 is removed as fast as it is introduced. For this reason, the equilibrium level represents a hard cap on accumulation of CO_2 in the atmosphere: an upper bound on the anthropogenic perturbation. It gradually drifts upward with increasing anthropogenic emission (13).

With α_{eff} determined (Fig. 12), the instantaneous equilibrium level, $r_A^{Eq}(t)$, follows directly from instantaneous anthropogenic emission, $E_A(t)$. Plotted in Fig. 14 is the increase in equilibrium level of anthropogenic CO_2 over the last half century (Magenta). It has an average of ~ 2 ppmv, close to the limiting level in Fig. 11 for constant emission representative of mean anthropogenic emission during its 20th century increase.

The actual perturbation of CO_2 introduced by anthropogenic emission must lie beneath the equilibrium level (shaded). Superimposed is the increase in observed CO_2 (Green). The anthropogenic perturbation of CO_2 can account for no more than a few percent of the observed increase.

From the IPCC's own estimates of extraneous carbon reservoirs, the anthropogenic contribution to increased CO_2 has been shown to be no more than 15% - 35% (Harde 2017; Harde 2019; Berry 2019; Harde and Salby 2021), recognized earlier from the strong interdependence of temperature and net CO_2 emission (Salby 2012). The present analysis does not rely upon such estimates, which are largely *ad hoc*. It shows that the anthropogenic perturbation is even smaller. This conclusion is confirmed in Part II of this two-part article, which demonstrates inde-

pendently through observed behavior that (i) the removal time of anthropogenic CO_2 is of order only a year and consequently (ii) the anthropogenic perturbation can represent but a few percent of increased CO_2. Much the same has been inferred from the satellite record of OCO-2 (Segalstad, 2017).

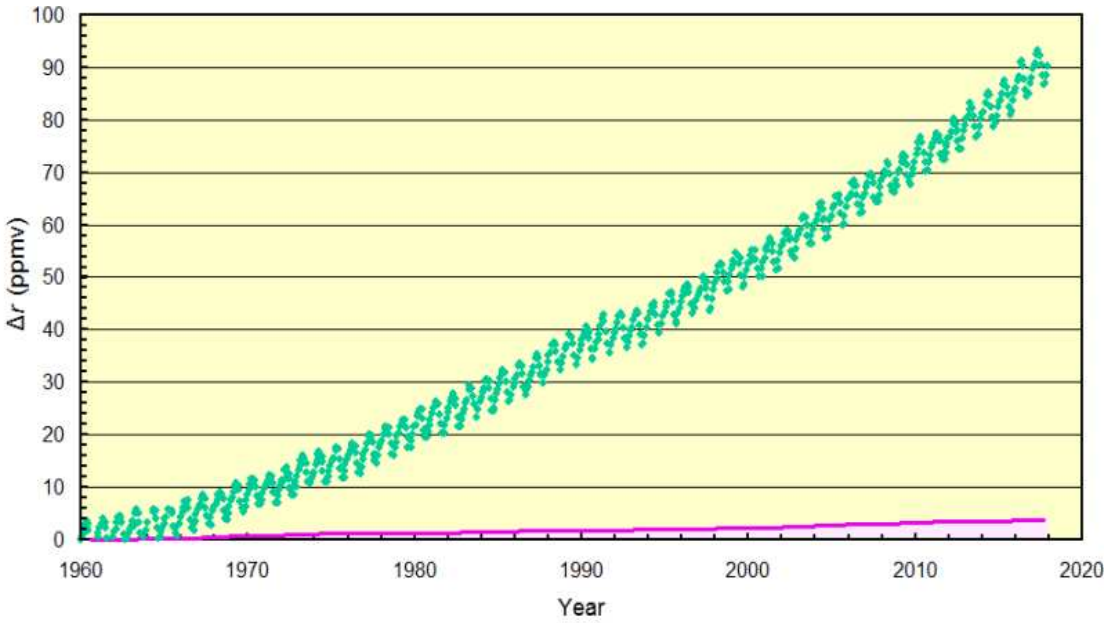

Figure 14: Increase of atmospheric CO_2 observed at Mauna Loa (Green). Superimposed is the instantaneous equilibrium level of anthropogenic CO_2 (Magenta), along with the possible range of the actual anthropogenic perturbation of CO_2 (Shaded).

The difference between the two curves in Fig. 14 represents the component of increased CO_2 that does *not* follow from anthropogenic emission. Dominating the observed increase of CO_2, it can only follow from changes of natural emission. That component has no relationship to nor can it be controlled by anthropogenic emission.

Funding

This research did not receive any specific grant from funding agencies in the public, commercial, or otherwise.

Guest-Editor: Prof. Jan-Erik Solheim; Reviewers were anonymous.

Acknowledgements

We are grateful for attention and comments provided during review and for editorial oversight by Prof. Jan-Erik Solheim and Geir Hasnes. Discussions with Zhenya Titova benefited this research before its scurrilous disruption. MS recognizes the special contribution to climate science made by Australia's Macquarie University: https://tinyurl.com/ClimateChangeCancelCulture.

References

Berry, E., 2019: *Human CO_2 emissions have little effect on atmospheric CO_2*, Intern. J. Atmospheric and Oceanic Sciences, v. 3(1), pp. 13-26, http://www.ijaos.org/article/298/10.11648.j.ijaos.20190301.13.

CDIAC, 2017: Carbon Dioxide Information Analysis Center, ESS-DIVE Archive, https://cdiac.ess-dive.lbl.gov/

Fang, C., J. Montcrief, 2005: *The variation of soil microbial respiration with depth in relation to soil carbon composition*, Plant and Soil, v. 268, pp. 243-253 doi:10.1007/s11104-004-0278-4

Harde, H., 2017: *Scrutinizing the carbon cycle and CO_2 residence time in the atmosphere*, Global & Planetary Change, v. 152, pp. 19-26, http://dx.doi.org/10.1016/j.gloplacha.2017.02.009.

Harde, H, 2019: *What humans contribute to atmospheric CO_2: Comparison of carbon cycle models and observations*. Earth Sciences, v. 8, pp. 139-158, doi: 10.11648/j.earth.20190803.13.

Harde, H. and M. Salby, 2021: *What controls the atmospheric CO_2 level?* Science Climate Change, v.1, no.1, pp. 54 - 69, https://doi.org/10.53234/scc202111/28

Holton, J., 2004: An Introduction to Dynamic Meteorology, 4th ed. Academic Press, San Diego, 535 pp.

IPCC, 2013: *Climate Change 2013*: Fifth Assessment Report of the Intergovernmental Panel on Climate Change, The Physical Science Basis. Cambridge University Press, Cambridge UK.

Levin, I., T. Naegler, B. Kromer, M. Diehl, R. Francey, A. Gomez-Pelaez, P. Steele, D. Wagenbach, R. Weller and D. Worthy, 2010: *Observations and modelling of the global distribution and long-term trend of atmospheric $^{14}CO_2$*. Tellus, v. 62B, pp. 26-46.

Maier M., V. Gartiser, A. Schengel and V. Lang, 2020: *Long term soil gas monitoring as tool to understand soil processes,* Appl. Sci., v. 10, pp. 8653-8683, doi:a10.3390/app10238653.

Salby, M., 2012: *Physics of the Atmosphere and Climate*, 2nd ed. Cambridge University Press, New York, 622 pp.

Salby, M. and H. Harde, 2021: *Control of atmospheric CO_2, Part II: Influence of Tropical Warming,* Science Climate Change, Vol. 1, No. 2, pp. N2 1 - 29, https://doi.org/10.53234/scc202112/211.

Segalstad, T. V., 1998: *Carbon cycle modelling and the residence time of natural and anthropogenic atmospheric CO2: On the construction of the "Greenhouse Effect Global Warming" dogma*, In: Bate, R. (Ed.): Global warming: the continuing debate. ESEF, Cambridge, U.K. (ISBN 0952773422), pp. 184-219.

Segalstad, T. V., 2017: CO_2 - *Friend or enemy*? In Nature Governs Climate (In Norwegian), Solheim, J.-E. (Ed), Klimarealistene, pp. 54-57.

Stenstrom, K., G. Skog, E. Georgiadou, J. Genberg and A. Johansson, 2011: *A Guide to Radiocarbon Units and Calculations*. Lund University, Internal Report LUNFD6(NFFR-3111)/1-17(2011).

Correspondence to
harde@hsu-hh.de

Vol. 1.2 (2021)
pp. 197-213

Control of Atmospheric CO_2 Part II: Influence of Tropical Warming

Murry Salby[1], Hermann Harde[2]

[1]Ex Macquarie University, Sydney, Australia

[2]Helmut-Schmidt-University, Hamburg, Germany

Abstract

Unlike much of the Earth, surface temperature in the tropics underwent a systematic and sustained increase during the satellite era. Due to the temperature dependence of surface processes which regulate CO_2 emission, that long-term change should exert a similar influence on atmospheric CO_2. We develop how this influence would manifest in the evolution of CO_2. Observed records are then used to investigate the interdependence of surface temperature and *net* CO_2 emission - the component of emission that actually changes CO_2.

Thermally-induced emission, especially from tropical land surface, is found to represent much of the observed evolution of net CO_2 emission. It accounts for sporadic intensifications of net emission that operate on interannual time scales, notably, during episodes of El Niño. Accounted for equally well is the long-term intensification of net emission during the last half century. Jointly, these unsteady components of net emission determine the thermally-induced component of anomalous CO_2. It closely tracks the observed evolution of CO_2.

Keywords: Carbon cycle; carbon 14 decay; CO_2 absorption time; tropical temperature change.

Submitted 2021-09-10, Accepted 2021-10-24. https://doi.org/10.53234/scc202112/12

1. Introduction

In Part I of this two-pronged study (Salby and Harde 2021; hereafter SH1), the record of anomalous carbon 14 revealed the effective absorption rate of atmospheric CO_2, which is emitted and absorbed at the Earth's surface. Coupled with the conservation law governing CO_2, the observed absorption provided an upper bound on the anthropogenic perturbation of CO_2. Only a couple of percent of the observed increase, it is much too small for anthropogenic emission to be responsible for the observed increase of atmospheric CO_2. The same conclusion follows from recent simulations of atmospheric carbon (Harde 2017 and 2019; Berry 2019; Harde and Salby 2021).

Here, we explore an important natural influence that likewise figures in the control of atmospheric CO_2. Surface processes which regulate emission and absorption of CO_2 depend intrinsically upon temperature. Many, like soil respiration, increase exponentially with temperature, typical of Arrhenius temperature dependence that operates in chemical reactions underpinning surface processes (e.g., Lloyd and Taylor 1994). In Section 2, we investigate the observed variation of temperature in major regions of the globe. How this influence would manifest in the observed record of CO_2 is developed in Section 3. Sections 4 and 5 then use observed records to explore the interdependence of surface temperature and *net* emission of CO_2, the component of emission that changes CO_2 and thus determines anomalous CO_2. From observed records of tropical surface temperature, we evaluate thermally-induced emission of CO_2. It is then compared against the observed evolution of CO_2.

2. Changes of Temperature

Global temperature today is ~ 0.7 K warmer than it was half a century earlier. The most (arguably the only) reliable record of global temperature is the operational satellite record from the Microwave Sounding Unit (MSU) suite of instruments. Plotted in Fig. 1 (Blue) is the record processed at the University of Alabama at Huntsville (Spencer et al. 2017). MSU is relatively free of manipulation and inter-calibration error that limit the surface network, which is inherently heterogeneous (dense over continents but sparse-nonexistent over ocean) and contaminated by urbanization surrounding measurement sites. By contrast, MSU retrieves temperature with homogeneous and near-global sampling of the Earth. And, because MSU measures microwave radiance, its temperature retrievals are unobstructed by cloud.

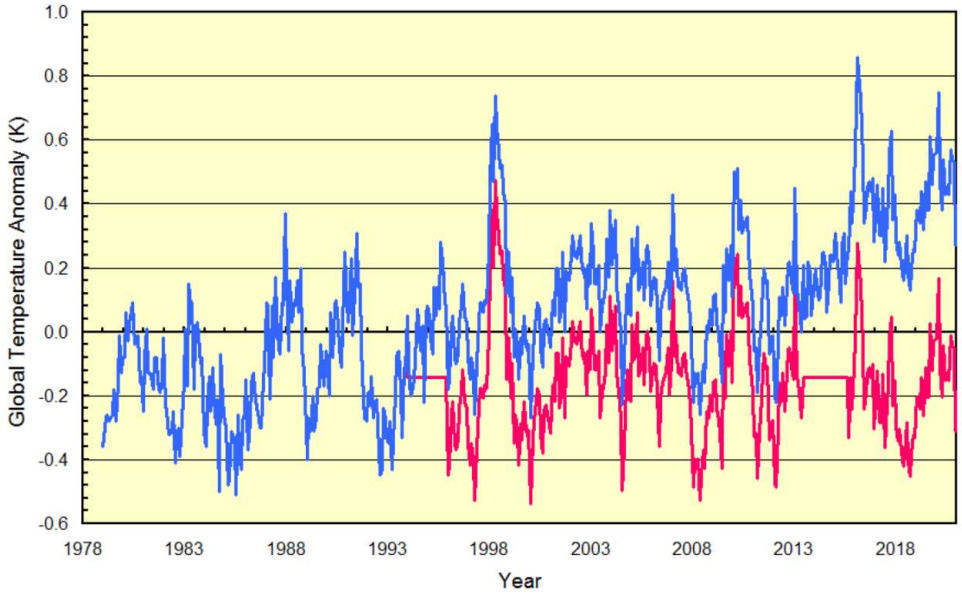

Figure 1: Anomalous global-mean temperature from the MSU suite of satellite instruments, retrieved by the University of Alabama at Huntsville (Blue). Omitting anomalous heating during two years preceding the El Niño of 1997 (1993.9 - 1995.9) and two years preceding the El Niño of 2016 (2013.4 - 2015.7), which represent only 10% of the record, results in the slightly-perturbed record that is superimposed (Red).

Although warmer today than at the start of the MSU record in 1979, global temperature has undergone virtually no systematic change. Notice that, before 1993, temperature fluctuated about a nearly constant mean. Much the same is apparent between 1996 and 2013. In fact, most of the increased temperature between the beginning and end of the record was introduced by just two brief intervals of sustained heating: one preceding the El Niño of 1997 (1993.9 - 1995.9) and another preceding the El Niño of 2016 (2013.4 - 2015.7). Those 4 years represent a mere 10% of the MSU record. Yet, omitting heating then, superimposed in Fig. 1 (Red), completely eliminates the temperature increase between the beginning and end of the global temperature record. The cumulative or *net* heating over the satellite era (which involves heating fluctuations of opposite sign) therefore vanishes. In the record of surface measurements, which extends back before the satellite era, much the same holds for the preceding 70 years (Salby 2018).

In the presence of systematic (e.g., ubiquitous) heating, as would follow the continuous increase of CO_2, eliminating the temperature offset in this manner would be virtually impossible. It can be shown that omitting a minor interval of heating would then result in only a minor reduction of the net temperature increase - because heating during the remaining 90% of the satellite era would still increase temperature. Yet, in the observed record, omitting heating during only 10% of the satellite era completely eliminates the net increase of temperature. It is for this reason that a trend ascribed to the warmer global temperature at the end of the record (which measures systematic warming during the satellite era) is not even close to being statistically significant (ibid).

Although true of global temperature, the absence of systematic warming need not be the case locally. Over the Arctic, MSU temperature does exhibit a gradual drift - but not consistently (Fig. 2a). While CO_2 increased monotonically, MSU temperature over the Arctic reversed: from weak cooling before 1993 to marginally-significant warming afterwards. How long before the onset of MSU measurements the cooling drift existed is unclear. Equally unclear is whether or not the warming drift has greater physical significance - viz. if, after sufficient time, it too will reverse.

Clouding such issues are uncertainties inherent to microwave observations of the atmosphere. Microwave retrievals are challenged by features that are prevalent over the Arctic. Central is surface emissivity, which is unknown but essential in the retrieval of temperature from microwave radiance - the property actually measured. Its role is especially important in the lowermost channel of MSU, from which lower-tropospheric temperature is retrieved. Owing to its key role, surface emissivity must be either presumed or modelled. The microwave emissivity of snow and ice is large and highly variable (e.g., Wang et al. 2017). It differs according to weather conditions, between ice and snow, even between new snow and old snow (Maslanic 2007; Rostosky et al. 2020; Cui et al. 2020). Especially problematic is high-altitude surface, like Greenland. There, unknown surface emissivity, which must be modelled, makes a disproportionate contribution to retrieved temperature in the lower troposphere.

Such limitations are a major source of discrepancy with ground-based measurements (McNally 2007; Tomaso and Bormann 2012). Notable are discrepancies associated with the melting and freezing of surface ice (Swanson 2003). A variety of approaches is being explored to address these limitations. To varying degree, all fill the observational void with surface properties that are modelled. Among them is estimating surface emissivity dynamically from weather forecasts (Tomaso et al. 2015).

Some insight into the physical significance of temperature drift over the Arctic comes from MSU temperature at midlatitudes. On long time scales, midlatitudes are largely free of snow and ice and, therefore, of the magnified uncertainty surrounding surface emissivity. Plotted in Fig. 2b is temperature at midlatitudes of the Northern Hemisphere. It exhibits little systematic drift. Following a step associated with the 1997 El Niño (cf. Fig. 1), temperature declined for about a decade before increasing after 2010. During the preceding decade, midlatitude temperature decreased. Much the same is apparent at midlatitudes of the Southern Hemisphere (Fig. 2c). There, warming after 2010 is largely offset by cooling during the preceding decade. Consequently, the slightly warmer temperature at the end of the record relative to that at the beginning derives chiefly from the brief interval of sustained heating before the El Niño of 1997 (cf. Fig. 1). Over the Antarctic (Fig. 2d), even the decadal swings of warming and cooling are absent. Devoid of ocean, the Antarctic exhibits no sustained change, not even on decadal time scales.

Figure 2 reveals that, over much of the Earth, surface temperature underwent no systematic change during the four decades that it was observed by MSU. Exceptional is surface temperature in the tropics. Plotted in Fig. 3, anomalous tropical temperature (Blue) systematically increased during the four decades observed by MSU. The sustained increase is mirrored in the independent record of anomalous sea surface temperature (SSTA) from the Hadley Centre (Kennedy et al. 2019), which is superimposed (Aqua). SSTA is offset to slightly-warmer temperature because MSU represents temperature a couple of km above and therefore cooler than the surface.

Nonetheless, the temperature of ocean (which comprises ~75% of the tropics) closely tracks MSU temperature - on short as well as long time scales. The two independent records make it clear that the tropics underwent systematic and sustained warming during the last half century, at least back to the onset of MSU measurements.[1] Owing to the dependence on temperature of

[1] Notice: The temperature increase over the tropics as a whole (viz. in MSU) is greater than only over ocean (in SSTA). Systematic warming of tropical land must therefore exceed that of tropical ocean.

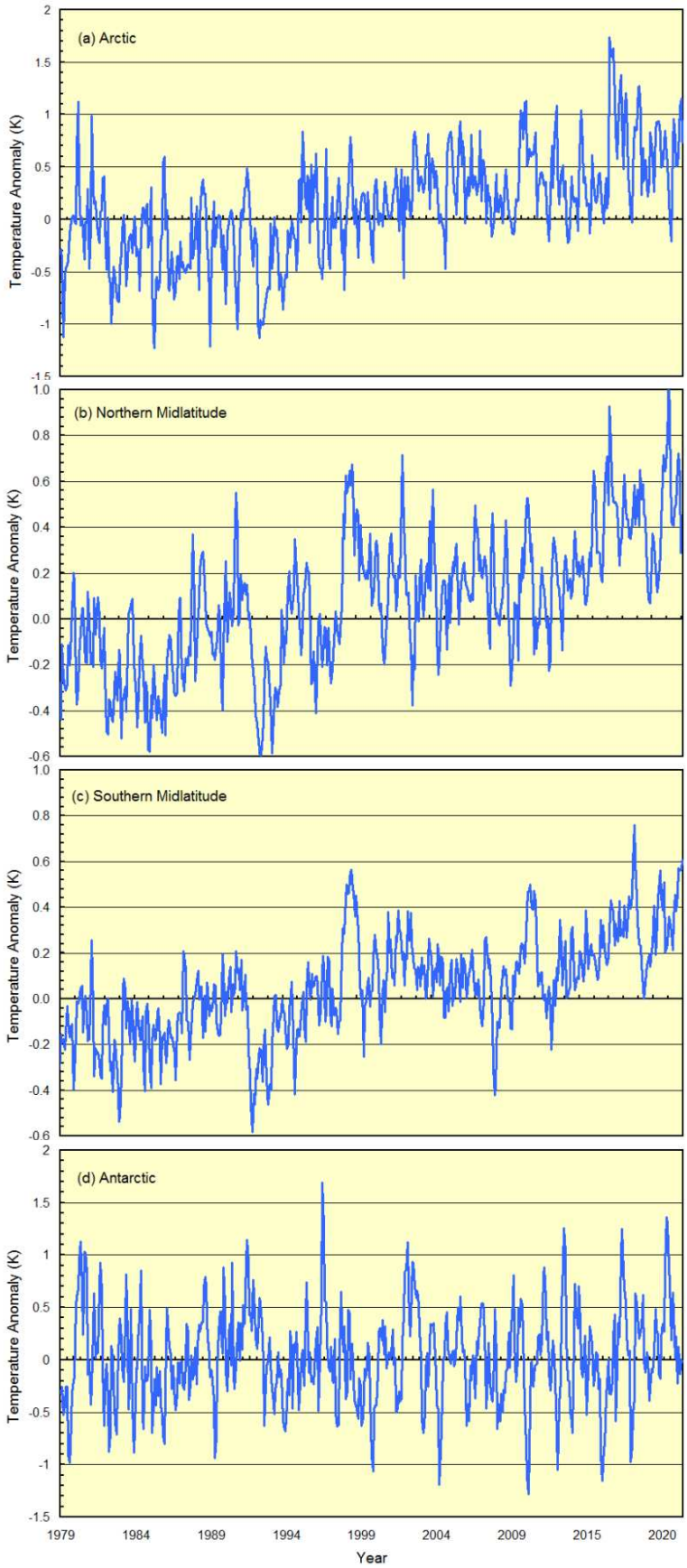

Figure 2: Anomalous temperature over (a) the Arctic (60N - 85N), (b) midlatitudes of the Northern Hemisphere (20N - 60N), (c) midlatitudes of the Southern Hemisphere (20S - 60S), and (d) the Antarctic (60S - 85S).

physical and chemical processes that regulate CO_2 emission, CO_2 must have experienced a parallel influence.

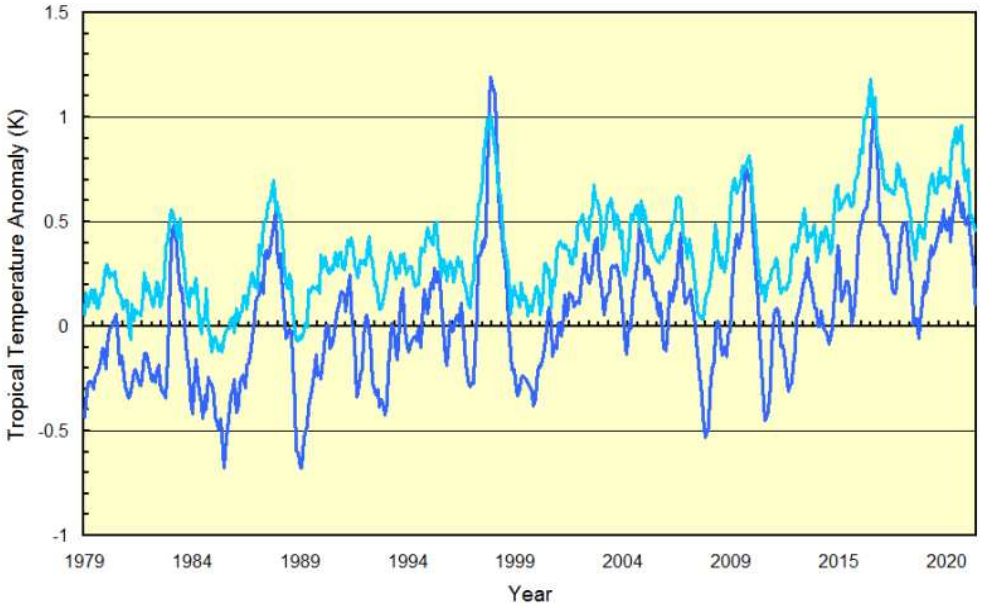

Figure 3: Anomalous temperature over the tropics (20S – 20N) observed by MSU, after being low-pass filtered by a 6-month running mean (Blue). Superimposed is the counterpart record of Sea Surface Temperature (Aqua).

3. Net Emission of CO_2

The longest continuous record of atmospheric CO_2 is that of measurements at Mauna Loa, Hawaii (CDIAC 2017). Removed from continents and positioned in the middle troposphere, Mauna Loa CO_2 is the only surface record that is largely free of local distortion by neighboring sources and sinks. For this reason, it approximates the global abundance of CO_2, which, on time scales longer than a month, is well mixed over the free troposphere. This feature is verified in recent satellite observations of CO_2, which track Mauna Loa CO_2 (SCIAMACHY 2006).

The change of global CO_2 is determined by emission and absorption, but only indirectly. Because CO_2 changes through their imbalance, it is the small residual of those opposing influences that forces changes of CO_2. Transient adjustment of the isotopic tracer $^{14}CO_2$, which was perturbed by nuclear testing, establishes that absorption of atmospheric CO_2 is directly proportional to the instantaneous abundance of atmospheric CO_2 (Harde and Salby 2021). An empirical fact, this fundamental feature is confirmed in independent simulations of CO_2 (ibid; SH1). The global abundance of atmospheric CO_2 is therefore governed by the conservation law:

$$\begin{aligned} \frac{dr}{dt} &= E - \alpha_{\text{eff}}\, r, \\ &= E_{\text{net}} \end{aligned} \qquad (1)$$

where r is the global-mean mixing ratio of CO_2 (which, hereafter, is used synonymously with "CO_2"), E is its global-mean emission rate (the rate at which CO_2 is introduced into the atmosphere), and α_{eff} is its global-mean rate of effective absorption (the rate at which CO_2 is removed from the atmosphere). The conservation law is used here to identify the components of emission responsible for observed changes of CO_2 (defining "anomalous CO_2"), as well as the respective time lag. In (1), E_{net} represents net emission: the imbalance between global emission and absorption. It measures the disequilibrium between the atmosphere and the Earth's surface, as developed in SH1. Equal to the instantaneous rate of change of r, E_{net} is the resultant of all con-

tributions. It is what actually determines if and how CO_2 changes.

Net emission is a minor residual between total emission and absorption, which mostly cancel one another. From the observed rate of CO_2 increase, E_{net} is of order 1-2 ppmv/yr (see, for example, Fig. 9). Emission and absorption, individually, are much greater. Approximately in balance, they are reflected in the magnitude of absorption. With effective absorption of $\alpha_{eff} = 0.1 - 1.0$ yrs^{-1} in (1) (see SH1; an historical overview of estimates can be found in Segalstadt 1996 and, more recently, in Harde and Salby 2021) and with $r \sim 400$ ppmv, emission and absorption are one to two orders of magnitude greater than E_{net}. Therefore, global-mean atmospheric CO_2 remains in a state of quasi equilibrium, wherein its emission in (1) is largely cancelled by its absorption. Through the slight imbalance between emission and absorption, CO_2 mixing ratio gradually drifts upward. Embodied in E_{net}, the disequilibrium responsible for the long-term drift of CO_2 is only a few percent of overall emission of CO_2.

Actual emission (E) is difficult to quantify because it is dominated by natural emission which, on a global basis, is not observed. E_{net}, on the other hand - what actually forces changes of CO_2 - *is* observed. In fact, E_{net} is observed as well as CO_2 itself. Through (1), net emission follows directly from the observed record as the instantaneous rate of change of CO_2.

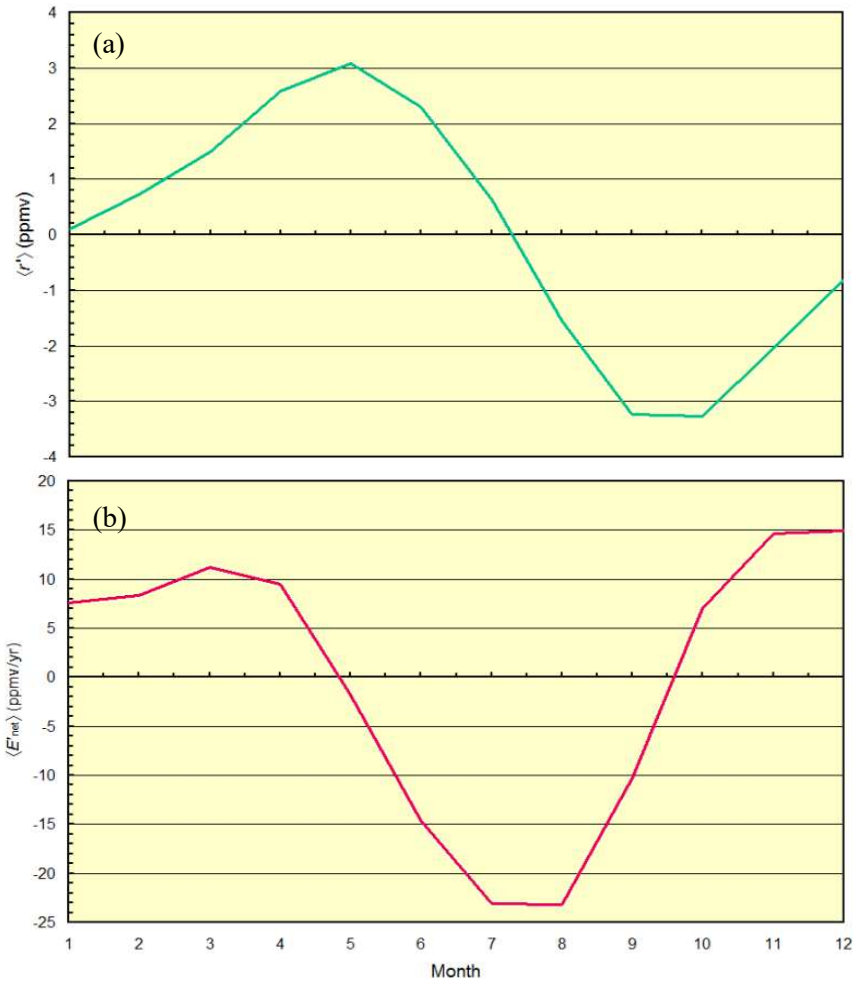

Figure 4: Zero-mean annual cycle of (a) anomalous CO_2 *mixing ratio and (b) net* CO_2 *emission.*

Changes of CO_2 that operate on time scales longer than annual are isolated by removing the zero-mean component of the mean annual cycle. Plotted in Fig. 4a, the zero mean annual cycle follows by averaging r during individual months. From October, $\langle r' \rangle$ increases by ~6 ppmv, before reversing direction in May and then decreasing by ~6 ppmv. In Fig. 4b is the net emis-

sion responsible for this annual variation of CO_2 (1). Instantaneously, $\langle E'_{net} \rangle$reaches 10 - 20 ppmv/yr. It is positive during Austral spring and summer (October - April), when $\langle r' \rangle$ increases each year. It is negative during Austral winter (May - September), when $\langle r' \rangle$ decreases each year. The net change of CO_2 introduced, however, vanishes - because net emission associated with this component of the annual cycle has zero mean. Consequently, removing the zero-mean annual cycle from the record of r has no impact on secular (long-term) changes of CO_2.

What remains, including random changes of the annual cycle, operates on interannual and longer time scales. Plotted in Fig. 5a is E_{net}, low-pass filtered to periods longer than a year (Red).[2] Net emission undergoes large interannual excursions - as large as 100% of the local mean. Conspicuous among them are strong intensifications of E_{net} during the El Niños of 1973, 1997, and 2016, when the tropical surface warmed abruptly.

Accompanying interannual excursions is a gradual intensification of net emission. From the onset of Mauna Loa measurements, E_{net} intensified: from less than 1.0 ppmv/yr to more than 2.0 ppmv/yr. This systematic intensification of E_{net} is responsible for the deviation from linearity in the evolution of CO_2 (see, for example, Fig. 9). The intensification extends back through the satellite era, beginning after the 1973 El Niño. Before 1973, E_{net} exhibits little systematic change, back to the onset of Mauna Loa measurements in 1959. Comparison with Fig. 3 reveals many of the same features in the record of tropical temperature during the overlapping period of MSU measurements.

4. Interdependence with Tropical Temperature

Net CO_2 emission in Fig. 5a and tropical temperature in Fig. 3 are, in fact, strongly coherent. Although present throughout the tropics, the strongest coherence is found over land. There, anomalous MSU temperature, T_{L}, and E_{net} have a correlation of 0.77. Resting on dozens of independent degrees of freedom (reflected in the number of random fluctuations in the two records), their correlation is significant at the 99.99% level. Hence, the strong correspondence between E_{net} and tropical temperature that is evident in Figs 3 and 5a is not by chance. Nor is it limited to interannual variability. Also evident in both records is a gradual but systematic increase.

The component of net CO_2 emission that operates coherently with tropical land temperature is evaluated by projecting the record of E_{net} onto the record of T_{L} from MSU. Representing thermally-induced emission, it is superimposed in Fig. 5a (Blue). $E_{\text{net}}(T_{\text{L}})$ closely tracks observed net emission, E_{net}. With a correlation of 0.80, their interdependence is highly significant. A cursory manifestation of the strong interdependence in Fig. 5a was identified earlier, in relation to global-mean temperature (Salby 2012).

Strong coupling of anomalous CO_2 to tropical temperature was previously noted by Humlum et al. (2013). They observed further that anomalous CO_2 appeared originally in the tropics but then advanced poleward into each hemisphere. Likewise noteworthy are recent satellite observations from GOSAT and OCO-2. They have revealed that tropical landmasses are a net emitter of CO_2 (Palmer et al. 2019). The magnified covariance between E_{net} and T_{L} evident in Fig. 5a, reflects a modulation of CO_2 emission by changes of tropical land temperature. Tropical land temperature, in turn, is largely imposed by surrounding ocean. In this manner, E_{net} would be perturbed most by tropical land surface, but operate coherently with temperature throughout the tropics.

Net emission of CO_2 is seen to vary nearly in phase with temperature over tropical land. The simultaneity of those changes is evident for interannual fluctuations of net emission, as well as for its long-term intensification. It is noteworthy that, although operat-

[2] Following the monthly record of r being subjected to two passes of Chapeau (1-2-1) convolution and the ensuing record of E_{net} being subjected to a 12-month Bartlett convolution (see, for example, Båth, 1974).

ing on disparate time scales, both components of thermally-induced emission derive from the same relationship to tropical surface temperature.

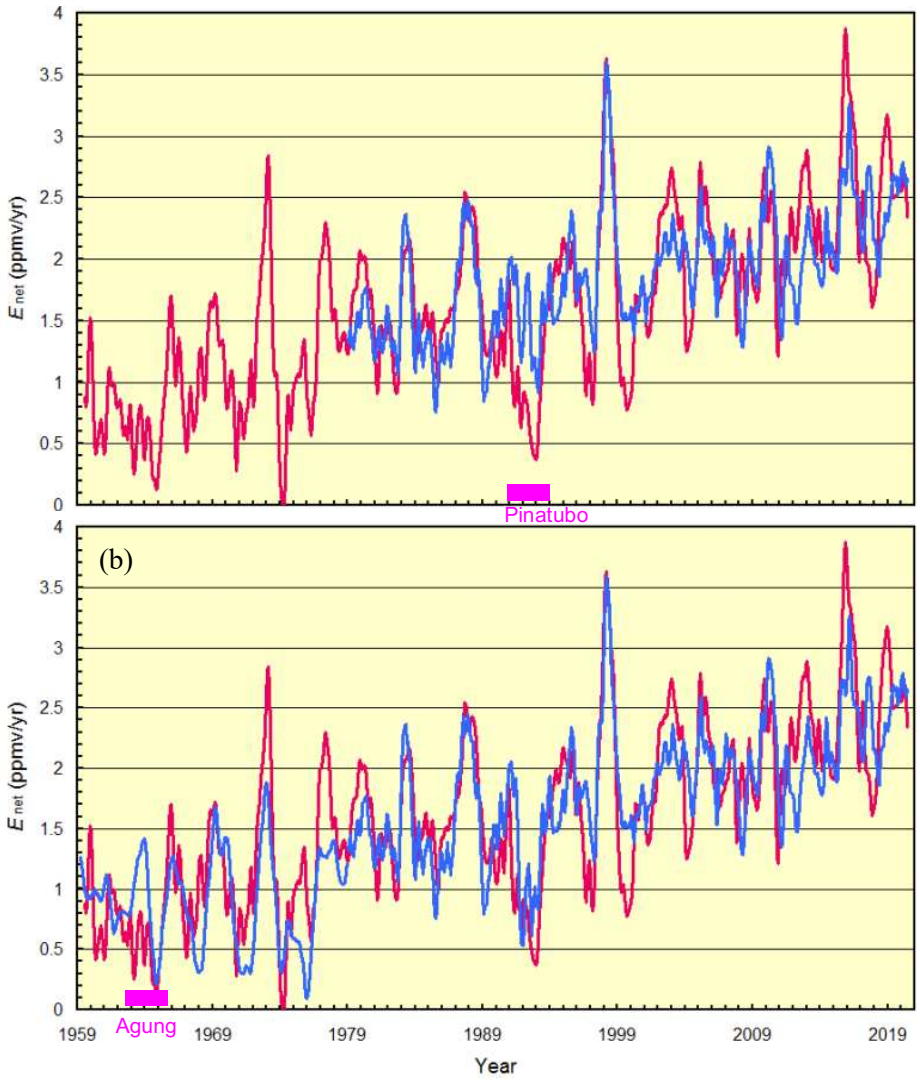

Figure 5: (a) Net emission of CO_2*, low-pass filtered to periods longer than 1 yr (Red). Superimposed is the component of net emission that operates coherently with temperature over tropical land observed by MSU (Blue). (b) As in (a), but with (i) the thermally-induced component of net emission also coherent with the perturbation of SW radiation that was introduced by the eruption of Mt. Pinatubo and (ii) extrapolated backward before the satellite era through the record of SSTA. Superimposed in (a) and (b) are the intervals perturbed by the volcanic aerosols of Mt. Pinatubo and Agung (Magenta).*

A brief interval when $E_{net}(T_L)$ and E_{net} deviated from one another occurred during 1991 - 1994. Observed CO_2 emission then fell short of that anticipated from thermally induced emission. This interval coincides with the major eruption of Mt. Pinatubo, which introduced volcanic aerosol into the stratosphere. Frozen in strong stability of the stratosphere, Pinatubo aerosol remained there for approximately 3 years. Plotted in Fig. 6 is anomalous shortwave (SW) radiation at the top of the tropical atmosphere, observed by the Earth Radiation Budget Experiment (ERBE). Increasing abruptly in 1991, it represents enhanced backscattering of SW radiation from the cloud of stratospheric aerosol introduced by Pinatubo. The enhanced backscattering corresponds to reduced SW radiation reaching the Earth's surface.

Beyond its impact on temperature, a perturbation of SW radiation influences vegetation and soil respiration directly (Keane and Ineson 2017). Projecting E_{net} onto the record of tropical land

temperature as well as the record of SW radiation obtains the perturbation of CO_2 emission by both environmental influences. In Fig. 5b is thermally-induced emission, inclusive of perturbed SW radiation. It tracks observed E_{net} even during the Pinatubo-perturbed years. The correlation with observed E_{net} is then increased to 0.82.

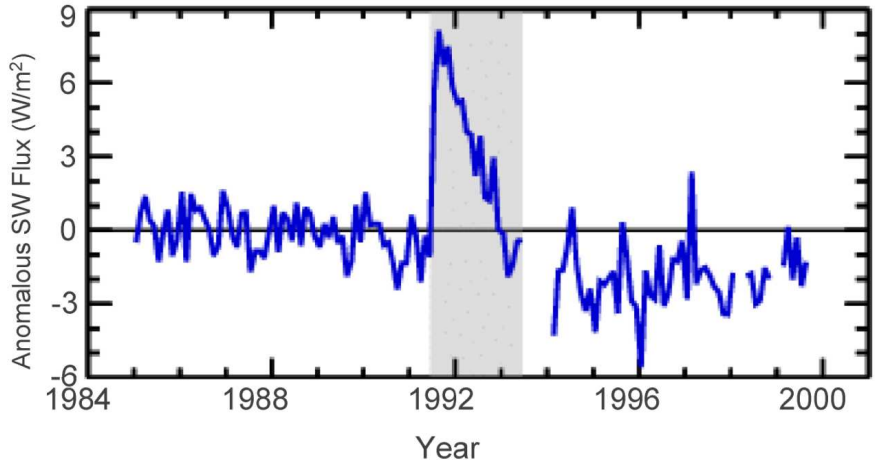

Figure 6: Anomalous outgoing SW flux observed by the Earth Radiation Budget Experiment. Adapted from Canty et al. (2013).

Before 1979, a record of temperature with complete coverage of the tropics does not exist. The record of SSTA, in principle, covers the tropical ocean, albeit with sparse sampling. However, it provides no direct information on temperature over tropical land, with which E_{net} operates most coherently during the satellite era. Nevertheless, temperature over tropical land is strongly controlled by temperature of surrounding ocean. During the MSU era, the two have a correlation of 0.94. We employ their strong interdependence to extend the thermally-induced component of net emission.

During the satellite era, when there is complete coverage of the tropics, the record of SSTA over ocean is first projected onto the record of MSU temperature over land. The ensuing projection represents the record of pseudo land temperature that is embodied in the SSTA record. It, in turn, extends back before the satellite era. Onto the extended record of tropical land temperature is then projected the observed record of CO_2 emission, E_{net}. Superimposed in Fig. 5b is the resulting net emission that operates dependently with tropical land temperature, extended back from the MSU record to the beginning of the Mauna Loa record. Despite the observational limitations, the SSTA extension of thermally-induced emission tracks observed emission of CO_2. In fact, the correlation between the concatenated record of $E_{net}(T_L)$ and the observed record, E_{net} , is 0.83 - as high as when the records are restricted to the satellite era. As noted earlier, the systematic intensification of E_{net} in the observed record develops only after the 1973 El Niño. Before then, net emission exhibits no systematic change. The same transformation is evident in thermally-induced emission, $E_{net}(T_L)$, which derives from tropical temperature.[3]

During the years 1963-1965, observed E_{net} fell short of that anticipated from $E_{net}(T_L)$, much like it did during the years perturbed by Pinatubo. The former years coincide with the eruption of Mt. Agung, the third-strongest eruption of the 20th century. It too invaded the stratosphere (Neimeier et al. 2019). Observations of perturbed SW radiation then, through which its impact on E_{net} could be represented, do not exist.

[3] Owing to the simultaneity of fluctuations in E_{net} and $E_{net}(T_L)$, induced changes of CO_2 lag changes of land temperature. From (1), anomalous r must lag anomalous T_L by a quarter cycle (Appendix A). The fluctuations in Fig. 5 have a mean period of 2.8 yrs. The lag required by the conservation law is thus ~ 8.5 months. It is close to the observed lag that emerges from the cross covariance between CO_2 and temperature (Humlum et al. 2013; Salby 2013).

The systematic intensification of E_{net} accelerates the growth of CO_2. It makes a major contribution to the net increase of CO_2 during the Mauna Loa era. Without it, CO_2 would have grown linearly at the rate observed in 1959: ~1 ppmv/yr; cf. Fig. 9. According to (1), cumulative net emission equals the net change of CO_2:

$$\int_{1959}^{t} E_{net}\, dt = \Delta CO_2 \,. \qquad (2)$$

It corresponds to the area under the curves in Fig 5b. Systematic intensification of E_{net} is seen to account for about half of the observed increase of CO_2 in the Mauna Loa record.

As is evident in Fig 5, thermally-induced emission accounts for the long-term intensification of net emission about as well as it accounts for interannual intensifications of E_{net}, like those introduced by El Niño. The two forms of variability involve widely-separated time scales. Nonetheless, their joint representation in $E_{net}(T_L)$ - through the same dependence on surface temperature - reflects a common physical mechanism, one that operates on both components of CO_2 emission.

5. Intensification of Emission: Seasonality

The long-term intensification of E_{net} in Fig. 5 is responsible for much of the net increase of CO_2 during the Mauna Loa era. It derives ultimately from changes in the raw monthly record of CO_2, wherein all variability is represented. Included is seasonality that remains after removal of the zero-mean annual cycle of CO_2 (Fig. 4).[4]

Plotted in Fig. 7 is the corresponding monthly record of E_{net} . Prevalent are quasi-annual fluctuations, with random amplitude and phase. Because they have non-vanishing mean, those fluctuations of net emission *do* introduce a net change of CO_2. The quasi-annual fluctuations have amplitudes initially of 2 - 4 ppmv/yr, much smaller than in the zero-mean annual cycle (Fig. 4b).

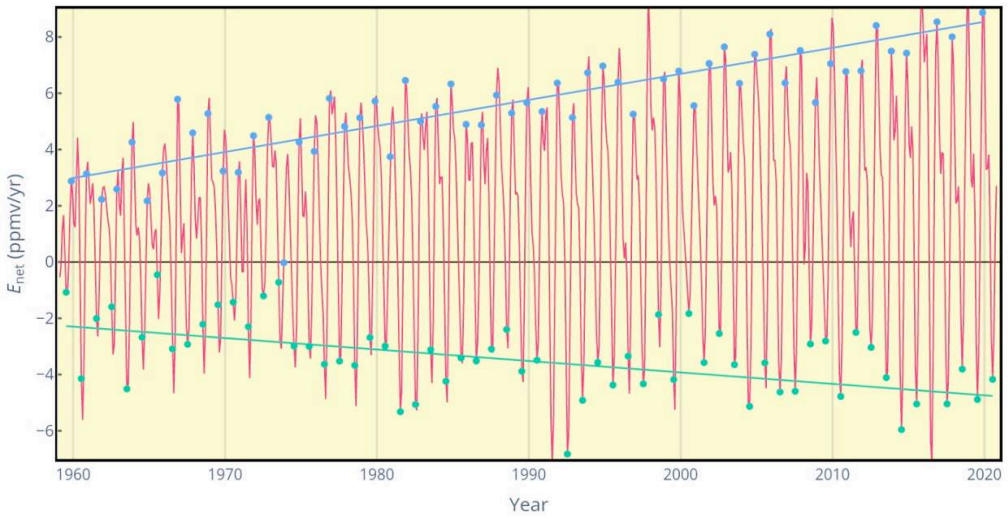

Figure 7: Monthly record of net CO_2 *emission, following removal of the zero-mean annual cycle. Superimposed is* E_{net} *during the months of July (Green) and the months of November (Blue).*

[4] In the frequency spectrum of CO_2, the annual variation of r is comprised of a Delta function (e.g., a spike of variance) concentrated at 1 cycle per year, flanked by a continuum of variance at neighboring frequencies. The continuum develops through nonlinear interaction with the monochromatic central frequency, from which variance leaks. As the zero-mean annual cycle is invariant from one year to the next, its elimination removes only the monochromatic spike. Remaining in the record of anomalous CO_2 are quasi-annual fluctuations that are aperiodic. They underpin the interannual and long-term changes of net emission in Fig. 5, which are seen to depend strongly upon tropical land temperature.

However, they systematically intensify, eventually attaining amplitudes that are twice as large as exist initially. Accompanying their amplification is an upward drift in baseline, equal to local-mean E_{net} .

The two secular changes of $E_{net}(t)$ are not independent. Were the quasi-annual swings in E_{net} symmetric (e.g., equal and opposite in conjugate months), they would result in no change of baseline. Superimposed in Fig. 7 is E_{net} during the months of July (Green). E_{net} during those months is uniformly negative. However, through changes of amplitude and phase, net emission during July fluctuates randomly. Nevertheless, the July values are clustered about minima of the quasi-annual swings. They gradually drift towards more-negative E_{net}, corresponding to a systematic weakening of net emission then. The drift represents a trend in July E_{net} of −0.04 ppmv/yr^2.

Also superimposed in Fig. 7 is E_{net} during the months of November (Blue). E_{net} then is uniformly positive. But, like E_{net} during July, it fluctuates randomly. Clustered about maxima of the quasi-annual swings, November values gradually drift towards more positive E_{net} , corresponding to an intensification of net emission then. The drift represents a trend in November E_{net} of approximately +0.09 ppmv/yr^2 - more than twice as fast as the negative trend during July. The imbalance of trend between conjugate months introduces the gradual drift in baseline. It corresponds to the long-term intensification of low-pass filtered E_{net} in Fig. 5.

Averaging values for individual months t_n yields the mean seasonality of net emission, $\langle E_{net}\rangle(t_n)$. Unlike the zero-mean component in Fig. 4b, this annual variation of net emission *does* introduce a net change of CO_2. Plotted in Fig. 8 (Solid), $\langle E_{net}\rangle(t_n)$ has an annual mean of ~ 1.6 ppmv/yr. However, it varies substantially with month. $\langle E_{net}\rangle(t_n)$ is positive during September - April, Austral spring and summer. It is negative during May - September, Austral winter. Those seasonal intervals are virtually identical to the intervals when E_{net} is positive and negative in the zero-mean annual cycle (Fig.4) - which introduces *no net change* of CO_2.

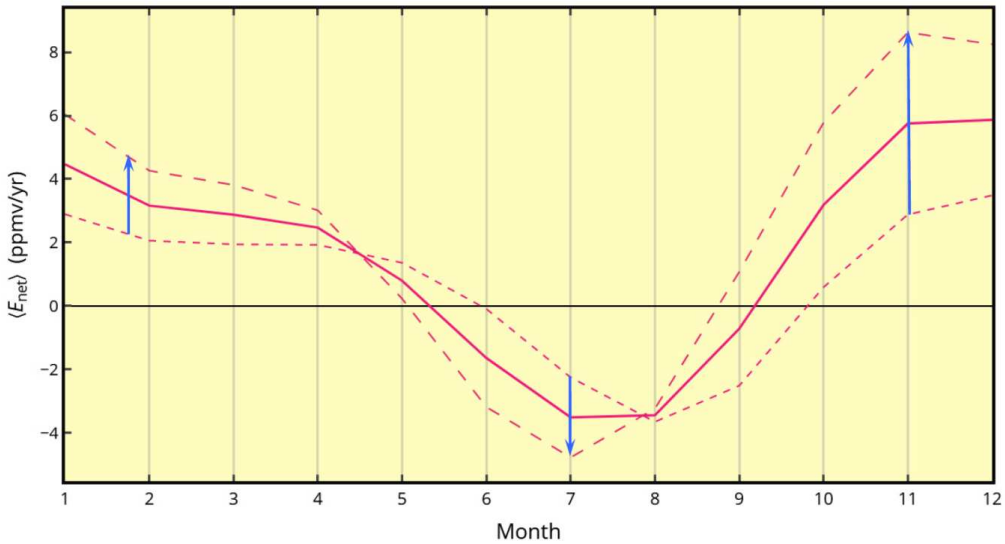

Figure 8: Mean annual variation of net emission, exclusive of zero-mean annual cycle, (Solid). Superimposed is the mean annual variation of E_{net} *at the beginning of the Mauna Loa record (Short Dashed) and at the end of the record (Dashed).*

Cumulative net emission in Fig. 8, integrated over a range of months, equals the respective increase of CO_2 (1). Notice that positive E_{net} during February - April (which increases CO_2 by 9.30 ppmv) is nearly cancelled by negative E_{net} during May - September (which decreases CO_2 by 9.33 ppmv). Therefore, cumulative net emission over the year follows chiefly from E_{net} during the remaining months: September - January, when E_{net} is large and positive. So too, therefore, must follow the annual increase of CO_2.

The annual mean of $\langle E_{net} \rangle$, ~1.6 ppmv/yr, is responsible for the average growth rate of CO_2, namely, the rate were CO_2 to have increased linearly during the Mauna Loa era. The gradual intensification of net emission (Fig. 5) causes CO_2 growth to accelerate. That intensification derives from the trend in the quasi-annual fluctuations of E_{net} , represented in Fig. 7. The trend in individual months modifies the seasonality of E_{net} between the beginning and end of the Mauna Loa record. Superimposed in Fig. 8 is the seasonality of E_{net} during 1959 (Short Dashed) and during 2020 (Long Dashed). Between the beginning and end of the record, the quasi-annual fluctuations of net emission undergo a systematic amplification: Large positive net emission becomes more positive. Large negative net emission becomes more negative. The increase of positive E_{net} (upward arrows), however, exceeds the decrease of negative E_{net} (downward arrows). The imbalance introduces an upward drift in the annual-mean of $\langle E_{net} \rangle$, which increases from 0.7 ppmv/yr during 1959 to 2.5 ppmv/yr during 2020.

The change of seasonality in Fig. 8 (arrows) mirrors the average seasonality of $\langle E_{net} \rangle$ (Solid). The latter, in turn, has the same form as E_{net} in the zero-mean annual cycle (Fig. 4b). As in the mean seasonality (Solid), acceleration of E_{net} between 1959 and 2020 during January - April (intensification of net emission) is largely cancelled by deceleration of E_{net} during May - August (weakening of net emission). Consequently, the long-term intensification of E_{net} in Fig. 5, which accelerates CO_2 growth, derives principally from an intensification of net emission during September - January, when instantaneous E_{net} is large and positive.

6. Conclusions

Net emission of CO_2, which is the resultant of all contributions, is concentrated at tropical latitudes - not at midlatitudes, where anthropogenic emission is concentrated. Represented in the interdependence of E_{net} and T_L is the sensitivity to temperature of net CO_2 emission. Largely invariant with time scale, the sensitivity is much the same for the long-term increase of temperature as it is for interannual fluctuations of temperature. Owing to this fundamental sensitivity, the observed intensification of E_{net} is an inevitable consequence of systematic warming in the tropics (Fig. 3).

In relation to CO_2, what is responsible for that warming is immaterial. Its influence on CO_2 should not be confused through circular reasoning. The observed warming, which forces increased CO_2 through intensified net emission, cannot itself be the result of increased CO_2. Were it, anomalous CO_2 and net emission that forces it would have increased twice as much as was observed: (i) the increase of CO_2 that hypothetically produced the observed warming plus (ii) the thermally-induced response to that warming, which has no dependence on what caused the warming yet induces an intensification of CO_2 net emission close to what is observed.

The direction of causation is also clear from the interdependence of net emission and temperature - for interannual fluctuations as well as for the long-term increase in those properties. In addition to having strong coherence with temperature, the two unsteady components of net emission have the same phase relationship to temperature: Both vary *in phase* with temperature (cf. Fig. 5b). The strong coherence and in-phase relationship to temperature reveal that, irrespective of time scale, changes of tropical temperature induce simultaneous changes of CO_2 net emission.

Under the opposite direction of causation, were the observed changes of tropical temperature induced by changes of CO_2, they would result in a fundamentally-different phase relationship. The time scale of thermal damping, which drives temperature towards thermal equilibrium, is only a couple of weeks (e.g., Salby 2012). It is much shorter than both unsteady time scales in Fig. 5b. Through anomalous radiative forcing, the comparatively gradual changes of CO_2 would therefore induce simultaneous changes of temperature, in phase with CO_2. However, net emission, which changes CO_2 through (1), must lead CO_2 by a quarter cycle (Appendix A). Net emission would thus also lead temperature by a quarter cycle. Under these circumstances, net

emission would lead and operate *in quadrature* with temperature - behavior contradicted by their in-phase relationship observed (Fig. 5b).

The observed contradiction invalidates the latter possibility. Through elimination, it unambiguously establishes the forcing of observed changes and the consequent response: Net emission of CO_2, which determines anomalous CO_2 (1), is forced by changes of tropical temperature - not vice versa.

The growth of atmospheric CO_2 follows from positive net emission (1). A small residual between emission and absorption, net emission is inherently seasonal. The seasonality of E_{net} is noteworthy. The component of E_{net} which introduces a net annual change of CO_2, (viz. the deviation from the zero-mean annual cycle in Fig. 8) has seasonality of the same form as seasonality in the zero-mean annual cycle (Fig. 4b), which introduces no net annual change of CO_2. The close correspondence of those unsteady components of net emission reflects a common physical mechanism. The processes responsible for the periodic annual swing of net emission should therefore also be responsible for its sporadic intensification, as occurs during episodes of El Niño. Much the same applies to the long-term intensification of net emission during the last half century.

The nexus between these unsteady components of net emission is underscored by the raw monthly record of E_{net} . Even after removal of the zero-mean annual cycle, monthly net emission fluctuates quasi annually (Fig. 7). Coupled to long-term changes, those fluctuations reflect a gradual amplification and distortion of the annual cycle of net emission. This modulation of the annual cycle underpins thermally-induced changes of emission, changes that represent interannual fluctuations of net emission as well as its long-term intensification (Fig. 5b).

Net emission determines the evolution of atmospheric CO_2 (1). Plotted in Fig. 9 is the observed evolution of CO_2 (Green). Also plotted is the evolution that CO_2 would have undergone had E_{net} remained constant after the 1973 El Niño (Dashed). About half of the observed increase follows from the systematic intensification of net emission; cf. Fig. 5b. Superimposed in Fig. 9 is the evolution of CO_2 that is introduced by thermally-induced emission in Fig. 5b (Blue). To within observational limitations, the observed evolution of CO_2 and the thermally-induced component of CO_2 are indistinguishable.

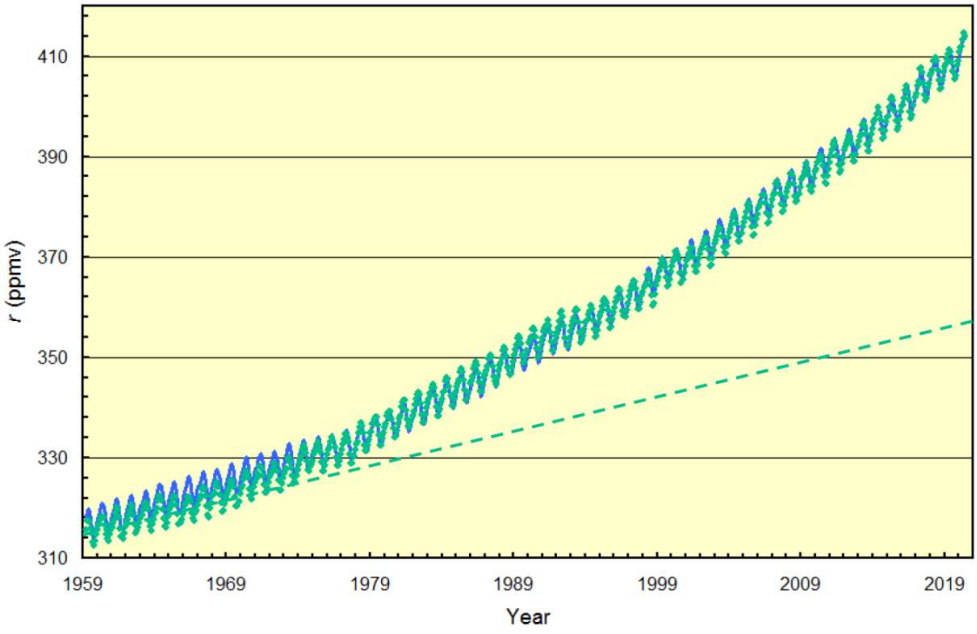

Figure 9: Evolution of CO_2 mixing ratio observed at Mauna Loa (Green), along with the evolution that would have occurred had net emission remained constant (Dashed). Superimposed is the evolution introduced by thermally induced-emission in Fig. 5 (Blue).

The veracity with which the thermally-induced component tracks the observed evolution of CO_2 has two important implications: (i) Through (2) and thermally-induced emission, tropical land temperature should be a robust predictor of atmospheric CO_2. By contrast, other contributions to net emission which operate incoherently with T_L afford virtually no predictive skill. Such is the case for anthropogenic emission, upon which climate projections of the IPCC rest. (ii) The anthropogenic perturbation of CO_2 must be small - so small, in fact, as to lie within the noise of the calculation. That, in turn, requires the removal time of anthropogenic CO_2 (which has not been specified in this calculation) to be quite short; cf. SH1 Figs 11, 13. It can be shown that, for the thermally-induced component of CO_2 to track the observed evolution so closely, the removal time of anthropogenic CO_2 must be of order only a year (Appendix B). Anthropogenic CO_2 is then removed from the atmosphere almost as fast as it is introduced, sharply limiting its accumulation in the atmosphere.

Funding

This research was performed without funding, from government or commercial source.

Guest-Editor: Prof. Jan-Erik Solheim; Reviewers were anonymous.

Acknowledgements

We are grateful for attention and comments provided during review and for editorial oversight by Prof. Jan-Erik Solheim and Geir Hasnes.

Appendix A

Phase Relationship between Anomalous CO_2 and Net Emission of CO_2

Net emission of CO_2 and anomalous CO_2 are related through the conservation law (1). Fourier transforming each side yields the conservation law for individual spectral components:

$$-i\omega\mathcal{R}(\omega) = \mathcal{E}_{\text{net}}(\omega), \tag{A1.1}$$

where

$$r(t) = \frac{1}{2\pi}\int_{-\infty}^{\infty}\mathcal{R}(\omega)e^{-i\omega t}d\omega, \tag{A1.2}$$

$$E_{\text{net}}(t) = \frac{1}{2\pi}\int_{-\infty}^{\infty}\mathcal{E}_{\text{net}}(\omega)e^{-i\omega t}d\omega \tag{A1.3}$$

and $\mathcal{R}(\omega)$ and $\mathcal{E}_{\text{net}}(\omega)$ are the spectral components of r and E_{net} at frequency ω.

Rearranging (A1.1) obtains

$$\begin{aligned}\mathcal{R} &= i\frac{\mathcal{E}_{\text{net}}}{\omega} \\ &= \frac{\mathcal{E}_{\text{net}}}{\omega}e^{i\varphi}\end{aligned}, \tag{A2.1}$$

where

$$\phi = \frac{\pi}{2} \tag{A2.2}$$

is the phase lag of $\mathscr{R}$ with respect to $\mathscr{E}_{\text{net}}$. Anomalous CO_2 is seen to vary *in quadrature* with net emission, lagging by a quarter cycle. Because it applies irrespective of time scale (ω), this consequence of the conservation law holds equally for interannual fluctuations and the long-term increase of net emission. As observed net emission varies in phase with anomalous temperature, on all relevant time scales (Fig. 5b), anomalous CO_2 must also lag anomalous temperature by a quarter cycle - as is, in fact, observed (Humlum et al. 2013; Salby 2013).

Appendix B

Effective Absorption Time of Anthropogenic CO_2

The thermally-induced component of CO_2 closely tracks the observed evolution of CO_2 (Fig. 9). For this to occur, the discrepancy from observed CO_2 introduced by the anthropogenic component of CO_2 and all other non-thermal contributions cannot exceed the observed discrepancy. In the average over time,

$$\begin{aligned} \left\langle \Delta r^2 \right\rangle &\cong \left\langle r_{\text{A}}^2 \right\rangle + \left\langle \Delta r_{\text{other}}^2 \right\rangle \\ &\geq \left\langle r_{\text{A}}^2 \right\rangle \end{aligned}, \tag{B1.1}$$

where angle brackets denotes time mean, Δr is the instantaneous discrepancy between the thermally-induced component of CO_2 and observed CO_2, r_{A} is the anthropogenic perturbation of CO_2, and Δr_{other} represents all other non-thermal contributions to anomalous CO_2 (which vary incoherently with systematically-increasing r_{A}). The root mean square discrepancy must therefore satisfy

$$r_{\text{A}}^{\text{rms}} \leq \Delta r^{\text{rms}}. \tag{B1.2}$$

As developed in Section 3 for all components of CO_2, the anthropogenic component remains close to its instantaneous equilibrium level (SH1),

$$r_{\text{A}}^{\text{Eq}}(t) = \frac{E_{\text{A}}(t)}{\alpha_{\text{eff}}^{\text{A}}}, \tag{B2}$$

where $\alpha_{\text{eff}}^{\text{A}}$ is the effective absorption rate of anthropogenic CO_2 and E_{A} is anthropogenic emission. The equilibrium level and, hence, anthropogenic CO_2 itself are seen to gradually drift with changes of anthropogenic emission. Together with (B2), (B1.2) requires

$$\alpha_{\text{eff}}^{\text{A}} \geq \frac{E_{\text{A}}^{\text{rms}}}{\Delta r^{\text{rms}}}. \tag{B3}$$

During the satellite era, when there was complete coverage of the tropics, the observed discrepancy from the thermally-induced component (Fig. 9) was $\Delta r^{\text{rms}} \cong 1.8$ ppmv. The rms discrepancy is comparable to the average equilibrium level of anthropogenic CO_2, 2.4 ppmv, which was evaluated independently from mean anthropogenic emission during its 20th century increase (SH1). For the same period, $E_{\text{A}}^{\text{rms}} \cong 2.2$ ppmv/yr (4.6 GtC/yr) is representative of anthropogenic emission. The effective absorption rate of anthropogenic CO_2 (B3) must therefore exceed

$$\alpha_{\text{eff}}^{\text{A}} \geq 1.2 \text{ yrs}^{-1}. \tag{B4}$$

Corresponding to a removal time shorter than a year, this empirical evaluation of $\alpha_{\text{eff}}^{\text{A}}$ is comparable to (in fact, slightly faster than) the effective absorption rate calculated independently through observed transience of carbon 14 (ibid).

References

Båth, M., 1974: *Spectral Analysis in Geophysics*. Elsevier, Amsterdam, 563 pp.

Berry, E., 2019: *Human CO_2 emissions have little effect on atmospheric CO_2*, Intern. J. Atmospheric and Oceanic Sciences, 3(1), pp. 13-26, http://www.ijaos.org/article/298/10.11648.j.ijaos.20190301.13.

Canty, T., N. Mascioli, M. Smarte and R. Salawitch, 2013: *An empirical model of global climate - Pat 1: A critical evaluation of volcanic cooling*, Atmos Chem Phys, 13, 3997-4031.

CDIAC, 2017: Carbon Dioxide Information Analysis Center, ESS-DIVE Archive, https://cdiac.ess-dive.lbl.gov/.

Cui, Z., Z. Zhao, Y. Zhai, Z. Sun, W. Cheng and C. Gu, 2020: *Use of double channel differences for reducing the surface emissivity dependence of microwave atmospheric temperature and humidity retrievals,* Earth an Space Science, 7, https://doi.org/10.1029/2019EA000854.

Harde, H., 2017: *Scrutinizing the carbon cycle and CO2 residence time in the atmosphere*, Global & Planetary Change, 152, pp. 19-26, http://dx.doi.org/10.1016/j.gloplacha.2017.02.009.

Harde, H, 2019: *What humans contribute to atmospheric CO_2: Comparison of carbon cycle models and observations*. Earth Sciences, 8, pp. 139-158, doi: 10.11648/j.earth.20190803.13.

Harde, H. and M. Salby, 2021: *What controls the atmospheric CO_2 level?* Science Climate Change, Vol.1, No.1, pp. 54 - 69, https://doi.org/10.53234/scc202111/28

Humlum, O., K. Stordahl and J.-E. Solheim, 2013: *The phase relation between atmospheric carbon dioxide and global temperature,* Global Planetary Change, 100, 51-69.

Keane, J. and P. Ineson, 2017: *Differences in the diurnal pattern of soil respiration reveal potential flaws in accepted sampling strategies,* Biogeosci, 14, 1181-1187.

Kennedy, J., N. Rayner, C. Atkinson and R. Killick, 2019: *An ensemble data set of sea surface temperature change from 1850: The Met Office Hadley Centre HadSST.4.0.0.0 Data Set*, JGR Atmospheres, 124, 7719-7763.

Lloyd, J. and J. Taylor, 1994: *On the temperature dependence of soil respiration*, Functional Ecology, 8 315-323.

Maslanik, J., 2007: *Effects of weather on the retrieval of sea ice concentration and ice type from passive microwave data,* Int. J. Remote Sensing, 13, 37-54.

McNally, T., 2007: *The use of satellite data in polar regions*. ECMWF Research Paper. https://www.ecmwf.int/sites/default/files/elibrary/2007/11088-use-satellite-data-polar-regions.pdf

Neimeier, U., C. Timmereck and K, Kruger, 2019: *Revisiting the Agung 1963 volcanic forcing - impact of one or two eruptions,* Atmos. Chem. Phys., 19, 10379-10390.

Palmer, P., L. Eng, D. Baker, F. Chevallier, H. Bosch and P. Somkuti, 2019: *Net carbon emissions from African biosphere dominate pan-tropical atmospheric CO_2 signal*, Nature Comm., https://doi.org/10.1038/s41467-019-11097-w

Rostosky, P., G. Spreen, S. Gerland, M. Huntemann and M. Mech, 2020: *Modeling the microwave emission of snow on Arctic sea ice for estimating the uncertainty of satellite retrievals,* JGR Oceans, doi.org/10.1029/2019JCO15465

Salby, M., 2012: *Physics of the Atmosphere and Climate*. Cambridge University Press, 252-254, 666 pp.

Salby, M., 2013: *Relationship between greenhouse gases and global temperature*, Video of lecture at Helmut-Schmidt-University, Hamburg, https://youtu.be/HeCqcKYj9Oc.

Salby, M., 2018: *What is really behind the increase of atmospheric CO_2?* Video of lecture at Helmut-Schmidt-University, Hamburg, https://youtu.be/rohF6K2avtY.

Salby, M. and H. Harde, 2021: *Control of atmospheric CO_2 - Part I: Relation of carbon 14 to the removal of CO_2*, Science Climate Change vol. 1, no. 2, pp. N1 1-36, https://doi.org/10.53234/scc202112/210

SCIAMACHY, 2006: European Space Agency, SCIAMACHY Carbon Dioxide, https://www.iup.uni-bremen.de/sciamachy/NIR_NADIR_WFM_DOAS/co2_nh_english.png

Segalstad, T., 1996: *Distribution of CO_2 between atmosphere, hydrosphere, and lithosphere*, in The Global Warming Debate, Report of the European Science and Environment Forum. Bourne Press, Dorset UK, 41-50.

Spencer, R., Christy, J., and D. Braswell, 2017: *UAH version 6 global satellite temperature products: Methodology and results*, Asia-Pacific J. Atm. Sci., 53, 121-130.

Swanson, R., 2003: *Evidence of possible sea-ice influence on microwave sounding unit tropospheric temperature trends in polar regions*, Geophys. Res. Lett., 30, doi:10.1029/2003GL017938.

Tomaso, E. and N. Bormann, 2012: *The assimilation of surface-sensitive microwave sounder radiances at ECMWF*, CIMSS Research Paper, https://cimss.ssec.wisc.edu/itwg/itsc/itsc18/program/files/links/4.38_DiTomaso_pa.pdf

Tomaso, E., N. Bormann and S. English, 2015: *Extending the use of microwave sounding data over sea-ice in the ECMWF system*, European Meteorological Satellite Research Paper, https://www.eumetsat.int/media/16218.

Wang, D., C. Prigent, L. Kilic, S. Fox, C. Harlow, C. Jimenez, F. Aires, C. Grasiotti and F. Karbou, 2017: *Surface emissivity at microwaves to millimeter waves over polar regions: Parameterization and evaluation with aircraft experiments*, J. Atm. Ocean Tech., 34, 1039-1059.

The Impact of Human CO_2 on Atmospheric CO_2

Edwin X Berry

Ed Berry, LLC, Bigfork, Montana 59911, USA

Correspondence to ed@aedberry.com

Vol. 1.2 (2021)

pp. 214-250

Abstract

A basic assumption of climate change made by the *United Nations Intergovernmental Panel on Climate Change* (IPCC) is natural CO_2 stayed constant after 1750 and human CO_2 dominated the CO_2 increase. IPCC's basic assumption requires human CO_2 to stay in the atmosphere longer than natural CO_2. But human CO_2 and natural CO_2 molecules are identical. So, human CO_2 and natural CO_2 must flow out of the atmosphere at the same rate, or e-time. The $^{14}CO_2$ e-time, derived from $\delta^{14}C$ data, is 10.0 years, making the $^{12}CO_2$ e-time less than 10 years. The IPCC says the $^{12}CO_2$ e-time is about 4 years and IPCC's carbon cycle uses 3.5 years. A new physics carbon cycle model replicates IPCC's natural carbon cycle. Then, using IPCC's natural carbon cycle data, it calculates human carbon has added only 33 [24-48] ppmv to the atmosphere as of 2020, which means natural carbon has added 100 ppmv. The physics model calculates if human CO_2 emissions had stopped at the end of 2020, the human CO_2 level of 33 ppmv would fall to 10 ppmv in 2100. After the bomb tests, $\delta^{14}C$ returned to its original balance level of zero even as $^{12}CO_2$ increased, which suggests a natural source dominates the $^{12}CO_2$ increase.

Keywords: carbon cycle; carbon cycle model; carbon dioxide; climate change; CO_2 increase; human carbon.

Submitted 26-09-2021. Accepted 11-11-2021. https://doi.org/10.53234/scc202112/13

1.Introduction

1.1 Definitions

The *Intergovernmental Panel on Climate Change* (IPCC) defines two carbon cycle domains, the *slow* carbon cycle and the *fast* carbon cycle. IPCC (2013, p. 470) explains,

> "The first is a fast domain with large exchange fluxes and relatively 'rapid' reservoir turnovers, which consists of carbon in the atmosphere, the ocean, surface ocean sediments and on land in vegetation, soils and freshwaters."
>
> "A second, slow domain consists of the huge carbon stores in rocks and sediments which exchange carbon with the fast domain through volcanic emissions of CO2, chemical weathering, erosion and sediment formation on the sea floor."

This paper uses the following definitions:

- "Natural carbon" is carbon from natural actions.
- "Human carbon" is from burning carbon fuels and producing cement.
- "Land carbon" is from human-caused land-use changes.

Human carbon moves carbon from the slow carbon cycle to the fast carbon cycle. Land carbon moves carbon from the land to the atmosphere, all within the fast carbon cycle.

This paper assumes human carbon transferred to the fast carbon cycle stays in the fast carbon cycle forever. This paper focuses on how long human carbon stays in the atmosphere in the fast carbon cycle.

The level or concentration of atmospheric CO_2 is in units of ppmv (parts per million by volume in dry air). However, it is customary to omit the "v" and write ppm. To convert CO_2 in ppmv into the mass of carbon in PgC (petagrams), multiply the ppmv by 2.12. GtC (Gigatons of car-

bon) is numerically equivalent to PgC.

1.2 The IPCC basic assumption

The IPCC, its supporting papers and climate models, assume that human CO_2 causes all or most CO_2 increase above 280 ppmv. This assumption is the basis of worldwide climate laws and treaties.

The IPCC (2013, p. 467, Executive Summary) says,

> "With a very high level of confidence, the increase in CO_2 emissions from fossil fuel burning and those arising from land use change are the dominant cause of the observed increase in atmospheric CO_2 concentration."

The IPCC (2013, pp. 470-471) assumes the natural CO_2 level remained at 280 ppm after 1750 and, therefore, human CO_2 caused all the CO_2 increase since 1750. This paper uses IPCC's own data to argue this IPCC assumption is incorrect.

Fig. # 1 (IPCC, 2013, p. 471, Fig. # 6.1) shows IPCC's natural carbon cycle (in black) and IPCC's human carbon cycle (in red). The title bar shows 589 PgC (278 ppmv) of *natural* carbon and 240 PgC (113 ppmv) of *human* carbon is in the atmosphere as of about 2005. So, according to the IPCC, human CO_2 has caused 29% (= 240/829) of the CO_2 in the atmosphere.

Fig. # 1 also shows annual *human* carbon emissions in 2005 are 8.8 PgC per year (7.8 PgC per year of human carbon and 1.1 PgC per year of land carbon) while *natural* carbon emissions are 168 PgC per year (107.2 PgC per year from land and 60.7 PgC from surface ocean).

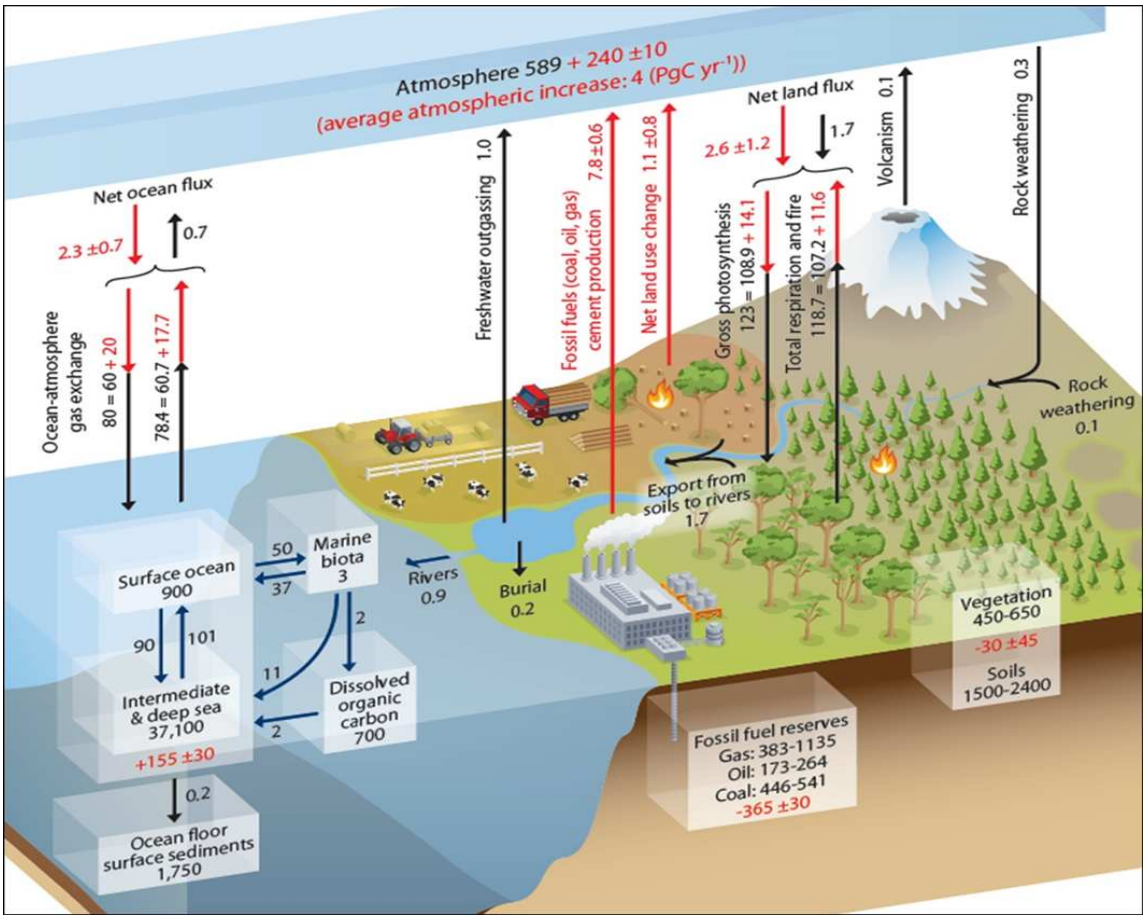

Figure 1. IPCC Figure 6.1 for 2010 shows IPCC's data for its natural and human carbon cycles.

Therefore, the IPCC assumes annual *human* emissions, which are only 5% of the total CO_2 inflow, have become 29% of the CO_2 in the atmosphere in 2010. Data for 2020 show 33%. How can 5% of the annual inflow become 29% or 33% of the total CO_2 in the atmosphere?

To achieve this result, the IPCC assumes *human* CO_2 stays in the atmosphere longer than *natural* CO_2. But this cannot be true because human and natural CO_2 molecules are identical. Therefore, they stay in the atmosphere for equal times. This is the *climate equivalence principle*.

IPCC's turnover time, which this paper calls "e-time," measures how long CO_2 stays in the atmosphere.

IPCC (2007, p. 948) defines turnover time to make outflow proportional to the first power of the level,

> "Turnover time (T) is the ratio of the mass M of a reservoir (e.g., a gaseous compound in the atmosphere) and the total rate of removal S from the reservoir: T = M / S. For each removal process, separate turnover times can be defined."

IPCC (2007, p. 948) says the turnover time (T) for natural CO_2 is about four years.

> *"Carbon dioxide* (CO_2) is an extreme example. Its turnover time is only about four years because of the rapid exchange between the atmosphere and the ocean and terrestrial biota."

However, IPCC (2013, p. 469) assumes human CO_2 turnover time is much larger than four years,

> "The removal of human-emitted CO_2 from the atmosphere by natural processes will take a few hundred thousand years (high confidence). Depending on the RCP scenario considered, about 15 to 40% of emitted CO_2 will remain in the atmosphere longer than 1,000 years. This long time required by sinks to remove anthropogenic CO_2 makes climate change caused by elevated CO_2 irreversible on human time scale. {Box 6.1}"

IPCC's Box 6.1, mentioned above, merely assumes the natural CO_2 level has remained at 280 ppmv while human CO_2 caused all the CO_2 increase. There are no data to prove this is the case.

This IPCC assumption requires *human* CO_2 to have a much longer turnover time (and therefore stay in the atmosphere much longer) than natural CO_2.

Turnover time is critical. If it is less than 10 years, then natural CO_2 caused most CO_2 increase. If it is greater than 100 years, then human CO_2 caused most CO_2 increase. The reason (more fully explained in Section 4) is CO_2 outflow from the atmosphere is fast when the turnover time is small and vice-versa. So, for a given inflow of human CO_2, more will remain in the atmosphere if the turnover time is large.

Revelle and Suess (1957) used ^{14}C data to calculate the turnover time "of a CO_2 molecule in the atmosphere … is of the order of 10 years," and correctly concluded,

> "This means most of the CO_2 released by artificial fuel combustion since the beginning of the industrial revolution must have been absorbed by the oceans."

Starr (1992) found several papers that assume human CO_2 caused all the CO_2 increase. By removing this assumption, Starr found the data show turnover time is 4 to 5 years. He correctly wrote,

> "The short residence time suggests that anthropogenic emissions contribute only a fraction of the observed atmospheric rise, and that other sources need be sought."

Segalstad (1998) lists 36 independent studies from 1957 to 1992 that used 6 different methods to estimate turnover time that show it is less than 10 years and dominantly between 5 and 10 years.

Rorsch et al. (2005) show if human and natural carbon have the same e-times, as physics re-

quires, then IPCC's assumption is wrong.

Essenhigh (2009) calculated the $^{12}CO_2$ e-time is about 4 years.

Ballantyne et al. (2012) found "there is no empirical evidence" that the ability of the land and oceans to absorb atmospheric CO_2 "has started to diminish on the global scale." This means human CO_2 has not changed the turnover time.

Munshi (2015a) shows the "detrended correlation of annual emissions with annual changes in atmospheric CO_2" is zero, which proves anthropogenic emissions are not the primary cause of the increase in CO_2 concentration. A non-zero correlation does not prove a cause-effect relationship is true, but a zero correlation proves there is no observable cause-effect. Correlations of time-series data must be detrended to remove overall trends before calculating cause-effect correlations.

Harde (2017, 2019) concluded the $^{12}CO_2$ e-time is about 4 years. Harde (2019) and Berry (2019) use one-reservoir models (that do not allow human carbon to flow of from land and oceans back into the atmosphere) to conclude that human emissions have added about 17 ppmv to 18 ppmv to the atmosphere.

Kohler et al. (2017) criticized Harde (2017), claiming human (but not natural) CO_2 reduced the "buffer capacity" of the carbonate system, conflicting with Ballantyne et al. (2012),

> "… the rise in atmospheric and oceanic carbon content goes along with an increase in the Revelle factor, a phenomenon which is already measurable. This implies that the oceanic uptake of anthropogenic carbon will become slower if we continue to increase anthropogenic CO_2 emissions. This is already seen in all CHIMP5 model simulations."

However, Kohler et al. arguments use the IPCC assumption – that human CO_2 dominated the CO_2 increase – to conclude human (but not natural) CO2 reduced ocean "uptake," caused the Revelle factor (that Ballantine et al. conclude is not measurable), and use CHIMP5 models that make the same assumption, to conclude (in circular fashion) the IPCC assumption is true so they can claim Harde (2019 is wrong.

Gruber et al. (2019) assume human carbon dominates the CO_2 increase to analyze their data to conclude the IPCC assumption is true.

1.3. The IPCC ice-core assumption

IPCC (2013, pp. 467-468) uses reconstructed ice core data to support its assumption that human CO_2 has caused all the CO_2 increase above 280 ppmv,

> "During the last 7000 years prior to 1750, atmospheric CO_2 from ice cores shows only very slow changes (increase) from 260 ppmv to 280 ppmv, in contrast to the human-caused increase of CO_2 since pre-industrial times."

IPCC's last phrase – "*in contrast to the human-caused increase of* CO_2 *since pre-industrial times*" – is IPCC's assumption that IPCC uses to conclude its assumption is true, which is circular reasoning.

The IPCC uses the *absence* of ice-core data – that show the natural CO_2 level was greater than 280 ppmv before 1750 – to assume natural CO_2 remained at 280 ppmv after 1750. Here are some problems for this IPCC ice-core assumption.

First, IPCC's antecedent is questionable.

- Segalstad (1998) shows why ice core reconstructions of CO_2 levels are not reliable.
- Kouwenberg (2004) and Kouwenberg et al. (2005 a, b) used conifer stomata data to reconstruct CO_2 levels that increased to 350 ppmv several times in the last 1200 years.
- Beck (2007) published thousands of direct chemical measurements of CO_2 that show much higher CO_2 levels than those reconstructed from ice cores.

- Jaworowski (2007) shows ice cores underestimate CO_2 levels.
- Salby (2012, pp. 21, 66) shows ice-core reconstructions of CO_2 levels do not accurately measure historical CO_2 levels.

Second, these papers negate IPCC's consequent:

- Segalstad (1998) shows the turnover time is 3.5 years to 5 years.
- IPCC (2007, p. 948) says the CO_2 turnover time is "about 4 years."
- IPCC (2013, pp. 470-471) Fig. # 1 shows the CO_2 e-time is 3.5 years.
- Harde and Salby (2021) show the $^{14}CO_2$ e-time is 10.0 years, which proves $^{12}CO_2$ e-time is much smaller, which proves human CO_2 did not cause all the CO_2 increase.
- The return of $\delta^{14}C$ to its original level of zero after the bomb tests, even as $^{14}CO_2$ and $^{12}CO_2$ increased, proves the added $^{12}CO_2$ came from a natural source that existed before the bomb tests (Section 6.1).

1.4 Isotope data show CO_2 increase is natural

IPCC (2007, p. 512) says,

> "The increase in atmospheric CO_2 concentration is known to be caused by human activities because the character of CO_2 in the atmosphere, in particular the ratio of its heavy to light carbon atoms, has changed in a way that can be attributed to addition of fossil fuel carbon."

This IPCC argument has no numbers. But isotope data contradict IPCC's assumption that human CO_2 caused all the increase and show the human effect is small (Segalstad, 1998; Quirk, 2009; Harde, 2017, 2019; Berry, 2019; Harde and Salby, 2021).

2. Method

2.1 The data

This paper uses these data,

- IPCC's natural carbon cycle data (IPCC, 2013, pp. 470-486)
- $\delta^{14}C$ data (Turnbull et al., 2017)
- ^{14}C data (Turnbull et al., 2017)
- ^{12}C data before 1960 (Etheridge et al., 1996; Jaworowski, 2007)
- ^{12}C data after 1960 (Keeling et al., 2001)
- Human carbon emissions data (Gilfillan et al., 2020)

2.2 The basics

According to the scientific method, data cannot prove an assumption is true, but only one contradiction to data proves an assumption is false.

IPCC (2013, p. 467, Executive Summary) says human CO_2 is the "dominant" cause of the increase. IPCC (2013, pp. 470-486) says human CO_2 caused all the increase. This paper shows both versions of IPCC's assumption conflict with IPCC's data.

The IPCC did not derive its human carbon cycle from IPCC's natural carbon cycle data, as it should have, but merely assumed that human CO_2 caused all the CO_2 increase above 280 ppmv. But scientific assumptions should be compatible with all available data.

This paper shows IPCC's assumed human carbon cycle contradicts IPCC's natural carbon cycle data. Therefore, IPCC's assumed human carbon cycle cannot be true.

2.3 The physics carbon cycle model

The physics carbon cycle model, derived in this paper, has only one hypothesis, namely, outflow is proportional to level. The IPCC (2013, p. 470, turnover time) uses this same hypothesis, so the physics carbon cycle model agrees with IPCC's natural carbon cycle (Section 3.1).

IPCC's natural carbon cycle (Fig. # 1) has four main carbon reservoirs, e.g., land, atmosphere, surface ocean, and deep ocean, in that order. The land connects only with the atmosphere and the deep ocean connects only with the surface ocean. The atmosphere and surface ocean have two connections.

IPCC's natural carbon cycle shows data for each of the four levels and the six flows between the four reservoirs at equilibrium.

The physics carbon cycle model uses IPCC's levels and flows to calculate the turnover times (now e-times) for the six outflow nodes. With these six e-times, the physics carbon cycle model calculates how the carbon levels change when the carbon cycle is not at equilibrium.

The physics model is a systems model where levels calculate flows, and flows calculate new levels.

For verification, the physics carbon cycle model replicates IPCC's natural carbon cycle. Then the physics model calculates the human carbon cycle using IPCC's natural carbon cycle e-times.

The atmospheric CO_2 e-time for IPCC's natural carbon cycle is 3.5 years (Equation 23), which approximates IPCC's (2007, p. 948) estimated turnover time of about 4 years.

This physics model is an extensible, documented, open-source model that other researchers can use to make carbon cycle calculations.

2.4 Data contradict IPCC's basic assumption

The IPCC assumes natural CO_2 stayed constant at 280 ppmv after 1750 while human CO_2 caused all the CO_2 increase above 280 ppmv. This assumption contradicts data.

First, $^{14}CO_2$ data show its e-time is 10 years, making the $^{12}CO_2$ e-time less than 10 years (Section 6.1). This contradicts IPCC's assumption.

Second, the return of $\delta^{14}C$ data to its original balance level of zero even as $^{12}CO_2$ increased, suggests the added $^{12}CO_2$ has a natural source independent of human emissions (Section 6.1).

Third, IPCC's assumption requires human CO_2 to have a much larger e-time than natural CO_2 to dominate the CO_2 increase. But human and natural e-times are the same because human and natural CO_2 molecules are identical. Different e-times would require a "carbon demon" in the atmosphere to separate human from natural CO_2 and then restrain the human CO_2 from flowing out of the atmosphere as fast as natural CO_2.

Fourth, the physics carbon cycle model uses IPCC data to show human carbon has added only 33 [24-48] ppmv to the atmosphere as of 2020, which means natural carbon has added 100 ppmv.

The physics model calculates if human CO_2 emissions had stopped at the end of 2020, the human CO_2 level would fall from 33 ppmv in 2020 to 16 ppmv in 2040, to 10 ppmv in 2100, and to 5 ppmv by 2180.

Fig. # 1 (IPCC, 2013, p. 471, Fig. # 6.1) shows the total natural carbon in the fast carbon cycle is 41,089 PgC and the added human carbon is 365 PgC as of about 2010. So, human carbon has added only 0.89% to the carbon in the carbon cycle as of 2010. This change of less than one percent diffuses arguments that human CO2 changed the e-times.

The physics carbon cycle model calculates IPCC's land use effect adds little carbon to the atmosphere because this carbon moves quickly from the atmosphere, through the surface ocean, and on to the deep ocean, without adding new carbon to the carbon cycle.

The physics model calculates, deductively, the consequences of IPCC's natural carbon cycle data. Therefore, these calculations are independent of outside data.

2.5 The Bern model

The Bern model (Siegenthaler and Joos, 1992; Strassmann and Joos, 2018) uses IPCC's assumption that human CO_2 dominates the CO_2 increase.

The Bern model uses Green's functions to calculate the evolution of one pulse in the atmosphere. Section 5.4 compares the Bern model with the physics model for a single carbon pulse in the atmosphere. The Bern model uses long e-times that leave 15% of carbon in the atmosphere at equilibrium. The physics model uses IPCC's e-times that leave only 1.4% of total carbon in the atmosphere at equilibrium.

Then, to calculate the results of continuing pulses, the Bern model must integrate successive Green's functions. The physics model for a single pulse could use Green's functions, but that would require integrating sequential Green's functions, which is unnecessary.

The physics model uses recursive calculations to quickly solve for any scenario in a single process. The physics model is a true systems model that allows levels to set flows and these flows to set new levels. It is simpler and more versatile than the Bern model.

The physics model (Section 4) shows how inflow sets a balance level where outflow equals inflow. The level always moves to the balance level. Once at the balance level, continuing constant inflow does not change the level.

3. Carbon data review

3.1 IPCC's carbon cycle data

IPCC (2013, p. 470) introduces IPCC's carbon cycles,

> "Atmospheric CO_2 represents the main atmospheric phase of the global carbon cycle. The global carbon cycle can be viewed as a series of reservoirs of carbon in the Earth System, which are connected by exchange fluxes of carbon. Conceptually, one can distinguish two domains in the global carbon cycle."
>
> "The first is a fast domain with large exchange fluxes and relatively 'rapid' reservoir turnovers, which consists of carbon in the atmosphere, the ocean, surface ocean sediments and on land in vegetation, soils and freshwaters."
>
> "Reservoir turnover times, defined as reservoir mass of carbon divided by the exchange flux, range from a few years for the atmosphere to decades to millennia for the major carbon reservoirs of the land vegetation and soil and the various domains in the ocean."
>
> "A second, slow domain consists of the huge carbon stores in rocks and sediments which exchange carbon with the fast domain through volcanic emissions of CO_2, chemical weathering, erosion and sediment formation on the sea floor."

IPCC's reference to "turnover times" clarifies that it defines outflows to be directly proportional to the reservoir levels and that IPCC's data include biogeochemical processes for the carbon cycle.

Fig. # 1 (IPCC, 2013, p. 471, Fig. # 6.1) shows IPCC's carbon cycle with its four major carbon reservoirs – land, atmosphere, surface ocean, and deep ocean – and its separation of the natural (in black) and human (in red) carbon cycles.

IPCC (2013, p. 470) says its Fig. # 6.1 applies to the fast domain,

> "A schematic of the global carbon cycle with focus on the fast domain is shown in Figure 6.1. The numbers represent the estimated current pool sizes in PgC and the magnitude of the different exchange fluxes in PgC/year averaged over the time-period 2000-2009."

IPCC (2013, p. 471) Fig. # 6.1 legend says it is a "simplified schematic of the global carbon cycle. Numbers represent reservoir mass in PgC and annual carbon exchange fluxes (in PgC per year)."

Fig. # 1 separates the natural carbon cycle (in black) from the human carbon cycle (in red),

> "Black numbers and arrows indicate reservoir mass and exchange fluxes estimated for the time prior to the Industrial Era, about 1750."
>
> "Red arrows and numbers indicate annual 'anthropogenic' fluxes averaged over the 2000-2009 time-period."
>
> "Uncertainties are reported as 90% confidence intervals. Individual gross fluxes and their changes since the beginning of the Industrial Era have typical uncertainties of more than 20%, while their differences are determined from independent measurements with a much higher accuracy."

The Gilfillan et al. (2020) data for human carbon emissions show human carbon inflow was 7.8 PgC per year in about 2005 and the accumulated human carbon emissions was 365 PgC in 2010, agreeing with Fig. # 1 data for the 2000-2009 time-period.

3.2 IPCC's natural carbon cycle

Fig. # 1 shows annual natural carbon emissions to the atmosphere are 107.2 PgC per year from the land and 60.7 PgC from the surface ocean for a total of 168 PgC per year.

IPCC's natural carbon cycle is at equilibrium. Fig. # 1 shows IPCC's net natural flows between the reservoirs are near zero, but they must be at net zero to truly be at equilibrium.

Fig. # 2 shows IPCC's natural net flows set to zero (a 1% adjustment to IPCC's data) to keep the IPCC's reservoir levels constant. The boxes represent reservoirs, and the arrows represent flows between the reservoirs. The origins of the arrows are "nodes."

Fig. # 2 uses IPCC's assumption that the natural level remained constant at 589 PgC (278 ppmv) after 1750. The Land 2500 PgC in Fig. # 2 is the total of averages of Vegetation (550 PgC) and Soils (1950 PgC) in Fig. # 1.

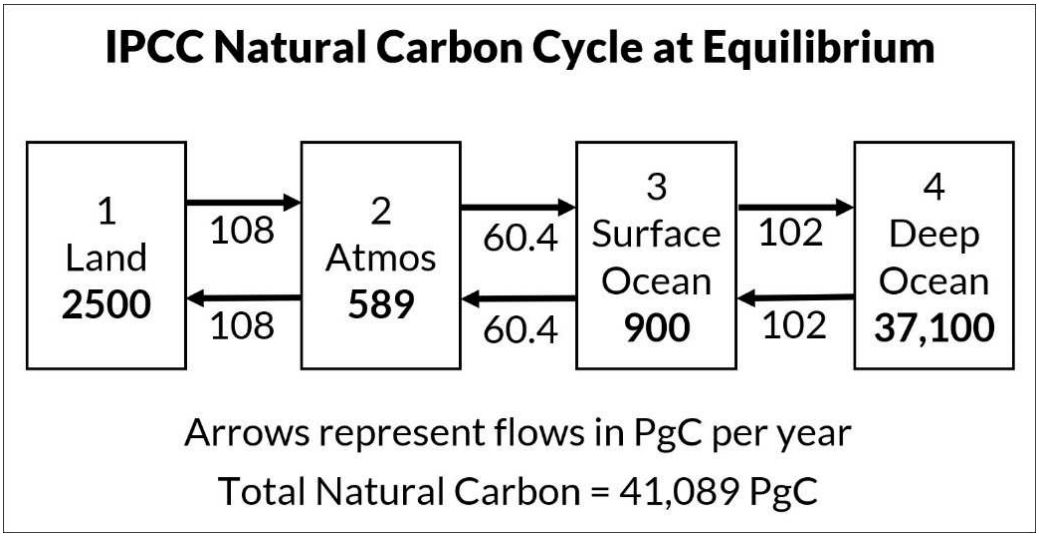

Figure 2. Levels and flows for IPCC's (2013) natural carbon cycle shown in Figure 1. The boxes represent the reservoirs and arrows represent the flows between the reservoirs.

Fig. # 3 shows the percent of natural carbon in each reservoir from Fig. # 2. Only 1.43% of natural carbon is in the atmosphere and 90% is in the deep ocean.

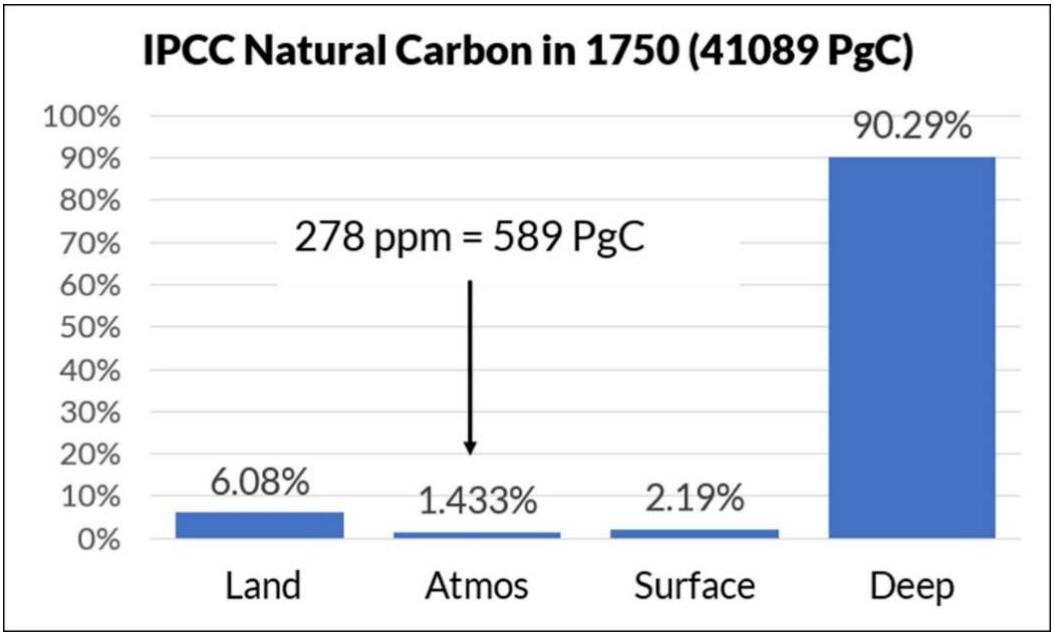

Figure 3. The percent of natural carbon in each reservoir for IPCC's natural carbon cycle in Figure 2.

The Fig. # 3 reservoir percentages are a fingerprint of the IPCC's natural carbon cycle at equilibrium. Since human carbon has the same turnover times as natural carbon, the human carbon cycle will have this same equilibrium fingerprint. If all human carbon emissions were to stop, the human carbon percentages would move toward the natural carbon percentages shown in Fig. # 3.

3.3 IPCC's human carbon cycle

Fig. # 1 shows annual human carbon emissions in 2005 were 7.8 PgC per year and land carbon emissions were 1.1 PgC per year for a total of 8.8 PgC per year which is 5% of the annual natural emissions of 168 PgC per year.

Fig. # 4 shows IPCC's human carbon cycle values in Fig. # 1 for the 2000-2009 time-period. Fig. # 4 shows human carbon emissions added 365 PgC to the human carbon cycle as of 2010.

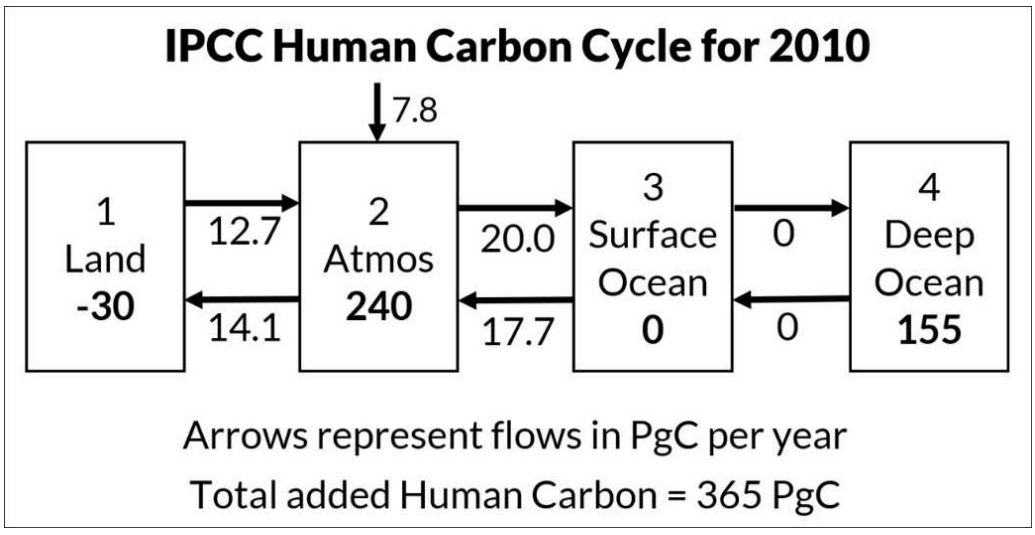

Figure 4. Levels and flows for IPCC's human carbon cycle shown in Figure 1. The boxes represent the reservoirs and arrows represent the flows between the reservoirs.

Fig. # 5 shows the percent of the 365 PgC of human carbon in each reservoir for IPCC's human carbon cycle shown in Fig. # 4. These percentages show 8% of 365 has moved from the land to the atmosphere to the deep ocean, 66% is in the atmosphere, and 42% is in the ocean.

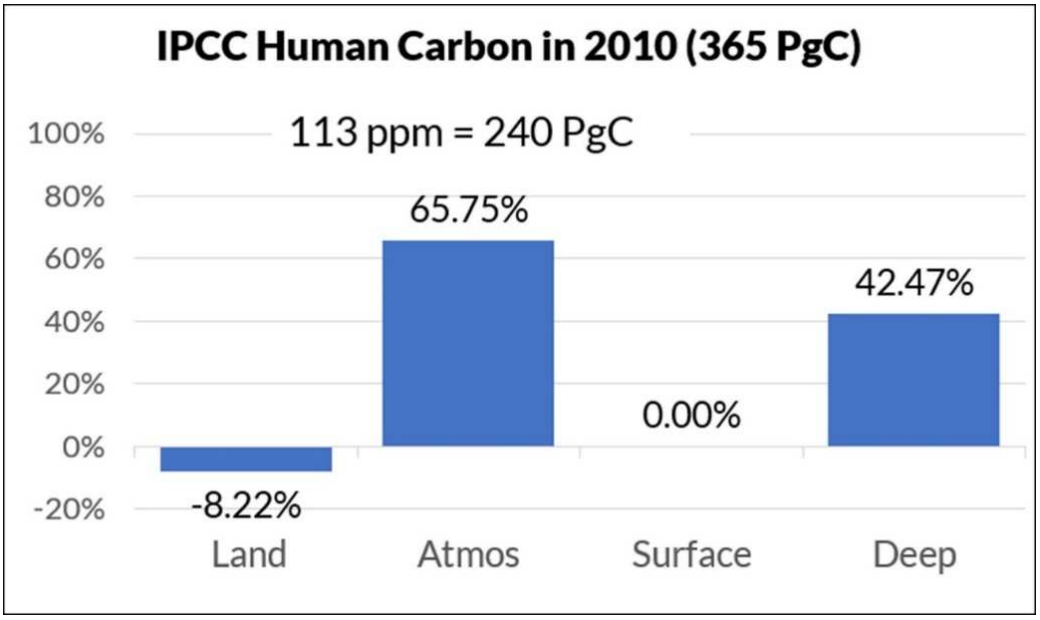

Figure 5. The percent of human carbon in each reservoir for IPCC's human carbon cycle in Figure 4.

Ignoring the 8% percent loss in the land carbon, which has large errors and could even be positive, Fig. # 5 shows the IPCC's human carbon cycle percentages do not resemble IPCC's natural carbon cycle percentages in Fig. # 3.

This difference suggests that IPCC's human carbon cycle uses different physics than IPCC's natural carbon cycle. Rather than calculate a human carbon cycle, the IPCC simply assigned 240 PgC or 66% of the human carbon 365 PgC to the atmosphere based solely on its assumption that natural CO_2 remained at 280 ppmv while human carbon caused all the increase in atmospheric CO_2. Then the IPCC assigned the remaining human carbon to the deep ocean.

IPCC's human carbon data in Fig. # 1 are from IPCC's (2013, p. 486) Table 6.1 "Global anthropogenic CO_2 budget" for the decade 2000 to 2009.

Table 1 shows IPCC's Table 6.1 with the Row 3 signs reversed to show positive flow from the atmosphere to the ocean. Positive flux numbers are in the direction of the flux title. IPCC writes,

> "Global anthropogenic CO_2 budget, accumulated since the Industrial Revolution (onset in 1750) and averaged over the 1980s, 1990s, 2000s, as well as the last 10 years until 2011."

The uncertainty range is for a 90 confidence interval.

Table 1. IPCC's (2013, p 486) Table 6.1

IPCC (2013, p 486) Table 6.1. Row-3 signs reversed to show positive flow from atmosphere to surface ocean.	*1750-2011 Cumulative* PgC	*1980-1989* PgC/Year	*1990-1999* PgC/Year	*2000-2009* PgC/Year	*2002-2011* PgC/Year
Atmospheric increase	240 ± 10	3.4 ± 0.2	3.1 ± 0.2	4.0 ± 0.2	4.3 ± 0.2
Fossil fuel and cement production	365 ± 30	5.5 ± 0.4	6.4 ± 0.5	7.8 ± 0.6	8.3 ± 0.7
Atmosphere-to-ocean flux	155 ± 30	2.0 ± 0.7	2.2 ± 0.7	2.3 ± 0.7	2.4 ± 0.7
Land-to-Atmosphere flux	30 ± 45	-0.1 ± 0.8	-1.1 ± 0.9	-1.5 ± 0.9	-1.6 ± 1.0
Net land use change	180 ± 80	1.4 ± 0.8	1.5 ± 0.8	1.1 ± 0.8	0.9 ± 0.8
Residual land sink (inferred)	-150 ± 90	-1.5 ± 1.1	-2.6 ± 1.2	-2.6 ± 1.2	-2.5 ± 1.3

The IPCC calculates the "inferred" values of Residual land sink as follows,

> [Residual Land Sink] = [Fossil fuel and cement production] + [Net land-use change] – [Atmospheric increase] – [Atmosphere-to-Ocean flux]

This formula finds the Cumulative Residual land sink is -150 PgC rather than -160 PgC and Table 1 corrects this IPCC error.

This paper uses Table 1 values to calculate the effect of IPCC's net land use change on the human carbon cycle.

4. Physics model

(The casual reader may skip Section 4 that develops the mathematics for the physics model.)

4.1 Physics model for one reservoir

The physics carbon cycle requires a theoretical base. All models are approximations to reality. Scientists and engineers define systems to approximate a subset of nature. A system includes levels and flows between levels. Levels set flows and flows set new levels. The mathematics used in the physics model are analogous to the mathematics used to describe engineering and chemical systems.

Fig. # 6 shows the one-level physics model with one outflow for carbon in the atmosphere. The same model applies to all carbon in any reservoir.

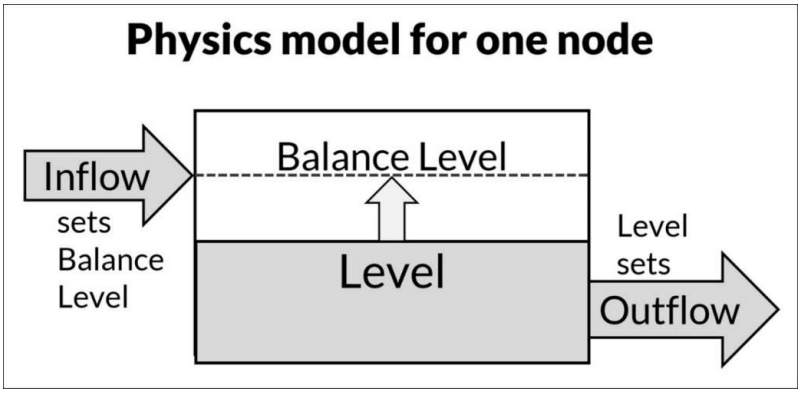

Figure 6. The physics model for one level and one outflow node.

Following Berry (2019), the physics model derivation begins with the continuity equation (1) which says the rate of change of level is the difference between inflow and outflow,

$$dL / dt = Inflow - Outflow \quad (1)$$

where,

L = carbon level (PgC)

t = time (years)

dL / dt = rate of change of L (PgC / year)

Inflow = carbon inflow (PgC / year)

Outflow = carbon outflow (PgC / year)

When *Outflow* = *Inflow*, then $dL/dt = 0$. The flows continue while the level is constant.

The physics model has only one hypothesis, outflow is proportional to level,

$$Outflow = L / T_e \quad (2)$$

where T_e is the "e-time," so defined because it is an exponential time. Equation (2) shows e-time *Te* is the same as IPCC's turnover time, *T*.

E-time is the time for the level to move (1 - 1/e) of the distance from its present level to its balance level.

Substitute (2) into (1) to get,

$$dL / dt = Inflow - L / T_e \quad (3)$$

When dL/dt is zero, the level will be at its balance level, L_b, defined as,

$$L_b = Inflow\ T_e \quad (4)$$

Substitute (4) for *Inflow* into (3) to get,

$$dL / dt = - (L - L_b) / T_e \quad (5)$$

Equation (4) shows how inflow sets the balance level. Equation (5) shows the level always moves toward the balance level set by the inflow. The variables L, L_b, and T_e are functions of time.

In the special case when L_b and T_e are constant, which means *Inflow* is constant according to (4), there is an analytic solution to (5). Rearrange (5) to get,

$$dL / (L - L_b) = - dt / T_e \quad (6)$$

Then integrate (6) from L_0 to L on the left side, and from 0 to t on the right side to get,

$$\text{Ln}\ [(L - L_b) / (L_0 - L_b)] = - t / T_e \quad (7)$$

where,

L_0 = Level at time zero ($t = 0$)

L_b = the balance level for a given inflow and T_e

T_e = time for L to move (1 – 1/e) from L to L_b

e = 2.7183

Define half-life, T_h, as the time for the level to fall to half its original level. Then (7) becomes,

$$\text{Ln}\,(1/2) = -\,T_h / T_e \tag{7a}$$

$$T_h = T_e\,\text{Ln}\,(2) = 0.6931\;T_e \tag{7b}$$

The original integration of (6) has two absolute values, but they cancel each other because both L and L_0 are always either above or below L_b.

Raise e to the power of each side of (7), to get the level as a function of time,

$$L(t) = L_b + (L_0 - L_b)\,\exp(-\,t / T_e) \tag{8}$$

Equation (8) is the analytic solution of (5) when L_b and T_e are constant.

All equations after (2) are deductions from hypothesis (2) and the continuity equation (1).

4.2 Physics model properties

The physics model's only hypothesis (2) is a linear function of level. This means the physics model applies independently and in total to human and natural carbon, and independently and in total to all definitions of carbon or CO_2 (Berry, 2019).

However, if outflow (2) were a strictly increasing function of level other than level to the power of one, then the physics model would *not* apply independently and in total to human CO_2 and natural CO_2.

The *superposition principle* says for all linear systems,

> the net response caused by two or more stimuli is the sum of the responses caused by each stimulus individually. So, if input A produces response X and input B produces response Y then input (A + B) produces response (X + Y).

Dalton's law of partial pressures applies to a linear system. It says,

> the total pressure in a mixture of non-reacting gases equals the sum of the partial pressures of the individual gases.

The linear physics model applies independently to human CO_2, natural CO_2, and their sums, and to $^{12}CO_2$, $^{13}CO_2$, and $^{14}CO_2$, and their sums.

Hypothesis (2) shows it is preferable to calculate the natural and human carbon cycles separately. Just add another instance of the physics model for each carbon definition. Then add the results of the separate calculations to produce the total carbon cycle.

Hypothesis (2) is compatible with all applicable physical and chemical laws. It is the simplest hypothesis for carbon cycle models, and it replicates IPCC's natural carbon cycle.

Harde and Salby (2021) show how carbon isotope data confirms this hypothesis is valid for carbon dioxide flows out of the atmosphere,

> "The exponential decline of anomalous $^{14}CO_2$ establishes that absorption of CO_2 is determined, not by extraneous reservoirs of carbon, but autonomously by the atmosphere. Specifically, the rate at which CO_2 is absorbed from the atmosphere is directly proportional to the instantaneous abundance of CO_2 in the atmosphere."

This statement supports hypothesis (2). Systems models must calculate outflows as functions of their levels. That the physics model replicates IPCC's natural carbon cycle shows there is no need to talk about uptakes. "Uptakes" cannot form a systems model because "uptakes" are not functions of their levels.

The physics model allows external processes to change reservoir levels only by changing the inflows, outflows, or e-times. The physics model *includes all effects of external processes* (chemical, biological, etc.) on the level of carbon in a reservoir because IPCC's natural carbon

cycle data include these effects.

Equation (5) shows how the level moves toward its balance level with a speed set by the e-time. When the level equals its balance level, outflow will equal inflow. At the balance level, constant inflow sets a constant level. Carbon will not accumulate in the reservoir.

The balance level (4) shows that neither human nor natural emissions accumulate in the atmosphere beyond their balance level. Constant inflows create constant outflows when the levels are at their balance levels.

4.3 Physics carbon-cycle model

All the definitions and properties of the physics model for one reservoir apply to the physics model for multiple reservoirs.

IPCC (2013) carbon cycle has four key carbon reservoirs, e.g., land, atmosphere, surface ocean, and deep ocean. We apply the physics model to each reservoir and each outflow node. The "level" of each reservoir is the mass of carbon in each reservoir.

The physics model is not a static mass balance, or a statistical curve fit to data. It is a dynamic flow model that accurately computes the evolution of levels and flows as functions of time, based on a given set of initial conditions, which define model outcomes. It may be the first fully functional mathematical model of IPCC's carbon cycle. It follows the numerical mathematics methods of Berry (1967, 1969) and Berry and Reinhardt (1974a, b, c, d) to calculate cloud droplet growth by stochastic collection.

Fig. # 7 shows the physics carbon cycle model with IPCC's four reservoirs and six outflows, where the arrows are all positive numbers. The origin of each arrow is a "node."

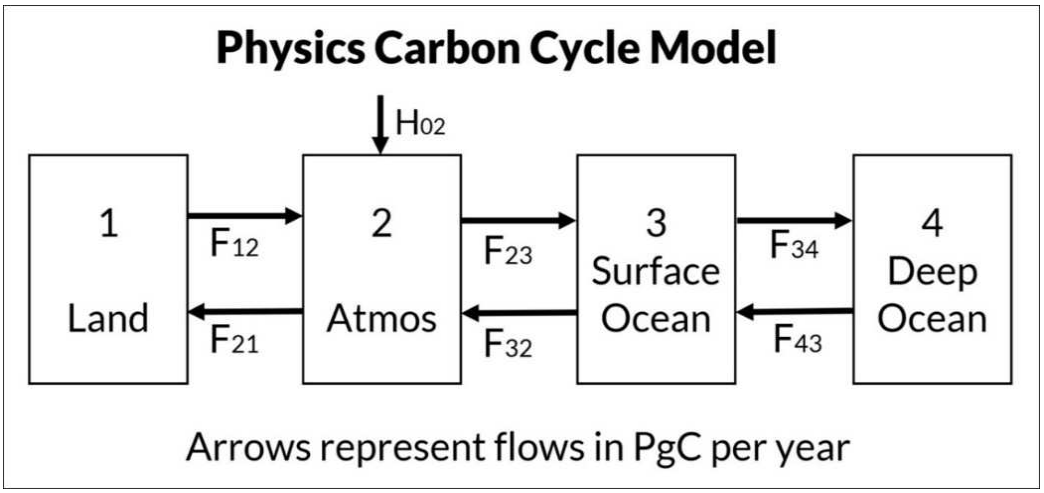

Figure 7. The physics carbon cycle model for IPCC's carbon cycles.

Define the Levels,

L_1 = level of carbon in the land

L_2 = level of carbon in the atmosphere

L_3 = level of carbon in the surface ocean

L_4 = level of carbon in the deep ocean

Define the individual flows out of the six nodes,

F_{12} = flow from land to atmosphere

F_{21} = flow from atmosphere to land

F_{23} = flow from atmosphere to surface ocean

F_{32} = flow from surface ocean to atmosphere

F_{34} = flow from surface ocean to deep ocean

F_{43} = flow from deep ocean to surface ocean

Define other variables,

t = time in years

H_{02} = human carbon flow to atmosphere

H_{12} = land carbon flow to atmosphere

Using (2), the flows out of the six nodes are,

$$\begin{aligned} F_{12} &= L_1 / T_{12} \\ F_{21} &= L_2 / T_{21} \\ F_{23} &= L_2 / T_{23} \\ F_{32} &= L_3 / T_{32} \\ F_{34} &= L_3 / T_{34} \\ F_{43} &= L_4 / T_{43} \end{aligned} \tag{9a}$$

The same equations in terms of e-times are,

$$\begin{aligned} T_{12} &= L_1 / F_{12} \\ T_{21} &= L_2 / F_{21} \\ T_{23} &= L_2 / F_{23} \\ T_{32} &= L_3 / F_{32} \\ T_{34} &= L_3 / F_{34} \\ T_{43} &= L_4 / F_{43} \end{aligned} \tag{9b}$$

Using (1) and (9), the rate equations for each reservoir are,

$$\begin{aligned} dL_1 / dt &= F_{21} - F_{12} - H_{12} \\ dL_2 / dt &= F_{12} - F_{21} + F_{32} - F_{23} + H_{02} + H_{12} \\ dL_3 / dt &= F_{23} - F_{32} + F_{43} - F_{34} \\ dL_4 / dt &= F_{34} - F_{43} \end{aligned} \tag{10}$$

The physics model uses (9) and (10) to calculate the natural and the human carbon cycles.

4.4 RC Network analogy

Fig. # 8 shows the RC network analogy to the physics carbon cycle model shown in Fig. # 7 (suggested by Happer and van Wijngaarden, 2020).

The four capacitors simulate the four reservoirs. The capacitor charge simulates the carbon levels. Charge is proportional to voltage, so voltage represents charge and carbon level.

The resistors simulate the "resistance to flow" between the reservoirs. Reservoir level differences drive flow. Voltage differentials drive the current between the capacitors, and current, which is flow of charge, simulates carbon flow.

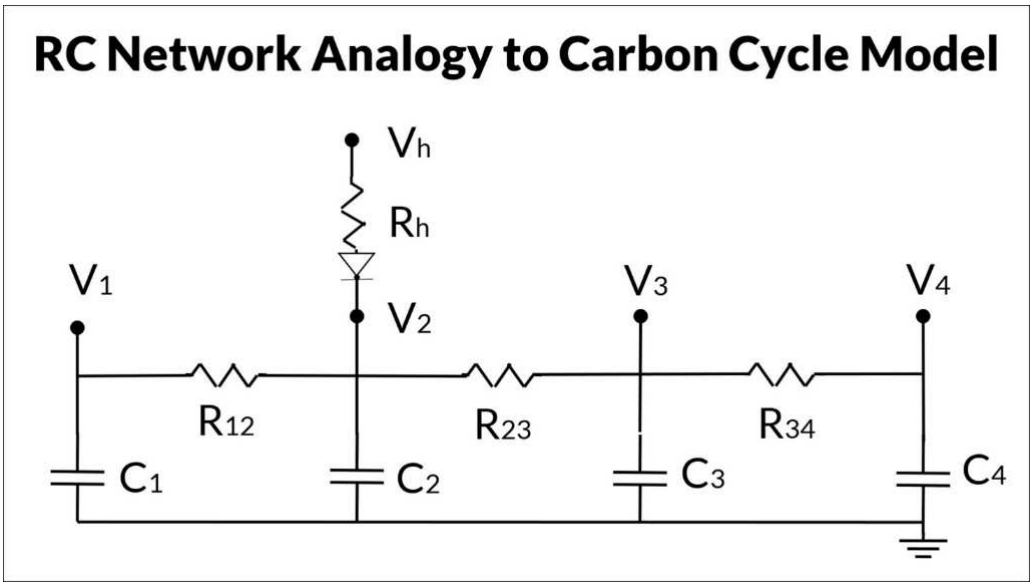

Figure 8. RC Network analogy to Physics carbon cycle model.

Fig. # 8 shows above V_2 a diode, resistor R_h, and voltage V_h, to simulate the inflow of human carbon into the atmosphere. The diode prevents reverse flow. To simulate human emissions, set $(V_h - V_2) / R_h$. To simulate the land-use effect shown in Fig. # 10, set $(V_1 - V_2) / R_{12}$.

The following derivations show how electrical circuit theory uses the physics model hypothesis (2).

The physics model defines the ends of each resistor as "nodes." Equation (11) shows how the outflow hypothesis (2) is the same as electrical circuit theory,

$$Outflow = L / T_e = I = V / R = Q / RC \tag{11}$$

where,

I = current outflow

V = voltage on the capacitor

R = resistance to outflow

Q = charge on the capacitor

C = capacitance

In electrical terms, Ohm's law requires the net flow between nodes to be,

$$Net\_F_{jk} = (V_j - V_k) / R_{jk} \quad (12a)$$

$$Net\_F_{jk} = F_{jk} - F_{kj} \quad (12b)$$

Therefore, the outflow from each node is,

$$F_{jk} = V_j / R_{jk} \quad (13)$$

where the resistance between nodes j and k is bidirectional,

$$R_{jk} = R_{kj} \quad (14)$$

The charge on a capacitor is the analog of the carbon level, L, so

$$V_j = L_j / C_j \quad (15)$$

Substituting (15) into (13), the flow out of each node is,

$$F_{jk} = L_j / R_{jk} C_j \quad (16)$$

Comparing (16) to (9) shows the capacitor analogy of T_e is,

$$T_{jk} = R_{jk} C_j \quad (17)$$

Therefore, the nodal flows for the capacitor analogy are the same as the nodal flows for the physics model (9) when (17) replaces the T_{jk} in (9).

At equilibrium, all V_j are equal. Therefore, (15) means,

$$L_j / C_j = L_k / C_k \quad (18)$$

In an electrical RC circuit, the time constant "*Tau*" is,

$$Tau \text{ (seconds)} = C \text{ (Farads)} * R \text{ (Ohms)} \quad (19)$$

The capacitor analogy uses the same equations and data as the physics carbon cycle model. Therefore, their results will be identical. Perhaps students can build a capacitor model.

4.5 Method of calculation

Set the flows in (9a) to equal IPCC's equilibrium flows shown in Fig. # 2 (in PgC/Year),

$$\begin{aligned} F_{12} &= L_1 / T_{12} = 108.0 \\ F_{21} &= L_2 / T_{21} = 108.0 \\ F_{23} &= L_2 / T_{23} = 60.4 \\ F_{32} &= L_3 / T_{32} = 60.4 \\ F_{34} &= L_3 / T_{34} = 102.0 \\ F_{43} &= L_4 / T_{43} = 102.0 \end{aligned} \quad (20)$$

Set the levels to equal IPCC's equilibrium levels shown in Fig. # 2 (in PgC),

$$\begin{aligned} L_1 &= 2500 \\ L_2 &= 589 \\ L_3 &= 900 \\ L_4 &= 37{,}100 \end{aligned} \quad (21)$$

Use (9b) to calculate the nodal e-times and use (17) to equate to RC e-times (in Years),

$$\begin{aligned} T_{12} &= 2500 / 108 = 23.1481 = R_{12}\, C_1 \\ T_{21} &= 589 / 108 = 5.4537 = R_{12}\, C_2 \\ T_{23} &= 589 / 60.4 = 9.752 = R_{23}\, C_2 \\ T_{32} &= 900 / 60.4 = 14.9007 = R_{23}\, C_3 \\ T_{34} &= 900 / 102 = 8.8235 = R_{34}\, C_3 \\ T_{43} &= 37100 / 102 \quad = 363.7255 = R_{34}\, C_4 \\ T_{43} &= 37100 / 102 \quad = 363.7255 = R_{34}\, C_4 \end{aligned} \tag{22}$$

The extended decimal places in (22) are not physically relevant. These decimal places are relevant only to those who wish to check the carbon cycle calculations.

Equation (22) shows the atmosphere has two outflows and two e-times, T_{21} = 5.4 years for flow to land and T_{23} = 9.8 years for flow to the surface ocean. The outflows (2) add up,

$$Outflow = L\,(1 / T_{21} + 1 / T_{23}) = L / 3.5 \tag{23a}$$

We can calculate the same e-time using the total outflow from the atmosphere in Fig. # 2, or

$$Te = L / Outflow = 589 / 168.4 = 3.5 \text{ years} \tag{23b}$$

Therefore, the overall e-time for atmospheric CO_2 for the IPCC (2013) natural carbon cycle is 3.5 years which is less than IPCC's estimate of about 4 years. Harde and Salby (2021) show this is a valid approximate e-time for atmospheric $^{12}CO_2$.

Happer and van Wijngaarden (2020) used a relaxation method to perform independent calculations using the equations in this paper and same input data. Their results matched the numerical calculations of this paper to two decimal places, which, of course, exceeds the accuracy of the data.

The numerical calculations use annual time steps,

1. Set initial levels.
2. Calculate nodal flows using (22) and (9a).
3. Calculate level rates of change using (10).
4. Multiply level rates of change by time step to get changes of levels.
5. Add changes of levels to the levels to get new levels.
6. Repeat for next time step.

The physics model allows the e-times to change with time. However, all calculations in this paper keep the (22) and (9a) e-times constant. Ballantyne et al. (2012) found "there is no empirical evidence" that the ability of the land and oceans to absorb atmospheric CO_2 "has started to diminish on the global scale."

Data and Calculations Availability gives links to download the Excel file that includes all the data, numerical calculations, and plots used in this paper.

5. Physics model results

5.1 The physics human carbon cycle

The physics carbon cycle model correctly simulates IPCC's natural carbon cycle. Since human carbon must obey the same physics as natural carbon, the physics carbon cycle model computes the human carbon cycle using the e-times found in IPCC's natural carbon cycle (22).

These calculations use Gilfillan et al. (2020) data for human carbon emissions from 1750 to 2017, and this paper's estimates of human emissions for 2018 and 2019.

The physics carbon cycle model hypothesis (2) allows independent calculations of natural and human carbon cycles. The sum of the human and natural carbon-cycles equals the total carbon cycle. Therefore, the physics model calculates the human carbon cycle independently.

The calculation begins with the human carbon levels at zero in 1750. Each numerical time step inserts human carbon and allows carbon to flow between reservoirs.

Fig. # 9 shows how the reservoir levels change with time for human carbon. The purple dashed line shows the cumulative human carbon inserted into the fast carbon cycle since 1750.

The solid bold line shows the measured atmospheric carbon level *above* 594 PgC (280 ppmv) using Etheridge et al. (1996) for Antarctic ice and firn data before 1960 and Keeling et al. (2001) for measured data thereafter.

Both natural and human carbon contribute to the measured carbon level, but the IPCC assumes human carbon caused all or most CO_2 increase above 280 ppmv. However, cumulative human carbon is greater than measured total carbon only after about 1955. Before 1955, it looks like natural carbon may have caused part of the increase.

Furthermore, the argument – that because cumulative human carbon exceeds the measured carbon level proves human carbon caused all the increase – is not valid because cumulative *natural* carbon is much greater than cumulative *human* carbon, and if natural carbon did not flow rapidly out of the atmosphere the measured carbon level would be much greater than the measured carbon level today. So, that argument omits proper account of the flow of human carbon out of the atmosphere.

Another invalid argument used to support the IPCC basic assumption is because nature absorbs human carbon from the atmosphere, therefore nature cannot add carbon to the atmosphere. This argument neglects the physics model *superposition principle* that explains why the natural carbon cycle is independent of the human carbon cycle.

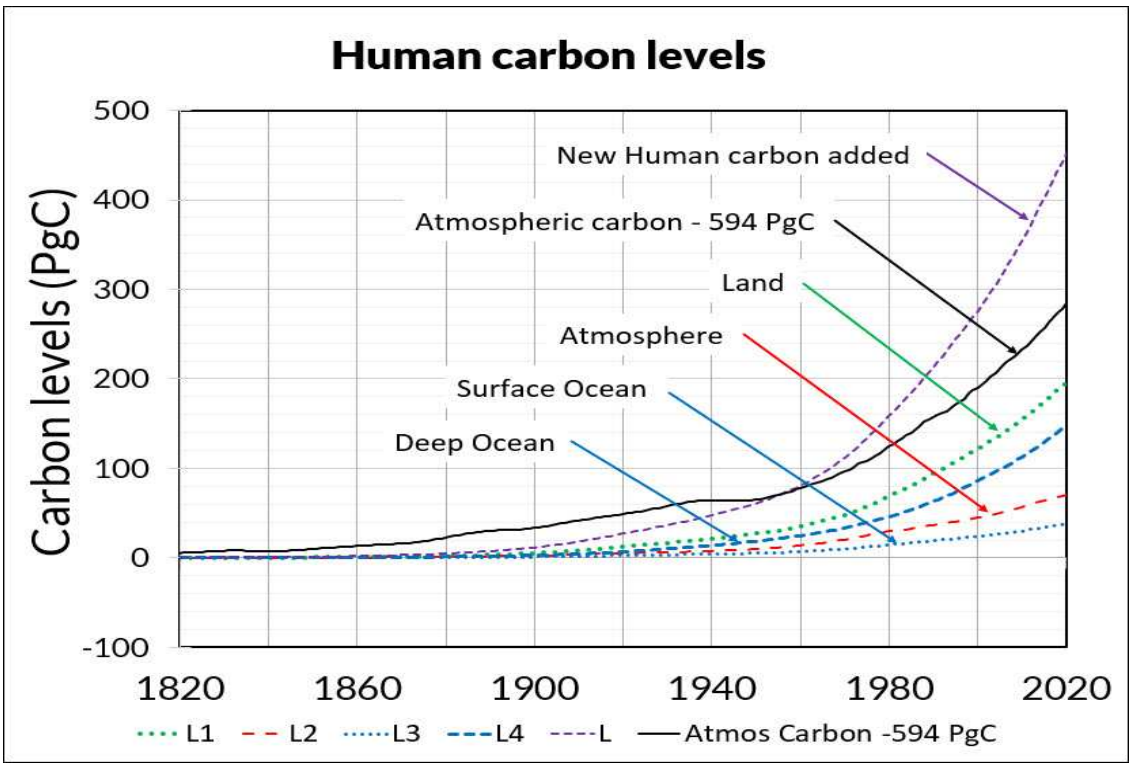

Figure 9. The dashed lines show the calculated human carbon levels for each reservoir.

Table 1 shows accumulated "Net Land Use Change" is 180 PgC over 260 years, for an average of 0.6923 PgC per year. These calculations use a larger land to atmosphere flow of 1.0 PgC per year beginning in 1750.

Net land use change of 1.0 PgC per year has almost no effect on atmospheric CO_2 because this carbon flows rapidly from the atmosphere to the deep ocean, and it adds no carbon to the carbon cycle.

Fig. # 10 shows the levels for land carbon.

Fig. # 11 shows the total effect (by adding them up) of human carbon and land carbon. Although calculated separately, this combination equals the sum of its two components.

Fig. # 9 and 11 show the total human carbon added to the carbon cycle is well below the measured atmospheric carbon before 1950, proving that nature has played a major part in the increase of atmospheric CO_2 after 1750, according to IPCC's data.

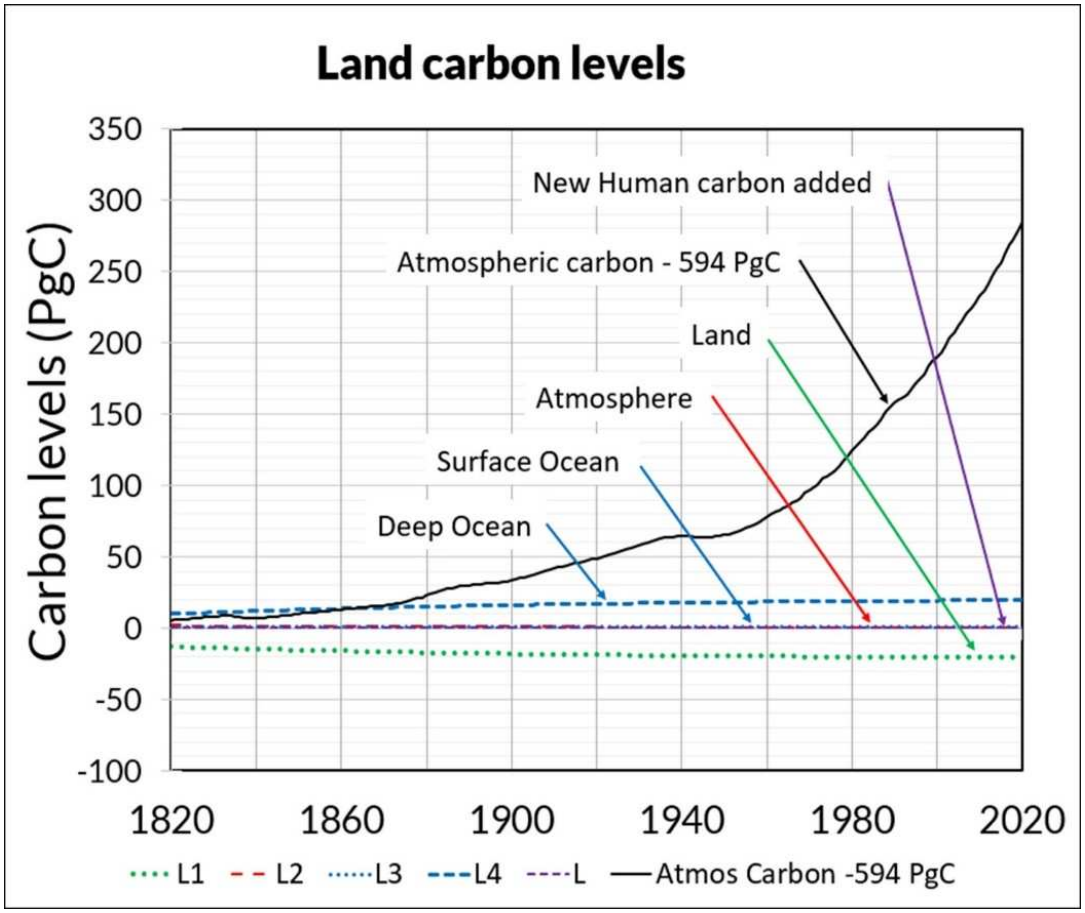

Figure 10. Same as Figure 9 but for Land carbon. Calculations set the land use change carbon flow from land to atmosphere at 1.0 PgC per year.

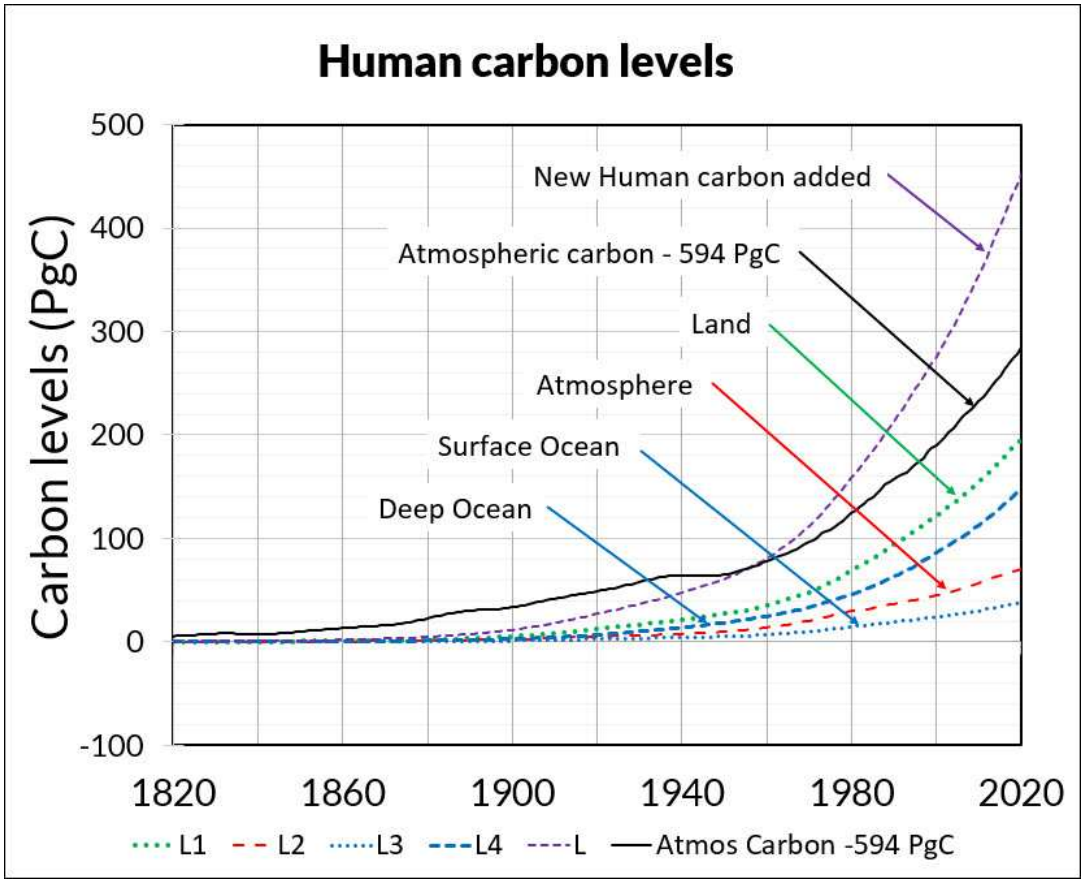

Figure 11. Same as Figure 9 but for all human carbon.

Tables 2, 3, and 4 show the calculated levels of human, land, and total carbon for selected years. All three calculations are independent, yet the independent values for human carbon in Table 2 and land carbon in Table 3, when summed, equal the total values for human carbon in Table 4. The levels for 2100 assume emissions of human carbon stop at the end of 2020.

Table 2. Calculated values of human carbon for selected years.

Year	*L_1*	*L_2*	*L_3*	*L_4*	*Total*	*L_2 ppmv*
1820	0.19	0.08	0.04	0.11	0.21	0.02
1900	5.27	2.49	1.18	2.84	11.78	1.17
2000	121.86	44.66	24.03	85.50	276.05	21.07
2010	154.35	57.05	29.98	112.77	354.14	26.91
2020	196.10	70.18	37.95	147.32	451.55	33.11
2100	110.77	21.31	17.14	302.33	451.55	10.05

Table 3. Calculated values of land carbon for selected years.

Year	L_1	L_2	L_3	L_4	*Total*	L_2 *ppmv*
1820	-13.02	1.89	1.27	9.87	0.00	1.06
1900	-18.00	1.00	0.83	16.17	0.00	0.47
2000	-20.45	0.56	0.62	19.26	0.00	0.27
2010	-20.58	0.54	0.61	19.43	0.00	0.25
2020	-20.69	0.52	0.60	19.58	0.00	0.24
2100	-21.29	0.41	0.55	20.33	0.00	0.19

Table 4. Calculated values of human carbon and land carbon for selected years.

Year	L_1	L_2	*L3*	L_4	*Total*	L_2 *ppmv*
1820	-12.82	1.97	1.31	9.98	0.21	1.08
1900	-12.73	3.49	2.01	19.01	11.78	1.64
2000	101.41	45.22	24.65	104.76	276.05	21.33
2010	133.77	57.59	30.58	132.20	354.14	27.16
2020	175.41	70.70	38.55	166.90	451.55	33.35
2100	89.48	21.72	17.69	322.67	451.55	10.25

Table 3 shows the flow of 1.0 PgC of land carbon to the atmosphere flows rapidly to the deep ocean, leaving little in the atmosphere, and it adds no new carbon to the fast carbon cycle.
Fig. # 12, 13, and 14 show the calculated level percentages for human carbon in Table 4 for the years 2010, 2020, and 2100, respectively.

Fig. # 12 shows in 2010, 16% of human carbon is in the atmosphere, 38% is in the land, and 37% is in the deep ocean. The percentages are significantly different than IPCC's (2013) human carbon cycle shown in Fig. # 5.

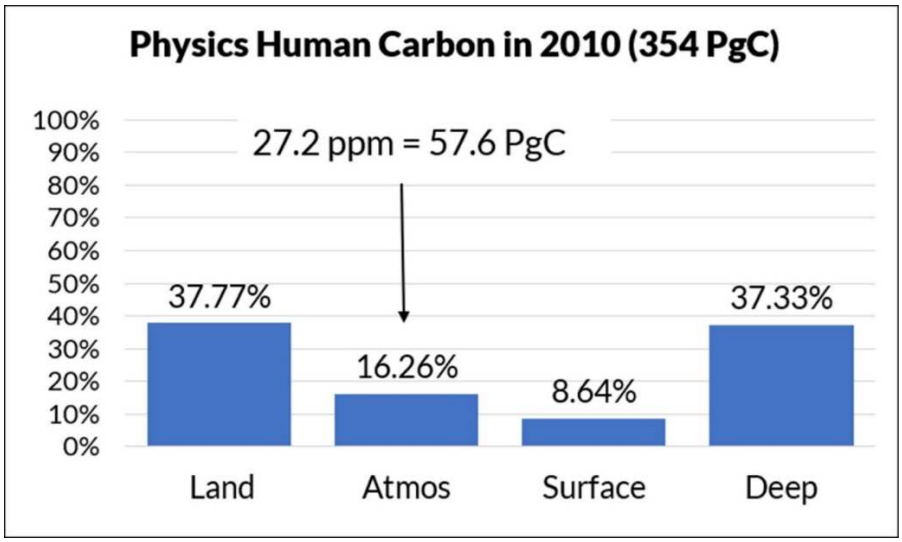

Figure 12. Physics model calculation of human carbon percentages in 2010.

Fig. # 13 for 2020 shows the percentage of human carbon in the atmosphere deep ocean have decreased while the percentage in the land has increased, while the total carbon has increased from 354 PgC in 2010 to 452 PgC in 2020. The 33 ppmv of human carbon in the atmosphere means nature added about 100 ppmv to the 280 ppmv in 1750 to get 413 ppmv.

Fig. # 14 for 2100 shows how fast human carbon in the atmosphere would flow to the deep ocean if all human emissions were to stop in 2020. The level percentages move toward IPCC's natural carbon cycle percentages shown in Fig. # 3.

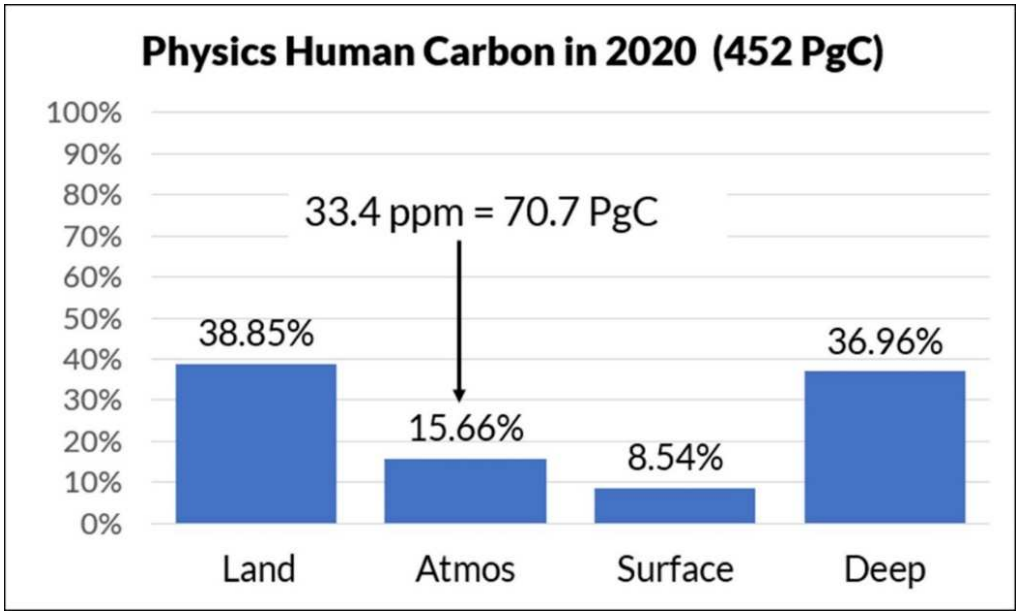

Figure 13. Physics model calculation of human carbon percentages in 2020.

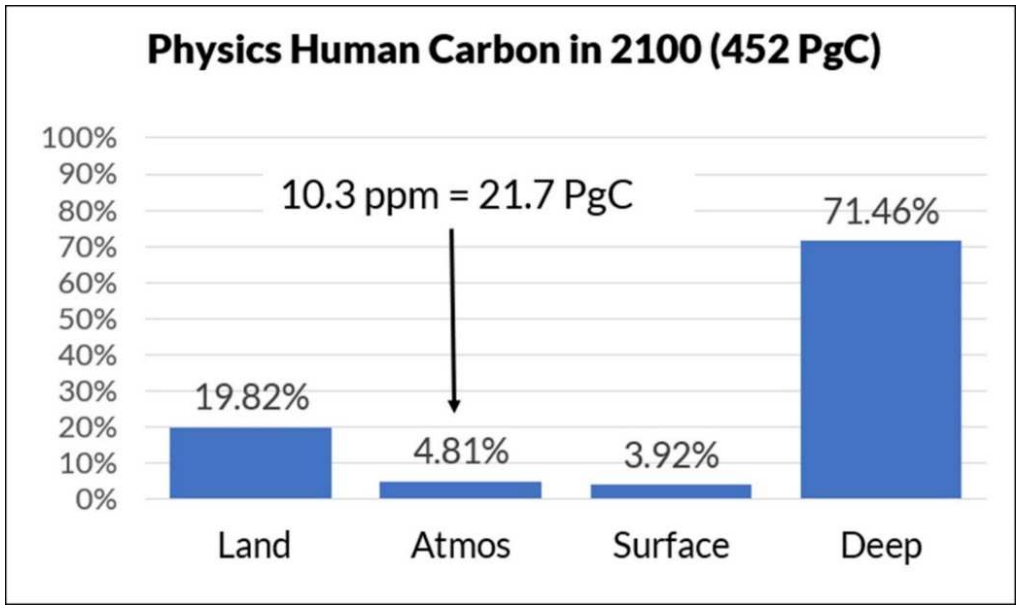

Figure 14. Physics model calculation of human carbon percentages in 2100 assuming all human carbon emissions were to stop in 2020.

Fig. # 15 shows the time plot of human carbon in the atmosphere. It peaks at 33 ppmv in 2020 and this level falls rapidly if human carbon emissions were to stop at the end of 2020, showing human carbon flows rapidly from the atmosphere.

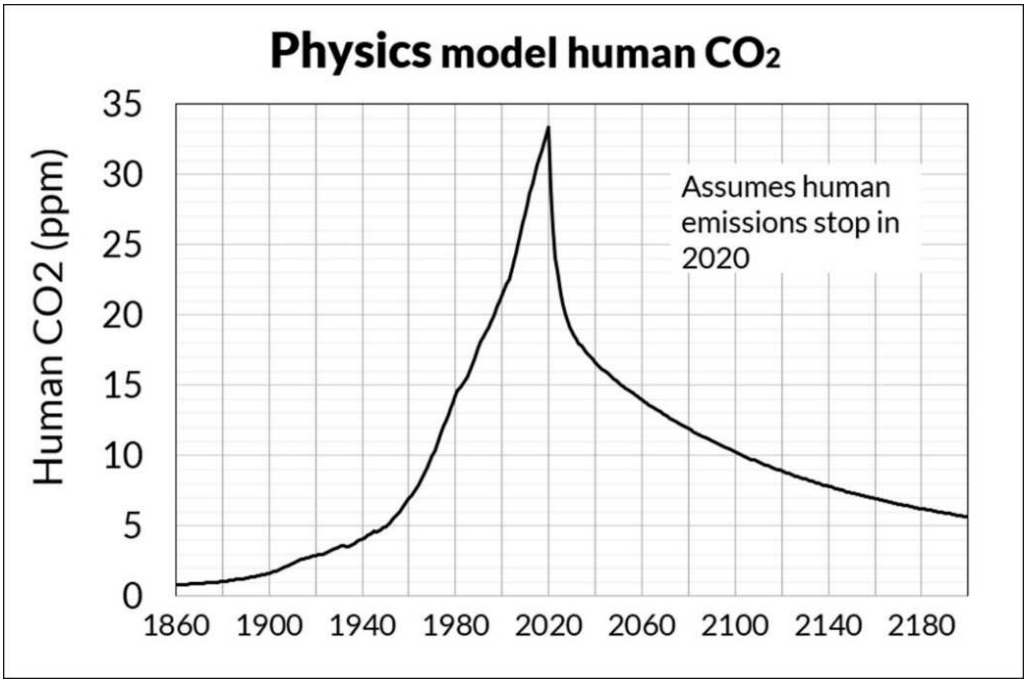

Figure 15. Physics model calculation of the human CO2 level from 1900 to 2100 assuming all human CO2 emissions stop in 2020.

5.2 Values at IPCC's extreme error bounds

IPCC (2013, p. 471) Fig. # 6.1 legend says,

> "Uncertainties are reported as 90% confidence intervals. Individual gross fluxes and their changes since the beginning of the Industrial Era have typical uncertainties of more than 20%, while their differences are determined from independent measurements with a much higher accuracy."

To find the extreme values for the physics human carbon cycle, adjust the e-times in (22) to their 20% borders that maximize and minimize the human CO_2 level. The deep ocean e-time has little effect on the level of atmospheric CO_2.

These e-times (years) maximize atmospheric CO_2 from 33 ppmv to 48 ppmv,

$$\begin{aligned} T_{12} &= (2500 / 108 = 23.1481) * 0.67 \quad = 15.43 \\ T_{21} &= (589 / 108 = 5.4537) * 1.20 \quad = 6.544 \\ T_{23} &= (589 / 60.4 = 9.752) * 1.20 \quad = 11.70 \\ T_{32} &= (900 / 60.4 = 14.9007) * 0.67 \quad = 9.98 \end{aligned} \tag{24}$$

These e-times (years) minimize atmospheric CO_2 from 33 ppmv to 24 ppmv,

$$\begin{aligned} T_{12} &= (2500 / 108 = 23.1481) * 1.49 \quad = 34.49 \\ T_{21} &= (589 / 108 = 5.4537) * 0.80 \quad = 4.36 \\ T_{23} &= (589 / 60.4 = 9.752) * 0.80 \quad = 7.80 \\ T_{32} &= (900 / 60.4 = 14.9007) * 1.49 \quad = 22.20 \end{aligned} \tag{25}$$

In summary, IPCC's natural carbon cycle data with 20% error bounds show human CO_2 has increased atmospheric CO_2 by 33 ppmv with a range of 24 ppmv to 48 ppmv, as of 2020. The

probability of occurrence of the extremes of 24 ppmv and 48 ppmv is small because all e-times were set to their limits.

5.3 Physics model carbon cycle pulse decay

Fig. # 16 shows how a single pulse of carbon in the atmosphere will flow to the other reservoirs in 100 years using IPCC's e-times for natural carbon.

After 10 years, only 15% of the carbon pulse is in the atmosphere. After 100 years, 5% of the carbon pulse is in the atmosphere, 28% is in the land, and 64% is in the deep ocean. This approximates the distribution of human carbon in Fig. # 13 for 2020.

The land reservoir is the fastest to accept carbon from the atmosphere. But after 10 years, the atmosphere level decreased so much that the land reservoir sends its carbon back to the atmosphere and thereby to the deep ocean. The land reservoir controls the initial decay of atmospheric carbon, but the deep ocean controls the final decay.

The atmosphere carbon does not have a constant e-time even though all six flows have constant e-times. The presence of multiple flow paths can make constant individual e-times appear to be variable e-times.

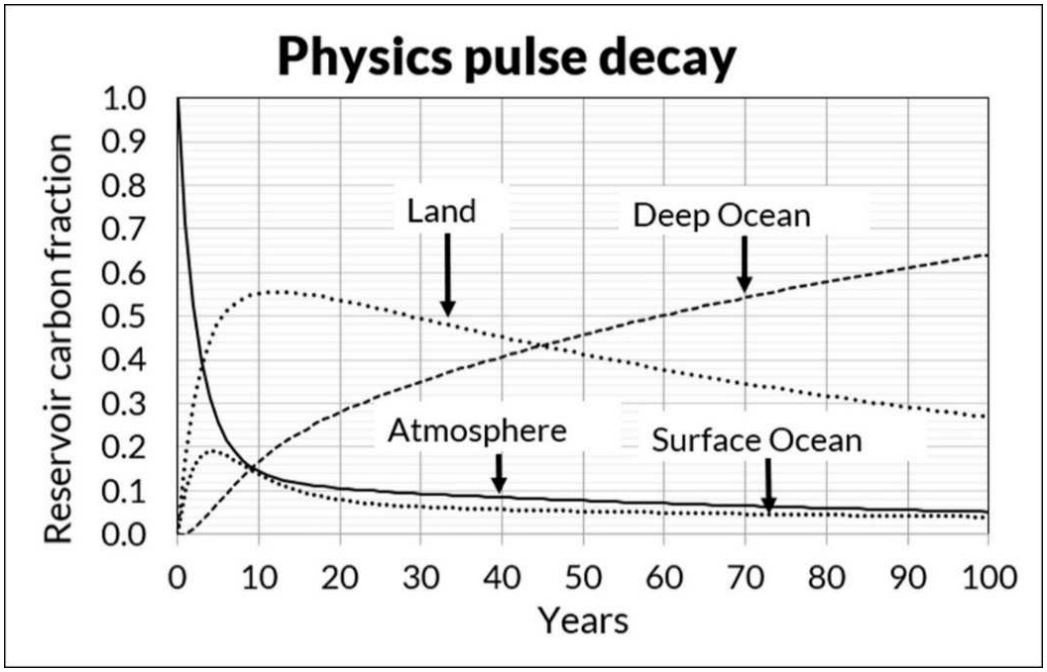

Figure 16. The physics model calculation of how a pulse of carbon in the atmosphere moves through the reservoirs.

5.4 The physics model vs the Bern model

Siegenthaler and Joos (1992) created the original Bern model. They used ^{14}C data to trace the flow of $^{12}CO_2$ from the atmosphere to the upper ocean and to the deep and interior oceans. However, they assumed human CO_2 caused all the increase to analyze their data.

The Bern model is based on IPCC's assumption that the human CO_2 causes all the CO_2 increase. This assumption requires the human CO_2 e-time to be much larger than ten years. Therefore, the Bern model prediction is wrong even though its math may be correct.

Joos (2002) calculated a Green's function for the Bern model. Then he assumed human carbon enters the atmosphere in sequential annual pulses and the carbon in each pulse flows out of the atmosphere independently according to his Green's functions.

To resolve the conflict with data that show e-time is less than 10 years, Joos assumed human

CO_2 (but not natural CO_2) decreases buffer capacity, which is incorrect because it has added less than one percent to the carbon in the natural carbon cycle.

To deconstruct Joos' integral equation, let inflow occur only in the year when *t*' equals zero. Then the integral disappears, and the Bern model becomes a level equation that depends on its starting level, L_o,

$$L(t) = L_0 \left[A_0 + A_1 \exp(-t / T_1) + A_2 \exp(-t / T_2) + A_3 \exp(-t / T_3) \right] \tag{26}$$

where,

t = time in years

L_0 = level of atmospheric CO_2 in year t = 0

$L(t)$ = level of atmospheric CO_2 in year t

Joos derived these TAR (Third Assessment Report) standard values for the Bern coefficients,

$$\begin{aligned} A_0 &= 0.152 \\ A_1 &= 0.253 \\ A_2 &= 0.279 \\ A_3 &= 0.316 \\ T_1 &= 171 \text{ years} \\ T_2 &= 18.0 \text{ years} \\ T_3 &= 2.57 \text{ years} \end{aligned} \tag{27}$$

where,

$$A_0 + A_1 + A_2 + A_3 = 1.000 \tag{28}$$

In (26), set t equal to infinity to get,

$$L = \mathrm{A}_0 L_0 = 0.152 L_0 \tag{29}$$

Equation (29), or the first term in (26) with values (27), predicts 15.2% of each one-year inflow will remain in the atmosphere forever.

For comparison, the (26) Green's function values for the physics carbon cycle (10) with the values of (20), (21), and (22) are,

$$\begin{aligned} A_0 &= 0.014 \\ A_1 &= 0.758 \\ A_2 &= 0.122 \\ A_3 &= 0.106 \\ T_1 &= 94.9 \text{ years} \\ T_2 &= 6.67 \text{ years} \\ T_3 &= 2.84 \text{ years} \end{aligned} \tag{30}$$

The physics model A_0 in (30) is one-tenth of the Bern model A_0 in (27). The A_0 in the Green's

functions are the equilibrium percentages for atmospheric CO_2 as shown in Fig. # 17. Thus, the physics model predicts only 1.4% of human carbon emissions will remain in the atmosphere forever while the Bern model predicts 15.2%.

Joos et al. (2013) compared the response of atmosphere-ocean models to a pulse emission of human CO_2 and found all the models predicted a "substantial fraction" of pulse would remain in the atmosphere and ocean for millennia. However, all models they compared assumed human carbon caused all the CO_2 increase.

Fig. # 17 compares the physics model (9) and (10) with the Bern model (27). The solid lines in Fig. # 16 and 17 are the same line for the physics pulse decay.

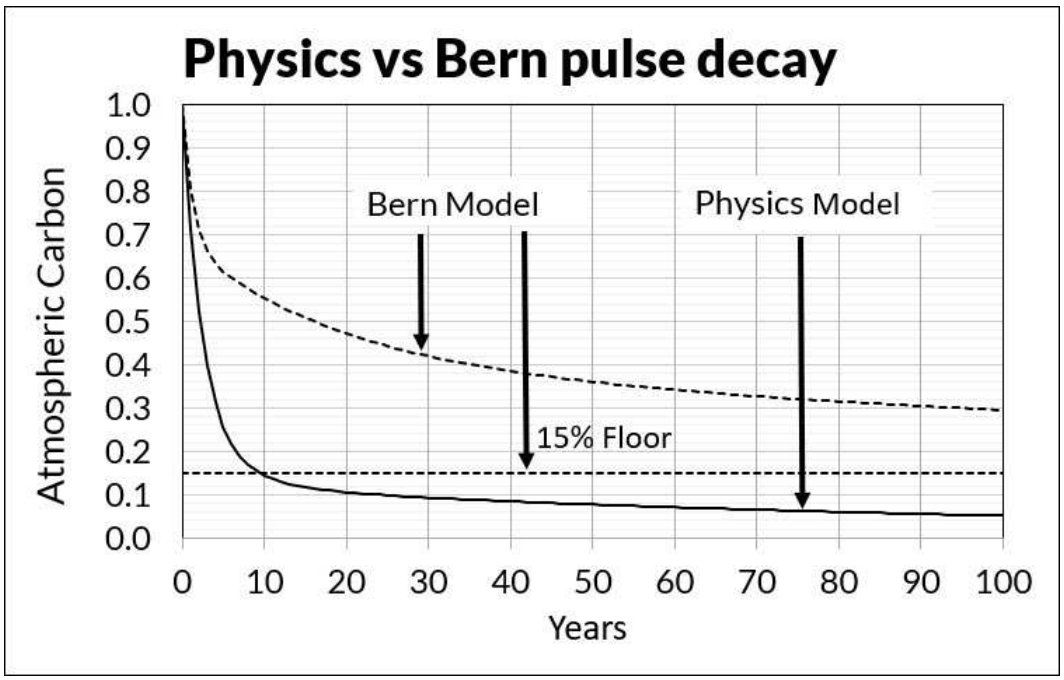

Figure 17. Pulse decay calculations by the physics model using (9) and (10), and the Bern model using (26).

In the Bern model, human CO_2 decays to 55% in 10 years and to 30% in 100 years and will never get below 15% because the Bern model's follows invalid assumption.

In the physics model, human CO_2 decays to 15% in 10 years and to 5% in 100 years and will never get below 1.4% because the physics model follows IPCC's natural carbon cycle data.

6. Discussion

6.1 $\delta^{14}C$ data show the CO_2 increase is natural

The above-ground atomic bomb tests in the 1950s and 1960s almost doubled the $\delta^{14}C$ in the atmosphere. $\delta^{14}C$ is the fractionation, age-corrected deviation from the standard pre-industrial atmospheric ^{14}C concentration (Stuiver and Polach, 1977).

The bomb tests ended in 1963 but it took about seven years for the $^{14}CO_2$ to mix between the hemispheres and to move from the stratosphere to the troposphere. The ^{14}C data in both hemispheres were virtually identical after 1970 (Turnbull et al., 2017).

Hua et al. (2013) processed $\delta^{14}C$ data for both hemispheres from 1954 to 2010. Turnbull et al. (2017) processed $\delta^{14}C$ data for Wellington, New Zealand, from 1954 to 2014. Their ^{14}C data are in units of $\delta^{14}C$ per mil where the $\delta^{14}C$ lower bound of -1000 equals the zero ^{14}C level. The "natural" $\delta^{14}C$ balance level, defined by the average measured level before 1950, is zero.

The physics model is based on hypothesis (2) that Outflow equals Level divided by e-time. All

physics model curve fits use both an e-time and a balance level.

Fig. # 18 plots these data,

- $\delta^{14}C$ data (black solid line) and its curve fit after 1970 (black dashed line).
- ^{14}CR or ^{14}C data relative to the $\delta^{14}C$ value in 1970 (blue sawtooth line) and its curve fit.
- $^{12}CO_2$ data in ppmv (red sawtooth line).

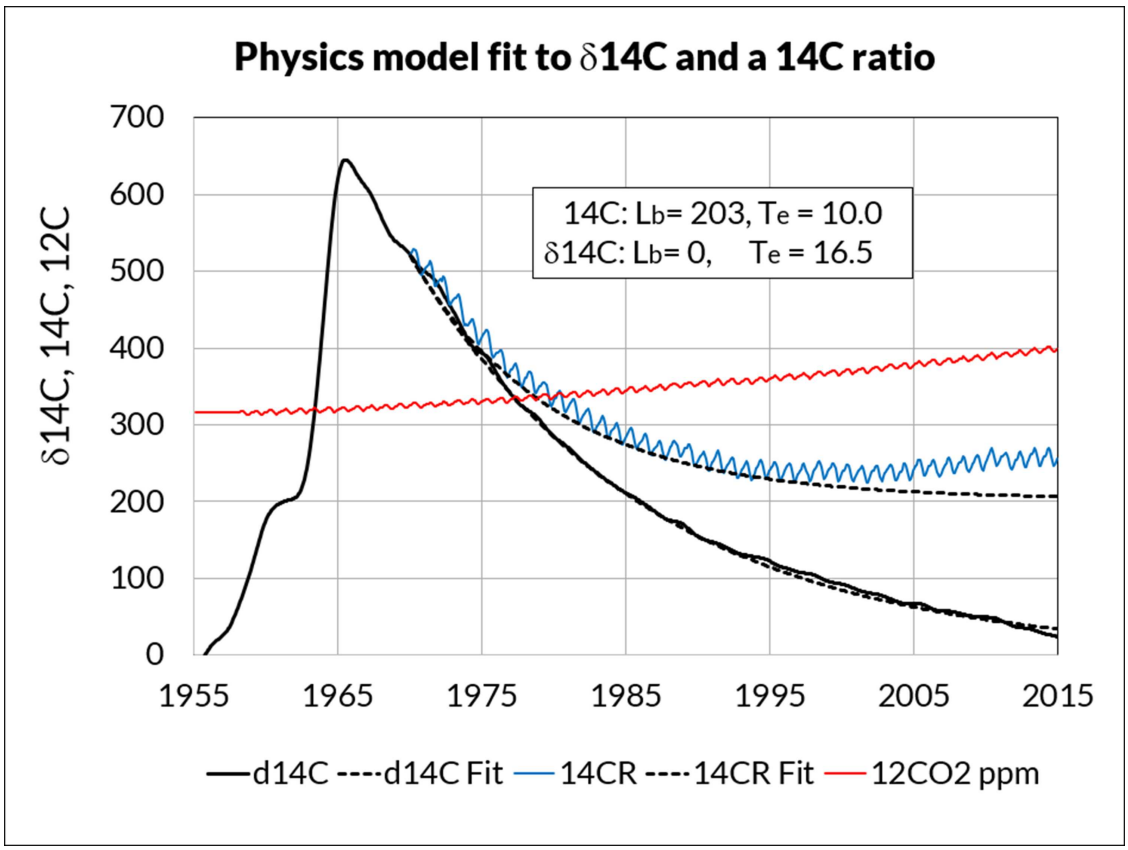

Figure 18. δ14C data (Turnbull et al., 2017, black line), the physics model fit to δ14C (black dashed line), 14CR (blue sawtooth line), physics model curve fit to 14CR (black dashed line), and 12CO2 ppmv (red line).

Equation (8) for a constant e-time fits the $\delta^{14}C$ data from 1970 to 2014 with a constant e-time of 16.5 years and a balance level of zero (Berry, 2019).

To plot ^{14}C on the scale of Fig. # 18, we define "^{14}CR" that will have the same e-time as ^{14}C.

To calculate ^{14}CR use,

$$^{14}CR = (\delta^{14}C + 1000)\ (^{12}CO_2 / {}^{12}CO_2\,(1970)) - 1000 \qquad (31)$$

Equation (8) fits ^{14}CR from 1970 to 1995 with e-time of 10.0 years and balance level of 203. Thereafter, ^{14}C is close to its balance level of 203, so it no longer follows its e-time curve.

The physics carbon cycle model has six different e-times. When a level is far from its balance level the level's own e-time dominates its return to its balance level and therefore is measurable. When a level approaches its balance level, other e-times control its path.

IPCC (2007, p. 948, Lifetime) explains why the "adjustment time" will equal the turnover time when the level is far from its balance level because it is unaffected by other reservoirs. However, "when several reservoirs are involved" (i.e., when it is near its balance level) then the adjustment time no longer equals the turnover time.

IPCC's "adjustment time" is not a physical parameter. Rather, it is IPCC's way to describe how

a level will approach its balance level in a multiple reservoir system.

Fig. # 18 is similar to Harde and Salby (2021, Figure 3) who also find the e-time for $^{14}CO_2$ is 10.0 years,

> "It operates with a single time scale, which reflects the collective absorption by all sinks of CO_2 at the Earth's surface. The long-term decline of anomalous $^{14}CO_2$ reveals an effective absorption time of about 10 years."

The $^{14}CO_2$ e-time of 10 years is an upper limit for the $^{12}CO_2$ e-time because the $^{14}CO_2$ isotope is heavier and slower (Van Langenhove, 1986).

The $\delta^{14}C$ curve is also significant because its return to its original balance level of zero even as ^{12}C has increased, means the dominant carbon flow into the atmosphere has its $\delta^{14}C$ equal to zero. This suggests the ocean, not human emissions, is the dominant source of the CO_2 increase after 1750.

Andrews (2020) criticisms of Harde (2019) and Berry (2019) are invalid because Andrews omits that the ^{14}C e-time of 10 years and the $\delta^{14}C$ return to zero show nature is the primary source of the CO_2 increase.

The physics model, using IPCC's natural carbon cycle data, calculates that human CO_2 adds only 33 ppmv to the atmosphere as of 2020.

However, Salby and Harde (2021) use short-term changes in ^{14}C between 1965 to 1970 to find the atmospheric CO_2 e-time is about 1 year rather than 3.5 years as used in the IPCC (2013) natural carbon cycle.

The physics model can simulate the Salby and Harde shorter e-time by reducing T_{21} from 5.45 to 1.56 years and T_{23} from 9.75 to 2.79 years (22), to get an overall CO_2 e-time of 1.0 years (23a). These revised e-times reduce the calculated human CO_2 increase from 33 ppmv to 10 ppmv as of 2020.

Quirk (2009) examined ^{13}C data and seasonal and hemispherical variations of CO_2, to find,

> "The constancy of seasonal variations in CO_2 and the lack of time delays between the hemispheres suggest that fossil fuel derived CO_2 is almost totally absorbed locally in the year it is emitted. This implies that natural variability of the climate is the prime cause of increasing CO_2, not the emissions of CO_2 from the use of fossil fuels."

6.2 How nature may have increased its CO_2 level

The physics model can show how nature may have increased its natural level of CO_2. To show how, we can apply the calculation method described in Section 4.5 by setting new e-times and calculating the result, through the recursive procedure, from 1750 to 2020.

For reference, Table 5 shows IPCC's natural carbon levels and Table 6 shows the e-times that keep IPCC's natural carbon equilibrium levels constant.

Table 5. IPCC's natural carbon cycle levels in PgC.

L_1	L_2	L_3	L_4
2500	589	900	37100

Table 6. Physics model e-times in PgC per year that keep IPCC's natural carbon levels constant.

T_{12}	T_{21}	T_{23}	T_{32}	T_{34}	T_{43}
23.15	5.45	9.75	14.90	8.82	363.73

Table 7 shows changes in T_{32} and T_{43} that would increase the natural CO_2 level by 100 ppmv.

Table 7. How changes in T32 and T43 would increase the natural CO2 level by 100 ppmv.

T_{32}	T_{43}	*Natural CO_2 level* (ppmv)	*Human CO_2 level*	*Simulation*
14.90	363.73	277.8	33.11	Equilibrium values
10.45	363.73	**377.9**	35.03	Desorption in surface ocean
14.90	**254.00**	**377.4**	33.54	Overturning of deep ocean

If T_{32} for the ^{12}C flow from the surface ocean to the atmosphere decreases from 14.90 to 10.45 PgC per year, the *natural* level of atmospheric CO_2 will increase by 100 ppmv, from 277.8 ppmv to 377.9 ppmv, simulating desorption of carbon in the surface ocean.

If T_{43} for the ^{12}C flow from the deep ocean to the surface ocean decreases from 363.73 to 254.00 PgC per year, the *natural* level of atmospheric CO_2 will increase by 100 ppmv, from 277.8 ppmv to 377.4 ppmv, simulating overturning of the deep ocean.

These e-time changes have insignificant effect on the calculated level of *human* CO_2 because the percent of human carbon in the ocean is still below its equilibrium levels.

Salby (2012, p. 253) uses data to derive an equation that shows how the rate of change of CO_2 level is a function of surface temperature *T*s. If all other things are constant, the rate of increase (dL_2 / dt) in the CO_2 level equals the rate of increase in the flow F_{32}. Then Salby's equation becomes,

$$dF_{32} = 3.5 \text{ (ppmv/year /K) } dTs \tag{32}$$

The above reduction of T_{32} from 14.90 to 10.45 increases the flow F_{32} by 25.7 PgC per year, from 60.4 to 86.1 PgC per year.

Using (32), an increased flow F_{32} of 25.7 PgC per year, or 12.1 ppmv per year, would require a surface temperature increase of (12.1 / 3.5) = 3.5 C.

Salby shows how the increase in *Ts* since the Little Ice Age in 1650 explains the increase in the level of atmospheric CO_2 from 1750 to 2020.

Harde (2017) concluded that natural CO_2 causes most of the CO_2 increase above 280 ppmv,

> "These results indicate that almost all of the observed change of CO_2 during the Industrial Era followed, not from anthropogenic emission, but from changes of natural emission. The results are consistent with the observed lag of CO_2 changes behind temperature changes (Humlum et al., 2013; Salby, 2013), a signature of cause and effect."

Harde (2017, Figure 3) shows how the CO_2 level has changed with surface temperature. His equation (17) is his curve fit to these data.

Fig. # 19, calculated using Harde's equation (17) and his dates in his Fig. # 3, shows how the natural CO_2 level has increased with surface temperature.

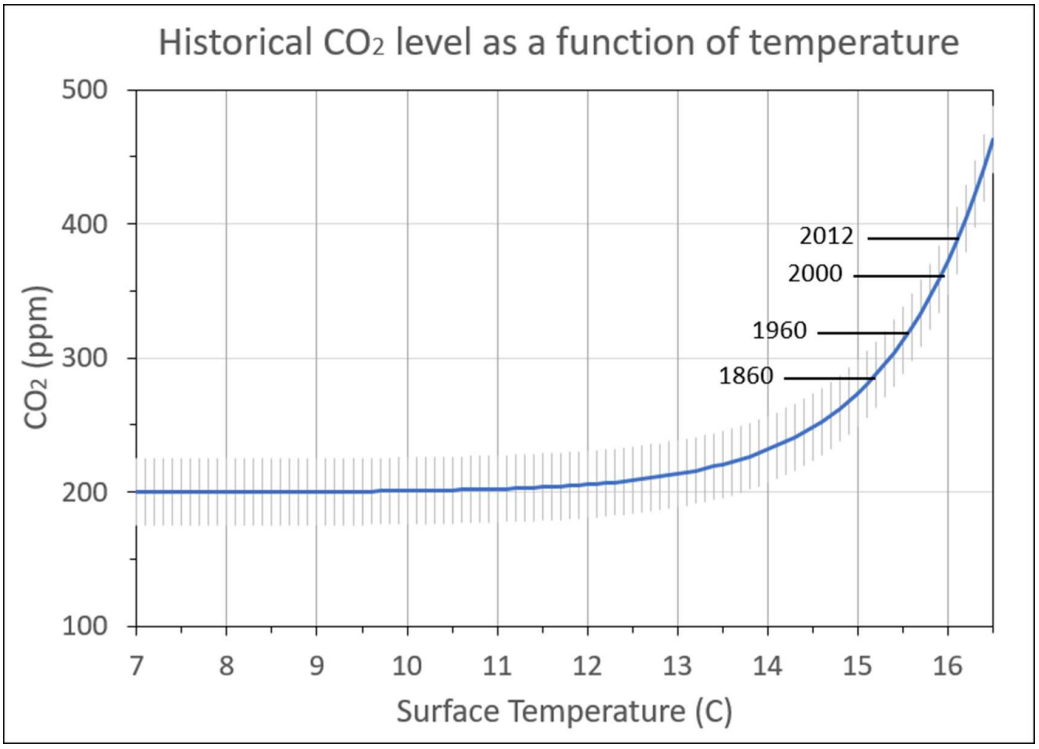

Figure 19. Harde (2017, Figure 3) curve fit by to CO2 and surface temperature data.

Kuo et al. (1990) uses time-series analysis to confirm that temperature and atmospheric carbon dioxide are significantly correlated and found that changes in atmospheric CO_2 lag temperature changes by five months.

Fischer et al. (1999) show the CO_2 increase in Antarctic ice cores increased occurred 600 ± 400 years after the warming of the last three deglaciations.

Caillon et al. (2003) show the CO_2 increase during the Antarctic Termination III occurred 800 ± 200 years after the Northern Hemisphere deglaciation.

Kouwenberg (2004) shows evidence that temperature controls the CO_2 level,

> "… temperature-driven changes in CO_2 flux between ocean surface waters and atmosphere may be invoked as a plausible mechanism to explain at least a substantial part of the reconstructed CO_2 variations over the last Millennium."

Rorsch et al. (2005) conclude the main cause of the CO_2 increase since 1750 is ocean outgassing.

MacRae (2008) found the rate of change of the CO_2 level (dL_2/dt) correlates with the surface temperature and thus atmospheric CO_2 changes lag atmospheric temperature changes by about nine months.

Humlum et al. (2013) show CO_2 increases do not correlate with human CO_2 emissions but consistently follow temperature increases by about 9 to 12 months. A correlation of zero between cause-effect data proves there is no observable cause-effect.

Salby (2013) shows how CO_2 follows changes in the integral of surface temperature.

Munshi (2015b) found there is no statistically significant correlation between the rate of human carbon emissions and the rate of change of global surface temperature even using time lags up to 20 years.

Quirk and Asten (2022) used CO_2 and 13C data from 1978 to 2017 to conclude that 50% of the CO_2 increase comes from the oceans and 50% comes from plants and fossil fuel emissions. If

fossil fuel and natural plant sources are about equal, then Quirk's results support the physics model predictions that about 25% of the increase comes from fossil fuel emissions.

Skrable et al. (2022) conclude from $d^{13}C$ and $\delta^{14}C$ data that the CO_2 increase after 1750 is due primarily to increasing net inputs of non-fossil CO_2 from the oceans due to temperature increases, not anthropogenic CO_2.

Courtney (2008) concludes that temperature can change carbon desorption from the oceans,

> "Qualitative consideration of the carbon cycle suggests the carbon cycle cannot be very sensitive to relatively small disturbances such as the present anthropogenic emissions of CO_2. However, the system could be quite sensitive to temperature. Indeed, the considerations suggest that the relatively large increase of CO_2 concentration in the atmosphere in the twentieth century is likely to have been caused by the increased mean temperature that preceded it. The main cause may be desorption from the oceans. The observed time lag of half a century is not surprising."
>
> "Assessment of this conclusion requires a quantitative model of the carbon cycle, but such a model cannot be constructed because the rate constants are not known for mechanisms operating in the carbon cycle."

Upon reviewing this paper's Preprint, Courtney (2019) wrote:

> "Your "physics model" quantifies the anthropogenic and natural contributions to changes in atmospheric CO_2 concentration without need for knowledge of rate constants for individual mechanisms. This is a breakthrough in understanding which [others] and myself all failed to make."

6.3 COVID-19 CO_2 data suggest the increase is natural

The Global Monitoring Laboratory (2020a, b) asks if the 2020 emissions reductions due to COVID-19 lowered the CO_2 level. The following approximate numbers illustrate how to answer this question.

The physics carbon cycle model calculates that reducing human CO_2 emissions by 20% in 2020 would reduce the CO_2 level from 33.5 ppmv in 2020 to 33.1 ppmv in 2021, which is unmeasurable, especially when added to an increasing natural CO_2 level.

However, if human carbon caused all the CO_2 increase of 133 ppmv, as the IPCC assumes, then reducing human CO_2 emissions by 20% would reduce the CO_2 level from 414.0 ppmv in 2020 to 412.4 ppmv in 2021, according to the physics model. This reduction would be measurable.

The Global Monitoring Laboratory (2020b) data show the COVID-19 decrease in human CO_2 did not affect the annual increase in CO_2, which contradicts IPCC's assumption.

6.4 The physics model will help future research

The physics model is a basis for future carbon cycle research. It can include more levels for land, atmosphere, and oceans to better simulate the carbon cycle. It can be adapted into a professional software platform to use monthly time steps and other numerical methods to improve its calculations.

Conclusions

IPCC's basic climate change assumption is natural CO_2 stayed constant after 1750 as human CO_2 causes all (or dominates) the increase in atmospheric CO_2.

To support its basic assumption, the IPCC claims "The removal of human-emitted CO_2 from the atmosphere by natural processes will take a few hundred thousand years (high confidence)." But the human carbon e-time must equal the natural carbon e-time because human and natural CO_2 molecules are identical.

The $^{14}CO_2$ e-time, derived from $\delta^{14}C$ data, is 10.0 years, making the $^{12}CO_2$ e-time less than 10 years. The IPCC says the $^{12}CO_2$ e-time is about 4 years and IPCC's carbon cycle uses 3.5 years.

After the bomb tests, $\delta^{14}C$ returned to its original balance level of zero even as $^{12}CO_2$ increased. This suggests the added $^{12}CO_2$ came from a natural source.

The physics model calculates, deductively, the consequences of IPCC's natural carbon cycle data. The physics model first replicates IPCC's natural carbon cycle. Then, using the same IPCC data, it calculates that human carbon has added only 33 [24-48] ppmv to the atmosphere as of 2020, which means natural carbon has added 100 ppmv. The physics model further calculates if human CO_2 emissions had stopped at the end of 2020, the human CO_2 level of 33 ppmv would fall to 10 ppmv by 2100.

The IPCC argues the *absence* of ice-core data – that might show the natural CO_2 level was greater than 280 ppmv before 1750 – supports its basic assumption. But the physics model shows IPCC's basic assumption, and therefore IPCC's ice-core assumption, contradict IPCC's natural carbon cycle data.

Data and Calculations Availability
Berry, E.X: BerryCarbonCycle_2021. Excel file that includes all the data and numerical calculations described in this paper. https://edberry.com/wp-content/uploads/Climate/BerryCarbonCycle-Atmosphere-2021.xlsx

Open discussion for readers of this paper: https://edberry.com/blog/climate/climate-physics/the-impact-of-human-co2-on-atmospheric-co2/

Guest editor: Jan-Erik Solheim, Referee: Stein Storlie Bergsmark

Acknowledgments:
The author thanks the following for their helpful comments during the preparation of this paper (without implying they agree with everything in this paper): William Happer and W.A. van Wijngaarden for their thorough review of the math and numerical calculations; and Hermann Harde, Richard Courtney, Tom Sheahen, Stein Bergsmark, Jan-Erik Solheim, Chuck Wiese, Nils-Axel Mörner, Camille Veyres, Laurence Gould, Jock Allison, Simon Aegerter, John Shanahan, John Droz, Jr., Alan Falk, Allan MacRae, Andre De Rick, Anthony Cox, Bob Webster, Case Smit, CD Marshall, Chic Bowdrie, Christopher Monckton of Brenchley, Dale Mullen, David Ayre, David Houghton, Dennis G. Sandberg, H. Douglas Lightfoot, Jacques- Raymond Børeng, JD Walker, John Finn, John Knipe, Larry Lazarides, Leif Asbrink, Mark Harvey, Marie Moranne, Massimo Polo, Mathew Fagan, Michael Beattie, Ralph Alexander, Ron Pritchett, Stephen Paul Anderson, Tim C., William Laser, and Ron Clutz for their valuable suggestions.

Funding: This research did not receive any specific grant from funding agencies in the public, commercial, or not-for-profit sectors.

Conflicts of Interest:
The Author declares he has no known competing financial interests or personal relationships that could have appeared to influence the work reported in this paper.

References

Andrews, D.E. 2020: **Correcting an Error in Some Interpretations of Atmospheric ^{14}C Data**, Earth Sciences, 9(4), pp. 126-129, https://doi:10.11648/j.earth.20200904.12. http://www.sciencepublishinggroup.com/j/earth

Ballantyne, A.P., Alden, C.B., Miller, J.B., Tans, P.P., and White, J.W.C. 2012: **Increase in observed net carbon dioxide uptake by land and oceans during the past 50 years**, *Nature*

488, pp. 70-73. doi:10.1038/nature11299. https://www.nature.com/articles/nature11299

Beck, E. 2007: **180 years of atmospheric CO_2 gas analysis by chemical methods**. *Energy & Environment*. Volume 18, No. 2. https://21sci-tech.com/Subscriptions/Spring%202008%20ONLINE/CO_2_chemical.pdf https://doi.org/10.1260/095830507780682147

Berry, E.X. 2019: **Human CO_2 emissions have little effect on atmospheric CO_2**. *International Journal of Atmospheric and Oceanic Sciences*. Volume 3, Issue 1, June, pp 13-26. http://www.sciencepublishinggroup.com/journal/paperinfo?journalid=298&doi=10.11648/j.ijaos.20190301.13

Berry, E.X. 1967: **Cloud droplet growth by collection**. J. Atmos. Sci. 24, 688-701. DOI: https://doi.org/10.1175/1520-0469(1967)024<0688:CDGBC>2.0.CO;2

Berry, E.X. 1969: **A mathematical framework for cloud models**. J. Atmos. Sci. 26, 109-111. https://moam.info/a-mathematical-framework-for-cloud-models-edberrycom_59a6a1c81723dd0c40321bda.html

Berry, E. X and Reinhardt, R.L. 1974a: **An analysis of cloud drop growth by collection. Part I. Double distributions**. *J. Atmos. Sci.*, **31,** 1814–1824. https://journals.ametsoc.org/view/journals/atsc/31/7/1520-0469_1974_031_1814_aaocdg_2_0_co_2.xml

Berry, E. X and Reinhardt, R.L. 1974b: **An analysis of cloud drop growth by collection. Part II. Single initial distributions.** *J. Atmos. Sci.*, **31,** 1825–1831. https://journals.ametsoc.org/view/journals/atsc/31/7/1520-0469_1974_031_1825_aaocdg_2_0_co_2.xml

Berry, E. X and Reinhardt, R.L. 1974c: **An analysis of cloud drop growth by collection. Part III. Accretion and self-collection**. *J. Atmos. Sci.*, **31,** 2118–2126. https://journals.ametsoc.org/view/journals/atsc/31/8/1520-0469_1974_031_2118_aaocdg_2_0_co_2.xml

Berry, E. X and Reinhardt, R.L. 1974d: **An analysis of cloud drop growth by collection. Part IV. A new parameterization.** *J. Atmos. Sci.*, **31,** 2127–2135. https://journals.ametsoc.org/view/journals/atsc/31/8/1520-0469_1974_031_2127_aaocdg_2_0_co_2.xml

Caillon, N., Severinghaus, J.P., Jouzel. J., Barnola, J., Kang, J., and Lipenkov, V.Y., 2003: **Timing of atmospheric CO2 and Antarctic temperature changes across Termination III**. *Science*, Vol. 299, No. 5613. https://www.science.org/doi/10.1126/science.1078758

Courtney, R.S. 2008: **Limits to existing quantitative understanding of past, present and future changes to atmospheric CO_2 concentration**. International Conference on Climate Change, New York. https://www.heartland.org/multimedia/videos/richard-courtney-iccc1. https://edberry.com/blog/climate/climate-physics/limits-to-carbon-dioxide-concentation/

Courtney, R.S. 2019: *Public email communication* to global-warming-realists@googlegroups.com, 21 November 2019. https://edberry.com/blog/climate/climate-physics/preprint3/

Essenhigh, R.E. 2009: **Potential dependence of global warming on the residence time (RT) in the atmosphere of anthropogenically sourced CO_2**. *Energy Fuel* 23, pp. 2773-2784. https://pubs.acs.org/doi/abs/10.1021/ef800581r

Etheridge, D.M., Steele, L.P., Langenfelds, R.L., Francey, R.J., Barnola, J.-M., and Morgan, V.I. 1996: **Natural and anthropogenic changes in atmospheric CO_2 over the last 1000 years from air in Antarctic ice and firn**. *Journal of Geophysical Research*. 101:4115-4128. https://www1.ncdc.noaa.gov/pub/data/paleo/icecore/antarctica/law/law_CO_2.txt

Fischer, H., Wahlen, M., Smith, J., Mastroianni, D., and Deck, B., 1999: **Ice core records of atmospheric co2 around the last three glacial terminations**. *Science*, Vol. 283, No. 5408. https://www.science.org/doi/10.1126/science.283.5408.1712

Gilfillan D., Marland, G., Boden, T., and Andres, R. 2020: **Global, Regional, and National Fossil-Fuel CO_2 Emissions: 1751-2017**. CDIAC-FF, Research Institute for Environment, Energy, and Economics, Appalachian State University. doi:10.15485/1712447.

Global Monitoring Laboratory. 2020a: **Trends in Atmospheric Carbon Dioxide: Monthly Average Mauna Loa CO_2.** Earth Systems Research Laboratories. https://www.esrl.noaa.gov/gmd/ccgg/trends/

Global Monitoring Laboratory. 2020b: **Can we see a change in the CO_2 record because of COVID-19?** Earth Systems Research Laboratories. https://www.esrl.noaa.gov/gmd/ccgg/covid2.html

Gruber, N., Clement, D., Carter, B., Feely, R., van Heuven S., Hoppema, M., Ishii, M., Key, R., Kozyr, A., Lauvset, S., Lo Monaco, C., et al. 2019: **The oceanic sink for anthropogenic CO_2 from 1994 to 2007.** Science, 15. March (363) pg. 1193. https://www.sciencemagazinedigital.org/sciencemagazine/15_march_2019_Main/MobilePagedArticle.action?articleId=1472451#articleId1472451

Happer, W., and van Wijngaarden, W.A. 2020: *Physics Rate Equations*. Princeton U. Princeton, NJ, USA. (Unpublished Work)

Harde, H. 2017: **Scrutinizing the carbon cycle and CO_2 residence time in the atmosphere**. Global and Planetary Change. 152, 19-26. https://www.sciencedirect.com/science/article/abs/pii/S0921818116304787

Harde, H. 2019: **What Humans Contribute to Atmospheric CO_2: Comparison of Carbon Cycle Models with Observations**. International Journal of Earth Sciences. Vol. 8, No. 3, pp. 139-159. http://www.sciencepublishinggroup.com/journal/paperinfo?journalid=161&doi=10.11648/j.earth.20190803.13

Harde, H. and Salby, M. L. 2021: **What Controls the Atmosphere CO_2 Level?** Science of Climate Change, Vol. 1, No. 1, August 2021, pp. 54-69. https://scienceofclimatechange.org/wp-content/uploads/Volume-1.1-August-2021.pdf

Hua, Q., Barbetti, M., and Rakowski, A.Z. 2013: **Atmospheric radiocarbon for the period 1950–2010.** Radiocarbon. Vol 55, pp. 2059–2072. Table S2c. https://doi.org/10.2458/azu_js_rc.v55i2.16177

Humlum, O., Stordahl, K., and Solheim, J.E. 2013: **The phase relation between atmospheric CO_2 and global temperatures.** Global and Planetary Change, 100, pp 51-69. https://www.sciencedirect.com/science/article/abs/pii/S0921818112001658

IPCC, 2013: Ciais, P., Sabine, C., Bala, G., Bopp, L., Brovkin, V., Canadell, J., Chhabra, A., DeFries, R., Galloway, J., Heimann, M., Jones, C., Le Quéré, C., Myneni, R.B., Piao, S., and Thornton, P. 2013: **Carbon and Other Biogeochemical Cycles.** In: Climate Change 2013: *The Physical Science Basis. Contribution of Working Group I to the Fifth Assessment Report of the Intergovernmental Panel on Climate Change* [Stocker, T.F., Qin, D., Plattner, G.-K., Tignor, M., Allen, S.K. Boschung, J., Nauels, A., Xia, Y., Bex, V., and Midgley, P.M. (eds.)]. Cambridge University Press, Cambridge, United Kingdom and New York, NY, USA. https://www.ipcc.ch/site/assets/uploads/2018/02/WG1AR5_Chapter06_FINAL.pdf

IPCC. 2007: *Climate Change 2007 - The Physical Science Basis. Contribution of Working Group 1 to the Fourth Assessment Report of the IPCC***.** Annex 1: Glossary: Lifetime. https://www.ipcc.ch/site/assets/uploads/2018/02/ar4-wg1-annexes-1.pdf

Jaworowski, Z. 2007: CO_2*:* **The greatest scientific scandal of our time.** 21st CENTURY Science & Technology. https://21sci-tech.com/Articles%202007/20_1-2_CO_2_Scandal.pdf

Joos, F. 2002: **Parameters for tuning a simple carbon cycle model.** UNFCCC. https://unfccc.int/resource/brazil/carbon.html

Joos, F., Roth, R., Fuglestvedt, J.S., Peters, G.P., Enting, I.G., von Bloh, W., Brovkin, V., Burke, E.J., Eby, M., Edwards, N.R., et al. 2013: **Carbon dioxide and climate impulse response functions for the computation of greenhouse gas metrics: a multi-model analysis**. Atmos. Chem. Phys. 13, 2793-2825. doi:10.5194/acpd-12-19799-2012, https://acp.copernicus.org/articles/13/2793/2013/acp-13-2793-2013.pdf

Keeling, C.D., Piper, S.C., Bacastow, R.B., Wahlen, M., Whorf, T.P., Heimann, M., and Meijer, H.A. 2001: **Exchanges of atmospheric CO_2 and 13CO_2 with the terrestrial biosphere and oceans from 1978 to 2000**. I. Global aspects, SIO Reference Series, No. 01-06, Scripps Institution of Oceanography, San Diego. 88 pages. https://scrippsCO_2.ucsd.edu/data/atmospheric_CO_2/primary_mlo_CO_2_record.html

Kohler, P., Hauck, J., Volker, C., Wolf-Gladrow, D.A., Butzin, M., Halpern, J.B., Rice, K., and Zeebe, R.E. 2017: **Comment on 'Scrutinizing the carbon cycle and CO_2 residence time in the atmosphere' by H. Harde**. Global and Planetary Change. 2017. https://www.soest.hawaii.edu/oceanography/faculty/zeebe_files/Publications/KoehlerGPC17.pdf

Kouwenberg, L.L.R. 2004: *Application of Conifer Needles in the Reconstruction of Holocene CO_2 Levels***.** Ph.D. Thesis. *Univ. Utrecht*, Netherlands. https://dspace.library.uu.nl/bitstream/handle/1874/243/full.pdf

Kouwenberg, L., Wagner, R., Kürschner, W., and Visscher, H. 2005a: Atmospheric CO_2 fluctuations during the last millennium reconstructed by stomatal frequency analysis of Tsuga heterophylla needles. *Geology*, 33 (1): 33–36. https://doi.org/10.1130/G20941.1

Kouwenberg, L., Wagner, R., Kürschner, W., and Visscher, H. 2005b: CO_2 fluctuations during the last millennium reconstructed by stomatal frequency analysis. https://plantstomata.wordpress.com/2019/03/18/CO_2-fluctuations-during-the-last-millenium-reconstructed-by-stomatal-frequency-analysis/

Kuo, C., Lindberg, C., and Thomson, D. 1990: **Coherence established between atmospheric carbon dioxide and global temperature.** Nature 1990, 343, 709–714. https://www.nature.com/articles/343709a0

MacRae, A. 2008: ***CO_2 is not the primary cause of global warming: the future cannot cause the past.*** Icecap. http://icecap.us/images/uploads/CO_2vsTMacRae.pdf)

Munshi, J. 2015a: **Responsiveness of Atmospheric CO_2 to Anthropogenic Emissions: A Note** (August 21, 2015). Available at SSRN: https://ssrn.com/abstract=2642639 or http://dx.doi.org/10.2139/ssrn.2642639

Munshi, J. 2015b: **Decadal Fossil Fuel Emissions and Decadal Warming: A Note** (September 19, 2015). Available at SSRN: https://ssrn.com/abstract=2662870 or http://dx.doi.org/10.2139/ssrn.2662870

Quirk, T. 2009: **Sources and sinks of CO_2**. Energy & Environment. Volume: 20 Issue: 1, pp. 105-121. https://journals.sagepub.com/doi/10.1260/095830509787689123

Quirk, T. and Asten, M. 2022: **Atmospheric CO_2 source analysis**. Melbourne, Victoria, Australia. (Preprint to be submitted) https://edberry.com/blog/climate/climate-physics/preprint-atmospheric-co2-source-analysis/

Revelle, R., and Suess, H. 1957: **CO_2 exchange between atmosphere and ocean and the question of an increase of atmospheric CO_2 during past decades**. Tellus. 9: 18-27. https://onlinelibrary.wiley.com/doi/epdf/10.1111/j.2153-3490.1957.tb01849.x

Rorsch, A., Courtney, R.S., and Thoenes, D. 2005: **The Interaction of Climate Change and the CO_2 Cycle.** Energy & Environment. Volume 16, No 2. https://journals.sagepub.com/doi/pdf/10.1260/0958305053749589

Salby, M.L. 2012: *Physics of the Atmosphere and Climate*. Cambridge University Press. 666 pp. https://www.amazon.com/Physics-Atmosphere-Climate-Murry-Salby/dp/0521767180/ref=mt_hardcover?_encoding=UTF8&me=.

Salby, M.L. 2013: *CO_2 follows the Integral of Temperature*, video. http://edberry.com/blog/climate-physics/agw-hypothesis/murry-salby-CO_2-follows-integral-of-temperature/.

Salby, M.L. and Harde, H. 2021: **Control of Atmospheric CO_2: Part I: Relation of Carbon 14 to the Removal of CO_2**. Science of Climate Change, 1, no.2. https://doi.org/10.53234/scc202112/210

Segalstad, T.V. 1998: **Carbon cycle modelling and the residence time of natural and anthropogenic atmospheric CO_2: on the construction of the Greenhouse Effect Global Warming dogma.** In: Bate, R. (Ed.): Global warming: the continuing debate. ESEF, Cambridge, U.K. (ISBN 0952773422): 184-219. http://www.CO_2web.info/ESEF3VO2.pdf

Siegenthaler, U. and Joos, F. 1992: **Use of a simple model for studying oceanic tracer distributions and the global carbon cycle.** *Tellus*, 44B, 186-207; https://onlinelibrary.wiley.com/doi/epdf/10.1034/j.1600-0889.1992.t01-2-00003.x

Skrable, K., and French, C.G. 2022: **World atmospheric CO_2, its ^{14}C specific activity, anthropogenic-fossil component, non-fossil component, and emissions (1750 - 2018).** (Accepted for Publication in the Health Physics Journal in 2022)

Starr, C. 1992: **Atmospheric CO_2 residence time and the carbon cycle**. Science Direct, 18, 12, pp. 1297-1310; https://www.sciencedirect.com/science/article/abs/pii/0360544293900178

Strassmann, K.M., Joos, F. 2018: **The Bern Simple Climate Model (BernSCM) v1.0: an extensible and fully documented open-source re-implementation of the Bern reduced-form model for global carbon cycle-climate simulations.** Geosci. Model Dev, 11, 1887-1908. https://gmd.copernicus.org/articles/11/1887/2018/

Stuiver, M. and Polach, H. 1977: **Discussion: Reporting of 14C data.** Radiocarbon, 19(3), 355-363. extension://bfdogplmndidlpjfhoijckpakkdjkkil/pdf/viewer.html?file=http%3A%2F%2Fwww.imprs-gbgc.de%2Fuploads%2FRadiocarbonSchool%2FReading%2Fstuier_polach.pdf

Turnbull, J.C., Mikaloff Fletcher, S.E., Ansell, I., Brailsford, G.W., Moss, R.C., Norris, M.W., and Steinkamp, K. 2017: **Sixty years of radiocarbon dioxide measurements at Wellington, New Zealand: 1954–2014.** Atmos. Chem. Phys., 17, pp. 14771–14784. https://doi.org/10.5194/acp-17-14771-2017

Van Langenhove, A. 1986: **Isotope effects: definitions and consequences for pharmacologic studies**. J. Clinical Pharmacology. https://doi.org/10.1002/j.1552-4604.1986.tb03545.x

The application of Classical simplicity to present-day mathematical problems

Correspondence to moncton@mail.com

Vol. 1.2 (2021)

pp. 251-270

Christopher Monckton of Brenchley

Gloucestershire, England

Abstract

Classical mathematicians valued simplicity, settling such complex questions as the irrationality of √2 by elementary methods. Today, too, refractory problems in pure as well as applied mathematics are resoluble by simple, Classical methods. For instance, though the Goldbach, Twin-Prime and Cousin-Prime Conjectures have withstood proof for 2-3 centuries, they are here proven by a method two millennia old. Likewise, a simple method shows that most lives lost in the COVID-19 could have been saved by a staged treatment protocol combining vaccines with off-label medications each proven to reduce severe outcomes somewhat. Simple mathematics logically applied also defeat the principal arguments for mitigating global warming – the threat of dangerously rapid warming and the cost of inaction. After correction of a grave error of physics that arose in the 1980s, when feedback formulism borrowed from control theory was misunderstood, global warming will be small enough to be net-beneficial. It is proven by Classical simplicity that Western net-zero emissions would mitigate warming undetectably by 2050, at disproportionate cost. The rational economic choice is to do nothing.

Keywords: Sieve of Eratosthenes; binary Goldbach conjecture; twin-prime conjecture; cousin-prime conjecture; COVID-19; global warming; spinning reserve; freedom equation.

Submitted ?-?-2021, Accepted 20-12-2021. https://doi.org/10.53234/SCC202112/33

Introduction: Some paragons of Classical simplicity

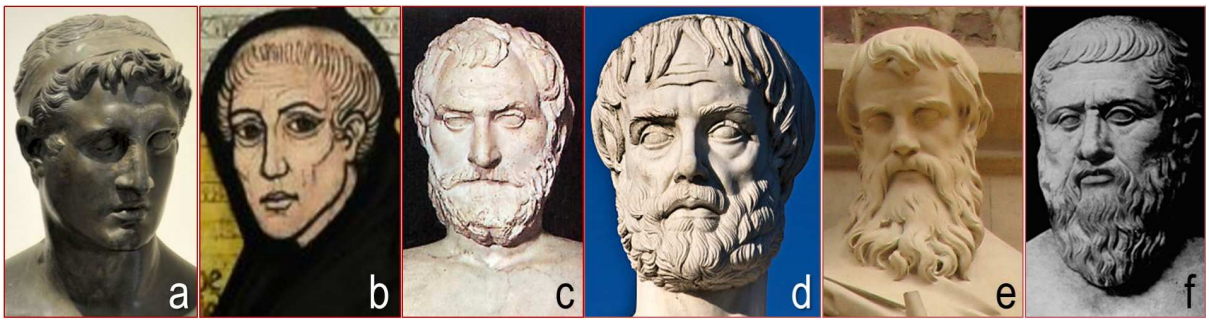

Figure 1: a) Callimachus; b) William of Ockham; c) Thales; d) Euclid; e) Aristotle; f) Eratosthenes

Callimachus, the librarian of Alexandria in the early third century BCE (Fig. 1a), wrote 800 books. Few survive. They were probably short: he is known for his epigram *μεγά βίβλιον μεγά κάκον* – the bigger the book the badder. By contrast, the first of three volumes of the *Sixth* and latest *Assessment Report* of the Intergovernmental Panel on Climate Change (IPCC 2021) has almost 4000 pages.

William of Ockham, the 14th-century Cambridge philosopher (Fig. 1b), is celebrated for his

simplicity principle: *essentia non sunt multiplicanda praeter necessitatem.* Where several explanations for a phenomenon compete, the least complicated is generally preferable. The art of Classical mathematics is not to find the most complex non-solution to a problem but to find the least complex solution. That straightforward principle may be usefully applied – but is not always currently applied – to apparently complex questions such as the COVID-19 pandemic and global warming.

Thales of Miletus (624-545 BCE: fig. 1c), the founder of the scientific method, is known for his theorem, an elegantly simple proof – here expressed in just two dozen words that will fit on a beermat (Fig. 2) – that the diameter of a circle subtends a right-angle to any point on the circumference.

Aristotle (384-322 BCE: Fig. 1d), the most influential of polymaths, studied biology, botany, chemistry, ethics, history, logic, metaphysics, rhetoric, psychology, philosophy of science, physics, poetics, political theory and zoology. At Plato's Academy, Aristotle wrote the *Topics,* on how to construct one's own argument, and the *Refutations of the Sophists,* on how to detect the dozen commonest logical fallacies in an interlocutor's argument. From these fallacies, Aristotle derived formal logic, in which an argument comprises one or more declarative premises leading to a conclusion. If the premises properly entail the conclusion, the argument is valid; if they are all true, it is sound and its conclusion is true. Aristotle codified the art and science of logic in his *Prior* and *Posterior Analytics.*

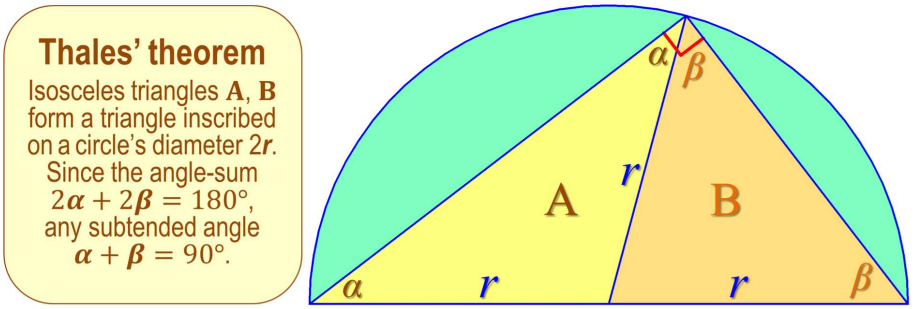

Figure 2: Beermat proof (left) of Thales' theorem (right)

Following Aristotle's logical method, Euclid (325-265 BCE: Fig. 1e) wrote the *Elements,* in which each new proposition was logically derived from a few axioms or from earlier propositions. His proof by contradiction (Proposition 117) that √2 is irrational is elegant in its simplicity. Let $\sqrt{2} = p_1/q_1$, so that $2 = p_1^2/q_1^2$. Since $2 \mid p_1$ and $2 \mid q_1$, let $p_2 = p_1/2$ and $q_2 = q_1/2$, so that $2 = p_2^2/q_2^2$, and so *ad infinitum.* But rational fractions cannot be indefinitely reduced. Therefore, $\sqrt{2}$ is irrational.

Euclid's beermat proof (Proposition 20) of the infinitude of the primes is also simple. Assume a greatest prime p_n. Let $P = (\prod_{i=1}^{n} p_i)$, and let $Q = P + 1$. Since each prime $p_i \in \{p_1, p_2 \ldots p_n\} \mid P$ by definition, $p_i \nmid Q$. Then Q is either a prime exceeding p_n or a composite each of whose prime factors exceeds p_n, so that that p_n cannot be the greatest prime.

Example: For $n = 4,\ p_n = 7$, so that $P = 2 \cdot 3 \cdot 5 \cdot 7 = 210$ and $P + 1 = Q =$ ($211 \in$ P) > 7.

Often even the most apparently complex and refractory problems, whether theoretical (such as the binary Goldbach conjecture in number theory), or practical (such as the COVID-19 pandemic or the climate question), may be usefully addressed by the combined simple mathematics and logic that were the Classical world's down-to-Earth gift to us. Each of these three problems will be subjected to the very simplest approaches: yet robust and reliable results will emerge. One of the many virtues of Classical simplicity is that results simply derived are not only more comprehensible than results derived by complex methods but also less error-prone, more tamper-proof and likelier to prove sound.

First, the Goldbach conjecture that any composite is the mean of two primes will be proven by the use of the sieve of Eratosthenes of Syene (Fig. 1f: 275-194 BCE), the polymath librarian of

Alexandria. Among Eratosthenes' many contributions to learning was his estimation of the Earth's circumference to within 4% by a simple method. He observed that at Syene (today Aswān), the Sun's rays fell vertically down a well-shaft on the summer solstice, but that in Alexandria on the same day the solar zenith angle was approximately one-fiftieth of a circle (7.2°).

Eratosthenes, who had earlier correctly concluded that the Sun was so large and so distant that its rays were effectively parallel, thus determined that the Earth's circumference was 50 times the distance from Syene to Alexandria. In reality, Syene does not fall exactly on the tropic of Cancer; it does not lie directly south of Alexandria, but SSE; and the angle subtended to the Earth's center by the great-circle arc between the two cities is more like 7.5° than 7.2°. Eratosthenes later revised his estimate to bring it within 1% of the true circumference – a profound result obtained by a simple method.

By the sieve of Eratosthenes, all multiples of successive primes $2, 3, 5, \ldots < p_x : p_x^2 \geq 2m - 3$ are eliminated from a given sequence of odd integers $3 \leq m \leq 2m - 3$. All surviving integers are primes.

Next, by a simple method the proposition will be evaluated that the COVID-19 pandemic may be ended by a simple multi-treatment protocol (to be applied only by a doctor) using safe, inexpensive and immediately-available pre-existing medications, whether or not accompanied by vaccination.

Finally, Classically simple approaches will be deployed to address three notions central to the climate-change narrative: that there is an "expert consensus" on climate change; that unmitigated anthropogenic warming will be large enough and rapid enough to be catastrophic; and that the welfare benefit of emissions abatement will exceed the substantial welfare loss. Nothing more complex than an ability to count and some simple logic will be needed, and yet powerful, policy-relevant conclusions will be derived. No small advantage of this approach is that even Western politicians – perhaps less numerate and less scientifically literate today than at any time since the Dark Ages – may perhaps be able to comprehend the simple arguments that will be set forth here.

2. Proof of the binary Goldbach conjecture

In 1742, Goldbach suggested the ternary conjecture (proven by Helfgott 2013) that any odd integer $2m + 1 \geq 7$ is the sum of three primes. Euler replied stating the binary conjecture (Waring 1770) that any even integer $2m \geq 4$ is the sum of two primes. Popper (1963) wrote: "We don't know: perhaps we may never know, and perhaps we can never know" its truth. Schnirelman (1930) showed that any $2m$ is the sum of ≤ 20 primes. Vinogradov (1937) and Chen Jing Run (1973) showed that any sufficiently large $2m$ is, respectively, the sum of ≤ 3 primes and of a prime and a composite with ≤ 2 prime factors.

2.1 . The method in outline

For any $2m \geq 6$, all the odd integers $3 \leq s \leq 2m - 3$ form $q = \lceil m/2 - 1 \rceil$ distinct partitions $\{s_1, s_2\}: s_1 + s_2 = 2m$. For p_x the greatest odd prime such that $p_x^2 \leq 2m - 3$, any $s : p_n \nmid s$ is prime for all primes $p_x \geq p_n \geq 3$. Partitions $\{s_1, s_2\} : p_n \mid s_1 s_2$ are successively eliminated in descending order $x \geq n \geq 1$. After the final sifting stage $n = 1$, the estimated minimum quantity of survivors $E_1 = |E_2/3| = |q/p_x|$ cannot exceed the true count T_1. Survivors will be Goldbach partitions (s_1, s_2 both prime). For all $2m : p_x \geq 5$, $T_1 \geq E_1 = |E_2/3| \geq |q/p_x| \geq |q_{\min}/p_x| \geq |(p_x - 1)/4| > 0$. Since Goldbach partitions also exist for all $2m : p_x = 2,3$, they exist for all $2m \geq 4$.

> Lemma 1: An integer $s < p_{x+1}^2$ lacking any prime factor $p_n \leq p_x$ is itself prime.
> *Proof:* For s the product of ≥ 2 prime factors each $> p_x$, $s > p_{x+1}^2$, contrary to the definition of *s*.

2.2 The partition count q for any even integer $2m \geq 12$

For any $2m \geq 12$, Eq. (1) gives the partition count $q : 3 \leq s_1 \leq s_2 \leq 2m - 3$. For any greatest prime divisor $3 \leq p_x \leq \infty$, Eq. (2) gives the least and greatest integers $2m_{\min}$, $2m_{\max}$, while Eq. (3) gives the partition counts $q_{\min}$, $q_{\max}$ such that, by Lemma 1, any odd integer $3 \leq s \leq 2m - 3$ not divisible by any odd prime $p_n \leq p_x$ will itself be prime. Given the infinitude of the primes (Euclid, Prop. 20), continuing *ad infinitum* will encompass all $2m \geq 12$. *Example:* See Table 1.

$$q = \lceil m/2 - 1 \rceil. \tag{1}$$

$$2m_{\min} = p_x^2 + 3 \quad | \quad q_{\min} = (m_{\min} - 2)/2 = (p_x^2 - 1)/4 \tag{2}$$

$$2m_{\max} = p_{x+1}^2 + 1 \quad | \quad q_{\max} = (m_{\max} - 1)/2 = (p_{x+1}^2 - 1)/4 \tag{3}$$

Remark: For any given q, two values of $2m$ exist. *Example:* For $q = 16$, $2m$ may be 66, with partitions from $\{3, 63\}$ to $\{33, 33\}$, or 68, with partitions from $\{3, 65\}$ to $\{33, 35\}$.

Table 1. Integers $2m_{\min}, 2m_{\max}$ and corresponding partition counts $q_{\min}, q_{\max}$ for $x \leq 6$

x	p_x	$2m_{\min}$	$q_{\min}$	p_{x+1}	$2m_{\max}$	$q_{\max}$
1	3	$3^2 + 3 = 12$	$(3^2 - 1)/4 = 2$	5	$5^2 + 1 = 26$	$(5^2 - 1)/4 = 6$
2	5	$5^2 + 3 = 28$	$(5^2 - 1)/4 = 6$	7	$7^2 + 1 = 50$	$(7^2 - 1)/4 = 12$
3	7	$7^2 + 3 = 52$	$(7^2 - 1)/4 = 12$	11	$11^2 + 1 = 122$	$(11^2 - 1)/4 = 30$
4	11	$11^2 + 3 = 124$	$(11^2 - 1)/4 = 30$	13	$13^2 + 1 = 170$	$(13^2 - 1)/4 = 42$
5	13	$13^2 + 3 = 172$	$(13^2 - 1)/4 = 42$	17	$17^2 + 1 = 290$	$(17^2 - 1)/4 = 72$
6	17	$17^2 + 3 = 292$	$(17^2 - 1)/4 = 72$	19	$19^2 + 1 = 362$	$(19^2 - 1)/4 = 90$

2.2 The sieve of Eratosthenes

The sieve is applied x times, taking each odd prime $p_x \geq p_n \geq p_1 = 3$ in descending order as the divisor, to eliminate all partitions $\{s_1, s_2\} : p_n \mid s_1\, s_2$. Where p_n is not common to both s_1 and s_2, after any sifting the estimated minimum survivors E_n will be $\lfloor E_{n+1}(p_n - 2)/p_n \rfloor$; E_n will be greater where $p_n \mid s_1$ and $p_n \mid s_2$. Then, after the final sifting stage, the true Goldbach count T_1 will be at least equal to $E_1 = \lfloor E_2(p_1 - 2)/p_1 \rfloor = \lfloor E_2/3 \rfloor = \lfloor q/p_x \rfloor \geq \lfloor q_{\min}/p_x \rfloor \geq \lfloor (p_x - 1)/4 \rfloor > 0$.

Example: For $m = 34$, $p_x = 7$. Then the successive prime divisors p_3, p_2, p_1 are 7,5,3 (Table 2). Dispose the odd integers $3 \leq s \leq (2m - 3 = 65)$ in $q = 16$ partitions $\{s_1, s_2\} : s_1 + s_2 = 2m$ from $\{3, 65\}$ to $\{33, 35\}$. After each sifting, $T_n \geq E_n$.

Table 2: The Sieve of Eratosthenes applied to 16 partitions $\{s_1, s_2\}$ for $m = 34 \Rightarrow q = 16$

	s_1	[3]	[5]	[7]	9	11	13	15	17	19	21	23	25	27	29	31	33	Survivors
n	s_2	65	63	61	59	57	55	53	51	49	47	45	43	41	39	37	35	$T_n \geq E_n$
3: $p_x = 7$			7							7	7						7	$12 \geq \lfloor 16\ (5/7) \rfloor = 11$
2: $p_2 = 5$		5					5	5				5	5				5	$7 \geq \lfloor 11\ (3/5) \rfloor = 6$
1: $p_1 = 3$			3		3	3		3	3		3	3		3	3		3	$2 = \lfloor 6\ (1/3) \rfloor = 2$

2.2 Relationship between true (T_1) *and estimated minimum* (E_1) *survivors*

For all $x \geq 4 \Rightarrow p_x \geq 11$, $E_1 = \lfloor E_2/3 \rfloor = \lfloor q/p_x \rfloor$ possesses certain implicit additional composite-denominated proper fractions, e.g. **7/9** and **13/15** in Eqs. (5-6), that are absent from T_1 in Eq. (4).

$$T_1 \geq \left\lfloor \left\lfloor \left\lfloor \left\lfloor \left\lfloor \left\lfloor \left\lfloor q \frac{p_x-2}{p_x} \right\rfloor \frac{p_x-4}{p_x-2} \right\rfloor \cdots \frac{15}{17} \right\rfloor \frac{11}{13} \right\rfloor \frac{9}{11} \right\rfloor \frac{5}{7} \right\rfloor \frac{3}{5} \right\rfloor \frac{1}{3} \right\rfloor \tag{4}$$

$$\geq E_1 = \left\lfloor \left\lfloor \left\lfloor \left\lfloor \left\lfloor \left\lfloor \left\lfloor q \frac{p_x-2}{p_x} \right\rfloor \frac{p_x-4}{p_x-2} \right\rfloor \cdots \frac{15}{17} \right\rfloor \frac{\mathbf{13}}{\mathbf{15}} \right\rfloor \frac{11}{13} \right\rfloor \frac{9}{11} \right\rfloor \frac{\mathbf{7}}{\mathbf{9}} \right\rfloor \frac{5}{7} \right\rfloor \frac{3}{5} \right\rfloor \frac{1}{3} \right\rfloor \tag{5}$$

$$= \left\lfloor q \frac{p_x-2}{p_x} \frac{p_x-4}{p_x-2} \cdots \frac{15}{17} \frac{\mathbf{13}}{\mathbf{15}} \frac{11}{13} \frac{9}{11} \frac{\mathbf{7}}{\mathbf{9}} \frac{5}{7} \frac{3}{5} \frac{1}{3} \right\rfloor = \left\lfloor \frac{q}{p_x} \right\rfloor \tag{6}$$

$$\geq \left\lfloor \frac{q_{\min}}{p_x} \right\rfloor = \left\lfloor \frac{p_x^2-1}{4p_x} \right\rfloor \geq \left\lfloor \frac{p_x-1}{4} \right\rfloor > 0 \quad | \quad p_x \geq 5 \tag{7}$$

By the prime number theorem, the fraction of composites among the integers $\leq 2m$ is approximately $1 - 1/\ln(2m)$, growing with $2m$ as the fraction $1/\ln(2m)$ of primes declines. The composite-denominated fractions in E_1 diminish E_1 compared with T_1. Then $T_1 - E_1$ will tend to increase for each additional such fraction in E_1 as m, q, p_x increase (Fig. 3).

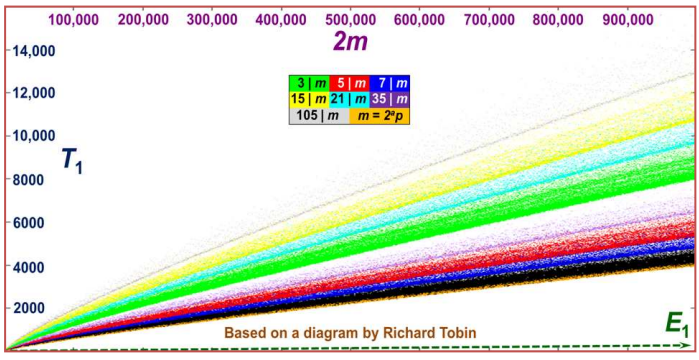

Figure 3: For $4 \leq 2m \leq 10^6$, *the estimated minimum quantity* $E_1 = \lfloor q/p_x \rfloor$ *of Goldbach partitions (dotted line), against the true quantities* T_1 *disposed as a Goldbach comet*

Inclusion of the composite-denominated proper fractions in E_1 permits the telescoping of E_1 in Eq. (6) to $\lfloor q/p_x \rfloor \geq \lfloor q_{\min}/p_x \rfloor \geq 0 : p_x \geq 5$ in Eq. (7). Since $T_1 \geq E_1 > 0$, Goldbach partitions must exist.

Example:
$x = 10^4 \Rightarrow p_x = 104{,}743 \Rightarrow q_{\min} = 2{,}742{,}774{,}012 \Rightarrow E_1 = \lfloor q_{\min}/p_x \rfloor = 26{,}185$. After the penultimate sifting using nested floor functions as in (4-5), $E_2 = 78{,}556$. After the last sifting, $E_1 = \lfloor E_2/3 \rfloor = \lfloor q_{\min}/p_x \rfloor = 26{,}185$. Here, $T_1 = 18{,}867{,}877 > 720E_1 \gg 0$.

In (5) as well as in (6), $E_1 = \lfloor q/p_x \rfloor$. *Proof:* For $p_x \mid q$, let $r = E_1 = q/p_x$. Then, for all q such that $r\,p_x \leq q < (r+1)p_x$, it follows that $E_1 = r\,p_x/p_x = \lfloor q/p_x \rfloor = r$. *Example:* see Table 3.

Table 3. Estimated minimum quantity E_n of survivors for $x = 4$, $p_x = 11$, q on $[30, 42]$ ($p_x \mid q$ **bold**)

q	30	31	32	**33**	34	35	36	37	38	39	40	41	42	(43)	**(44)**	$p_x \mid q$
$E_5 = \lfloor 9q/11 \rfloor$	24	25	26	**27**	27	28	29	30	31	31	32	33	34	(35)	**(36)**	$9r$
$E_4 = \lfloor 7E_5/9 \rfloor$	18	19	20	**21**	21	21	22	23	24	24	24	25	26	(27)	**(28)**	$7r$
$E_3 = \lfloor 5E_4/7 \rfloor$	12	13	14	**15**	15	15	15	16	17	17	17	17	18	(19)	**(20)**	$5r$
$E_2 = \lfloor 3E_3/5 \rfloor$	7	7	8	**9**	9	9	9	9	10	10	10	10	10	(11)	**(12)**	$3r$
$E_1 = \lfloor E_2/3 \rfloor$	2	2	2	**3**	3	3	3	3	3	3	3	3	3	(3)	**(4)**	r
$= r = q/11$	2	2	2	**3**	3	3	3	3	3	3	3	3	3	(3)	**(4)**	$q/11$
Lesser value of T_1	5	3	7	5	7	8	5	4	8	5	5	6	9	(7)	**(7)**	

By (4-5), $T_1 \geq E_1$. For all $m : p_x \geq 5$, since E_1 in (5-6) is at least as in (7), by (2-3) $E_1 = \lfloor q/p_x \rfloor$ is at least equal to $\lfloor q_{\min}/p_x \rfloor = \lfloor (p_x - 1)/4 \rfloor$. Then $T_1 \geq E_1 > 0$. Since Goldbach partitions are also known for all $m : p_x = 2, 3$, at least one Goldbach partition exists for any even integer $2m \geq 4$.

3. Proof of the twin-prime conjecture

In 1846, de Polignac conjectured an infinitude of consecutive primes differing by any gap $2g \geq 2$. Brun (1919) showed that the sum of the reciprocals of the twin primes ($2g = 2$) converges to his constant, which Brent (1976) and Nicely (2010ab) derived from the twin primes $< 10^{11}$ & $< 2 \times 10^{16}$ as 1.90216054 and 1.902160583209 respectively. Goldston, Pintz & Yıldırım (2009) proved the conjecture for $2g = 16$ assuming the Elliot-Halberstam conjecture. Zhang (2013) showed that, without assumptions, infinitely many consecutive primes differ by $\leq 7 \times 10^7$. Tao et al. (2014) reduced that gap to ≤ 246. Hardy & Wright (1976) wrote that proof "is at present beyond the resources of mathematics".

3.1 The method in outline

The pivot $s = p_x + 1$ is the mean of twin primes $\{p_x, p_x + 2\}$. Since $(p_x + 2)^2 - p_x^2 = 4p_x + 4$, $2p_x + 2$ even integers s fall on $[p_x^2 + 1, (p_x + 2)^2 - 1]$. However, for all $p_n \leq p_x$ no true pivot s may be congruent to $\pm 1 \pmod{p_n}$. Thus, $p_x^2 + 1$ & $(p_x + 2)^2 - 1$ cannot be true pivots, so that $q = 2p_x$. After the final sifting by $p_1 = 3$, all survivors are true pivots, so that $T_1 \geq E_1 = q/p_x = 2p_x/p_x = 2$.

Lemma 2: For any $p_n \leq p_x$, no candidate pivot $s \equiv \pm 1 \pmod{p_n}$.

Proof: Otherwise, either $p_n \mid p_x$ or $p_n \mid (p_x + 2)$, so that s is not the mean of twin primes.

3.2 Analog of the sieve of Eratosthenes

For primes $p_x \geq p_n \geq 3$ in descending order, all candidate pivots $s \equiv \pm 1 \pmod{p_n}$ are eliminated. By Lemmas 1, 2, after the last sifting each surviving pivot necessarily falls between twin primes. The estimated minimum $E_1 = q/p_x = 2$, the telescoped product in Eq. (8), includes composite-denominated proper fractions not in T_1, so that, for $p_x \geq 11$, $T_1 - E_1$ will tend to increase.

$$T_1 \geq \left\lfloor \left\lfloor \left\lfloor \left\lfloor \left\lfloor q\frac{p_x-2}{p_x} \right\rfloor \cdots \frac{9}{11} \right\rfloor \frac{5}{7} \right\rfloor \frac{3}{5} \right\rfloor \frac{1}{3} \right\rfloor \geq E_1 = q\frac{p_x-2}{p_x} \cdots \frac{9}{11}\frac{7}{9}\frac{5}{7}\frac{3}{5}\frac{1}{3} = \frac{q}{p_x} = \frac{2p_x}{p_x} = 2. \quad (8)$$

Example: Table 4 shows successive eliminations of candidate pivots $s \equiv \pm 1 \pmod{p_n}$ for $p_x = 11$. After all siftings, the two surviving candidates, ***138*** and ***150***, are true pivots. Thus, between 11^2 and 13^2 there exist two twin primes, $\{137,139\}$ and $\{149,151\}$.

Table 4. $2p_x = 2 \times 11 = 22$ candidate pivots on $[11^2 + 3, 13^2 - 3]$: residues $\pm 1 \pmod{p_n}$

Candidate pivot:	124	126	128	130	132	134	136	***138***	140	142	144	146	148
$\bmod p_x = 11$										–1	+1		
$\bmod p_3 = 7$					–1	+1						–1	+1
$\bmod p_2 = 5$	–1	+1				–1	+1				–1	+1	
$\bmod p_1 = 3$	+1		–1	+1		–1	+1		–1	+1		–1	+1

Candidate pivot:	***150***	152	154	156	158	160	162	164	166	$T_n \geq E_n$
$\bmod p_x = 11$								–1	+1	18 = 22 (9 /11) = 18
$\bmod p_3 = 7$						–1	+1			12 ≥ 18 (5 / 9) = 10
$\bmod p_2 = 5$			–1	+1				–1	+1	7 ≥ 10 (3 / 5) = 6
$\bmod p_1 = 3$		–1	+1		–1	+1		–1	+1	2 = 6 (1 / 3) = 2

As Table 5 shows, each of the first five twin primes $\{p_x, p_x + 2\}$ generates the estimated minimum quantity $E_1 = q/p_x = 2p_x/p_x = 2$ of new twin primes on $[p_x^2 + 3, (p_x + 2)^2 - 3]$. Thereafter, composite-denominated fractions in E_1 ensure that $T_1 - E_n$ will increase with p_x.

Table 5. All twin-prime pivots s on $[p_x^2 + 3, (p_x + 2)^2 - 3]$ for the first 10 twin primes

$\{p_x, p_x + 2\}$	Candidate pivots	New true twin-prime pivots on $[p_x^2 + 3, (p_x + 2)^2 - 3]$						
{3, 5}	12-22	12	18					
{5, 7}	28-46	30	42					
{11, 13}	124-166	138	150					
{17, 19}	292-358	312	348					
{29, 31}	844-958	858	882					
{41, 43}	1684-1846	1698	1722	1788				
{59, 61}	3484-3718	3528	3540	3558	3582	3672		
{71, 73}	5044-5326	5100	5232	5280				
{101, 103}	10,204-10,606	10,272	10,302	10,332	10,428	10,458	10,500	10,530
{107, 109}	11,452-11,878	11,490	11,550	11,700	11,718	11,778	11,832	

The first pair $\{3, 5\}$ of twin primes, on its own, generates an infinite series of further twin primes. On $[3^2 + 3, 5^2 - 3]$, two new twin primes exist: $\{11, 13\}$ and $\{17, 19\}$. On $[11^2 + 3, 13^2 - 3]$ another two exist: $\{137, 139\}$ and $\{149, 151\}$. Thenceforth, the composite-denominated factors in E_1 in (8) become influential. On the interval $[137^2 + 3, 139^2 - 3]$ there are 6 new twin primes: the first is $\{18{,}911, 18{,}913\}$. On $[18{,}911^2 + 3, 18{,}913^2 - 3]$ there are 250 new twin primes: the first is $\{357{,}626{,}021,\ 357{,}626{,}023\}$; and so *ad infinitum*.

Since the true quantity T_1 of new twin primes between the squares of pre-existing twin primes cannot be fewer than the estimated minimum $E_1 = 2$, an infinitude of twin primes exists.

3.3 Visual verification

The tails of the Goldbach and twin-prime comets (Fig. 4) straighten as expected, as the proper fractions with denominations close to p_x in T_1, E_1 asymptotically approach unity.

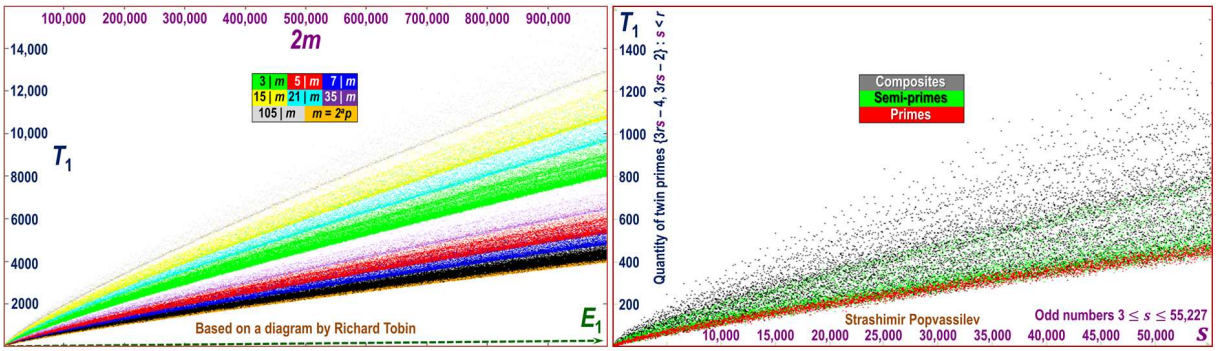

Figure 4: Similarity between two comets: Goldbach (left) and twin-prime (right)

4. Proof of the cousin-prime conjecture

The twin-prime conjecture concerns the least de Polignac prime gap $2g = 2$. The cousin primes, where $2g = 4$, are $\{p_x, p_x + 4\}$. For any p_x, all odd integers on $[p_x^2 + 4, (p_x + 4)^2 - 4]$ are candidate pivots. There are thus $4p_x + 5$ candidate pivots. Then the estimated minimum E_1 surviving after all siftings is $\lfloor (4p_x + 5)/p_x \rfloor = 4$. Here, no true pivot $s \equiv \pm 2 \pmod{p_n}$. *Example:* see Table 6.

Table 6. For $p_x = 7$, $g = 33$ candidate pivots on $[p_x^2 + 4, (p_x + 4)^2 - 4]$, sifted by $7, 5, 3$

mod p_n	53	55	57	59	61	63	65	67	69	71	73	75	77	79	81	83	85	87	89	91
mod 7					−2		+2					−2		+2					−2	
mod 5	−2		+2			−2		+2			−2		+2			−2		+2		
mod 3	+2	−2		+2	−2		+2	−2		+2	−2		+2	−2		+2	−2		+2	−2

mod p_n	93	95	97	99	101	103	105	107	109	111	113	115	117	$T_n \geq E_n$
mod 7	+2					−2		+2					−2	24 ≥ ⌊33 (5 / 7)⌋ = 23
mod 5	−2		+2			−2		+2			−2		+2	15 ≥ ⌊23 (3 / 5)⌋ = 13
mod 3		+2	−2		+2	−2		+2	−2		+2	−2		5 ≥ ⌊13 (1 / 3)⌋ = 4

The first pair $\{7, 11\}$ of cousin primes engenders an infinite family of further cousin primes. On $[7^2 + 4, 11^2 - 4]$ there are 5 new pairs of cousin primes: the first is $\{67, 71\}$. On $[67^2 + 4, 71^2 - 4]$ there are 10; the first is $\{4513, 4517\}$. On $[4513^2 + 4, 4517^2 - 4]$ there are 175; the first is $\{20{,}367{,}433,\ 20{,}367{,}437\}$ and so *ad infinitum*.

Since the quantity of new cousin primes on $[p_x^2 + 4, (p_x + 4)^2 - 4]$ for any p_x cannot be fewer than the estimated minimum $E_1 = 4$, and since the pivot $s = p_x + 2 \equiv 0 \pmod 3$ is composite,

so that $p_x, p_x + 4$ are consecutive primes, there exists an infinitude of cousin primes.

Remark: The general de Polignac conjecture (Guy 1994, p. 19) is not so readily established. Though the present method shows, *mutatis mutandis,* that infinitely many prime pairs are separated by any given gap $2g \geq 2$, for $2g > 4$ the two primes are not necessarily consecutive.

5. Ending the COVID-19 pandemic by a Classically simple method

Apparently refractory practical as well as theoretical present-day problems may be successfully addressed by Classically simple methods. The COVID-19 pandemic is an instance. Two years after SARS-COV2 first emerged, nearly all governments and most medical practitioners have deployed only one form of treatment – vaccines. In those countries where take-up has been significant, vaccines have greatly reduced severe disease and death. However, the emergence of the delta and omicron variants after most vaccines had been designed has diminished their efficacy in inhibiting both infection and transmission. In the largely-vaccinated United States, for instance, in September 2021 daily newly-reported infections were almost thrice, and daily deaths twice, what they had been in September 2020.

Vaccines are proving to be less efficacious in eradicating the pandemic than had been hoped. Nevertheless, governments have tended not only to confine their officially-recommended treatment to vaccination alone but also to blame the continuing high hospitalization and death rates chiefly on the unvaccinated. Compulsion is now widely deployed to ensure greater vaccine take-up. For instance, the United States administration, almost 200 pages into its 2500-page 2021 budget reconciliation Bill, included a well-concealed provision that would fine any large employer up to $700,000 for each employee who remained unvaccinated. However, more scientifically literate and more libertarian administrations, such as the State governments in Uttar Pradesh, Bihar and Goa, India, realizing that vaccines were unaffordable and thus not widely available to them at the outset, sourced and supplied to every infected citizen a treatment pack comprising several safe, inexpensive and widely-available pre-existing medications each of which had proven somewhat efficacious against the pathogen. The program was very successful in reducing severe outcomes. States using multi-treatment protocols have the lowest fatality rates in India and among the lowest in the developing countries.

Dr Peter McCullough of Texas is one of many medical practitioners who, having studied the repurposing of pre-existing medications to prevent and to treat the infection, devised treatment protocols, similar to those of the Indian States, that would be efficacious even in the unvaccinated. Dr McCullough's staged protocol – first prophylaxis and then several stages of treatment with pre-existing medications before admission to hospital – has reduced morbidity and mortality in his patients by 85%, an odds ratio r similar to that of vaccination itself. A summary of his protocol is at Annex A.

Scientifically, then, who is right – illiberal governments and medical practitioners who recommend or compel vaccination as the sole method of containment, despite its shortcomings, or the minority who recommend not only vaccination but also simultaneous administration of several pre-existing medications each known to be safe, inexpensive and somewhat efficacious? Thousands of medications are now available, and repurposing them for off-label use has long been commonplace. In the United States, for instance, a quarter of all prescriptions are for off-label uses. It would be surprising if none of these medications had any effect on a new pathogen. As it turns out, several have been shown individually to deliver modest reductions in severe outcomes when administered against SARS-COV2.

It is not the objective here to recommend any particular treatment. However, the usual reasons given by governments and medical practitioners for not recommending sufficiently large doses of such oft-advocated treatments as intravenous Vitamin C, oral Vitamin D3, zinc and other dietary supplements, anti-parasitics (such as hydroxychloroquine and ivermectin), steroids, anticoagulants and anti-inflammatories are that few of these treatments on its own, though passionately argued for by their supporters, have been shown to reduce the risk of severe outcomes to a

statistically-significant degree.

The epidemiological rule of thumb in reporting clinical trials is that any reduction of less than 50% in the risk of severe outcomes – i.e., an odds ratio $r > 0.5$ – is statistically insignificant except in the very largest and costliest trials. However, suppose that more than one medication is taken, and suppose also that each medication has, on average, an odds ratio $r = 0.67$ – i.e., that on its own it reduces the risk of severe outcomes by $100(1-0.67) = 33\%$. A reduction of just one-third in morbidity and mortality is not on its own statistically significant. However, combining several safe, inexpensive, readily-available medications allows combination of their odds ratios. *Example:* Table 7 gives the odds ratios r_n for n treatments in combination, where the odds ratio for each individual treatment is 0.67.

Table 7. Risk reductions and their significance for 1-5 treatments each with an odds ratio 0.67.

Qty. *n* of treatments	1	2	3	4	5
Odds ratio r_n	0.67	$0.67^2 = 0.45$	$0.67^3 = 0.30$	$0.67^4 = 0.20$	$0.67^5 = 0.14$
Risk reduction d_n %	100(1 – 0.67) = 33%	100(1 – 0.45) = 55%	100(1 – 0.30) = 70%	100(1 – 0.20) = 80%	100(1 – 0.14) = 86%
Significant?	**No**	**Yes**	**Yes**	**Yes**	**Yes**

In general, for n treatments with odds ratios $r_1 \dots r_n$, Eq. (9) gives the percentage risk reduction d_n if a patient takes advantage of all n treatments.

$$d_n = 100\left(1 - \prod_{i=1}^{n} r_n\right) = 100\,(1 - r_1\, r_2\, r_3 \dots\, r_{n-1}\, r_n)\,\% \tag{9}$$

The vaccines, on their own, typically exhibit a statistically-significant period mean odds ratio $r_0 = 0.3$ in the period from double vaccination to some months after receipt of a booster injection, reducing risk of severe outcomes by a useful $100(1 - 0.3) = 70\%$. Similarly, if there were just three standard prophylactic medications having statistically-insignificant odds ratios $r_1 = 0.6$, $r_2 = 0.65$ and $r_3 = 0.7$, implying small risk reductions of 40%, 35% and 30% respectively, by Eq. (9) the three treatments combined would reduce morbidity and mortality by $100(1 - r_1 r_2 r_3) = 73\%$.

By this method, even those reluctant to be vaccinated would reduce their risk of severe outcomes by 73% – about the same as if they had received the vaccine – if they were to take three such non-vaccine treatments in combination. Even though few of those individual treatments, on their own, would pass the test for statistical significance, in combination the risk reduction would be similar to or even greater than that of the vaccine itself, eliminating any justification for the imposition of punitive sanctions upon those reluctant to be vaccinated. Of course, combining the odds ratios for vaccination and the individual treatments would achieve a combined risk reduction of $100(1 - r_0 r_1 r_2 r_3) = 92\%$. In practice, the risk reduction would be even greater, since, for instance some studies (see e.g. Borsche et al. 2021) have found that 5000 IU Vitamin D3 (cholecalciferol) daily, combined with a small dose of Vitamin K2, has on its own an odds ratio similar to that of the vaccines.

Accordingly, the simple equation (9), readily solvable using nothing more complicated than a pocket calculator, is all that is required to demonstrate that Dr McCullough and separately governments such as those of Uttar Pradesh, Bihar and Goa are right, and that less liberal administrations such as those of the United States and the United Kingdom are wrong. Pandemics such as that of COVID-19 may in future be ended not by reliance on a sole method of treatment, and certainly not by brute force of law, but by simple mathematics logically applied – the very essence of the Classical approach.

6. Climate change assessed by Classically simple methods

Figure 5: Fabius the Dodger

Quintus Fabius Maximus Verrucosus (d. 203 BCE: Fig. 5) was a Roman general and statesman whose strategic delaying tactics deployed against the invading Carthaginian army of Hannibal earned him the soubriquet *cunctator*, the Dodger. His brilliantly-executed delaying tactics were successful enough to earn him the devotion of his nation, so that by the time of his death he had served as a *pontifex* for 12 years and an *augur* for a then-unprecedented 62 years. It will here be explained why the Fabian strategy of waiting and seeing, rather than acting precipitately and expensively with the intention of abating future anthropogenic global warming, is the scientifically and economically rational course.

Our centennial effect on global temperature is thought to be similar to equilibrium doubled-CO_2 sensitivity (ECS). IPCC (2021) estimates 3 [2 to 5] K ECS. The CMIP6 models (Zelinka et al. 2020) predict 3.9 [1.8 to 5.6] K. Yet Stern (2006), Murphy (2009) and the deliberately extreme RCP8.5 21st-century emissions scenario predict as much as 11 K. Many other authorities find the midrange estimate to be of order 1 K. The estimates of our impact on global temperatures this century thus range from 1 K to 11 K – an order-of-magnitude uncertainty.

As Monckton of Brenchley (2021) demonstrated, an error of physics that arose when climatologists borrowed feedback formulism from control theory misled then into imagining that ECS must be approximately 3-4 K. The CMIP6 models (Zelinka et al. 2020) estimate the midrange doubled-CO_2 radiative forcing as $3.52\ \mathrm{W\,m^{-2}}$. The product of this forcing and the $0.3\ \mathrm{K\,W^{-1}m^2}$ Planck sensitivity parameter (Schlesinger 1988) is the 1.06 K direct warming or reference sensitivity before allowing for the feedback response that constitutes the difference between reference and equilibrium temperatures. Feedback response is an additional warming dependent upon and proportional to the reference signal. The principal feedback response is caused by more water vapor, a greenhouse gas, in warmer air. At midrange, all other feedback processes self-cancel.

In 1850, before we had any measurable influence on global temperature, the natural greenhouse effect was 32.5 K and reference sensitivity to preindustrial noncondensing greenhouse gases was 7.6 K. All of the 24.9 K difference was feedback response.

Climatology erroneously takes the system-gain factor as the ratio of equilibrium to reference *sensitivities*: i.e., $32.5/7.6 > 4$ in 1850. For instance, Lacis et al. (2010) stated that direct warming represents 25% of the total greenhouse effect, the remaining 75% being feedback response to the 25%, implying a system-gain factor $100\%/25\% = 4$. Since reference sensitivity to doubled CO_2 is little more than 1 K, the implication was that ECS, the product of 1.06 K reference sensitivity and the system-gain factor, and consequently 21st-century anthropogenic global warming from all sources, which is approximately equal to ECS, would be of order 4 K.

Similarly, in 2021, based on Zelinka (*op. cit.*), midrange direct and final warming in the CMIP6

ensemble are 1.05 K and 3.9 K respectively. By the erroneous current method, then, ECS would again appear to be of order 4 K.

The corrected method in Monckton of Brenchley (*op. cit.*) takes the system-gain factor as the ratio of equilibrium to reference *temperatures.* Thus, in 1850 the system-gain factor was not $32.5/7.6 > 4$ but $(255.2 + 32.5)/(255.2 + 7.6) < 1.1$, implying ECS not of 4 K but of a harmless and net-beneficial 1.1 K. Feedback processes necessarily respond not merely to reference *sensitivities* but to the entire reference *temperature*, which, in 1850, was the 262.8 K sum of the 255.2 K emission temperature and the 7.6 K reference sensitivity directly forced by preindustrial noncondensing greenhouse gases.

In the 77 years since the end of the Second World War, the global warming rate has indeed been equivalent to 1.1 K century^{-1} (HadCRUT4: Morice et al. 2012, updated). It is unlikely that the rate of warming in the rest of this century will greatly exceed that rate, particularly since there has been no statistically-significant global warming for almost a decade.

Furthermore, given that the entire feedback response to 7.6 K direct warming by preindustrial noncondensing greenhouse gases was only 0.7 K, it is extremely unlikely that the feedback response to just 1.06 K direct warming by doubled CO_2 will be anything like the 2.84 K implicit in the 3.9 K CMIP6 midrange equilibrium doubled-CO_2 sensitivity.

However, even a 1% increase in the system-gain factor would increase ECS by 250% (Table 8). Since the uncertainty in feedback strengths exceeds 1% by 1-2 orders of magnitude (Table 9), the corrected method shows that it is not possible to make accurate predictions of global warming, since any increase in feedback strength amplifies not only reference sensitivity but the entire reference temperature.

The 95% certainty currently claimed by IPCC for its 3 [1.5, 4.5] K ECS interval is accordingly as baseless as all other such predictions. Unfortunately, governmental and intergovernmental policies are founded upon such predictions: today's governing class are not Plato's philosopher-kings.

Table 8. The impossibility of predicting global warming accurately

System-gain factor and ECS	Erroneous method		Corrected method	
1850 system-gain factor	32.5 / 7.6	4.275	287.7 / 262.7	1.095
ECS with 1.06 K reference sensitivity	4.275 x 1.06 K	4.5 K	1.095 x 1.06 K	1.2 K
ECS with 1% rise in system-gain factor	**4.318** x 1.06 K	**4.5 K**	**1.106** (262.7 + 1.06) – 287.7	**4 K**
% increase	**+1%**	**+1%**	**+1%**	**+250%**

After correction of climatology's error, large and dangerous global warming is no longer near-certain. It remains possible, but is no longer likely, for there is no good reason to suppose that the feedback regime that obtains today differs at all from that which obtained in 1850.

What is certain, however, is that no individual feedback is directly quantifiable by measurement, and that current estimates of feedback strengths are manifestly excessive. It is no surprise that the currently-published uncertainties in the short-term, policy-relevant feedback strengths are substantial (see e.g. Table 9).

Since the relationship between the feedback sum and the system-gain factor is rectangular-hyperbolic, so that a small change in the first engenders a large change in the second, the system-gain factor, and hence ECS, are among the least well-constrained quantities in the history of physics.

Table 9. Estimates of sensitivity-relevant feedbacks based on IPCC (2013, p. 818, table 9.5)

Temperature feedbacks		Lower	Midrange	Upper	*Timescale*
Water vapor feedback λ_1	(W m^{-2} K^{-1})	+1.3	+1.6	+1.9	*Hours*
Lapse rate feedback λ_2	(W m^{-2} K^{-1})	–1.0	–0.6	–0.2	*Hours*
Cloud feedback λ_3	(W m^{-2} K^{-1})	–0.4	+0.3	+1.1	*Days*
Surface albedo feedback λ_4	(W m^{-2} K^{-1})	+0.2	+0.3	+0.4	*Years*
Feedback sum $\lambda = \sum_{i=1}^{4}(\lambda_i)$	(W m^{-2} K^{-1})	+0.1	+1.6	+3.2	*Years*
Feedback fraction $f = 0.3\,\lambda$	(Unitless)	[+0.0]	+0.5	[+1.0]	
System-gain factor $A = 1/(1-f)$	**(Unitless)**	**[1.0]**	**2.0**	**[∞]**	

There is reasonable confidence that reference doubled-CO_2 sensitivity (RCS) is of order 1 K, but, after correction of climatology's error, there can be no confidence in any particular value of the feedback sum, of the system-gain factor or of ECS. Since it is no longer near-certain that global warming will be large enough to be other than net-beneficial, the question arises whether it is worthwhile to endure the economic cost of abating greenhouse-gas emissions and mitigating future global warming at all.

Table 10 shows that only 1 W m^{-2} of anthropogenic greenhouse-gas forcing has occurred over the past 30 years (NOAA AGGI: Butler & Montzka 2020). That forcing increased near-linearly at 1/30 W m^{-2} year^{-1} throughout. Therefore, assuming that all nations were to move in a straight line from the current emissions trajectory to net-zero by 2050, 0.5 W m^{-2} of new emissions would be abated. IPCC predicts 3 K midrange final warming in response to almost 4 W m^{-2} doubled-CO_2 forcing. On that basis, the warming abated if all nations on Earth attained net-zero emissions by 2050 would be only $0.5 \times 3/4$, or less than 3/8 K. However, after correcting climatology's control-theoretic error, the warming abated by global net-zero would be just $0.5 \times 1.06/4$, or little more than 1/8 K.

Table 10. Quantum of global warming abated, 2021-2050, and cost of abating 3 K warming by 2100

Item	Source or method	IPCC	Corrected
30 years' anthropogenic forcing	NOAA AGGI 2020	1 W m^{-2}	**1 W m^{-2}**
Warming abated by straight line to net-zero by 2050	1 W m^{-2} / 2	0.5 W m^{-2}	**0.5 W m^{-2}**
Equilibrium-sensitivity parameter	(3 K **or 1 K**) / 4 W m^{-2}	3/4 K W^{-1} m^2	**1/4 K W^{-1} m^2**
Abated by global net-zero emissions, 2021-2050,	1/2 of (3/4 **or 1/4**)	3/8 K	**1/8 K**
… by Western nations' net-zero emissions by 2050,	1/5 of (3/8 K or **1/8 K**)	1/13 K	**1/40 K**
… and by UK net-zero emissions by 2050 (**$4.2 tn**)	1% of (3/8 K or **1/8 K**)	1/250 K	**1/700 K**
Cost of mitigating 3 K warming by 2100	**$4.2 tn** x 3(250 or **700**)	**>$3 qn**	**>$9 qn**

Western nations alone are obliged to abate greenhouse-gas emissions under the Paris accords: other high-emitting nations, such as China, India and Russia, have made it clear that they have no immediate plans for significant abatement. However, the West accounts for only 20% of new emissions. Therefore, the warming abated, even if the West attained net-zero emissions by 2050, would be only 1/13 K (if climatology were correct about how much warming we may cause), or just 1/40 K (after correction of climatology's error).

Each nation's individual contribution to global-warming reduction would be so minuscule as to be inconsequential. The UK, for instance, represents little more than 1% of global greenhouse-gas emissions. If the UK were to attain net-zero emissions by 2050, which is unlikely, she would succeed in forestalling less than 1/250 K global warming on the basis of climatology's error, or less than 1/700 K after correction of that error. In the UK, the first nation to propose net-zero emissions by 2050, the national electricity grid authority has estimated that the present value of attaining net zero by 2050 would be $4.2 trillion.

Thus, the cost of abating the 3 K currently-predicted global warming by 2100 would be well above $3 quadrillion before correcting climatology's error of physics, and 2-3 times that after correction.

7. The utility of the freedom equation

Classical simplicity may also be applied to questions such as how to maximize the economic freedom of the members of a given population. Eq. (10), the economic freedom equation, provides a simple starting-point. Economic freedom F is equal to the ratio of the availability A of resources R to the product of the cost C of those resources and the population P to which those resources are available.

$$F = \frac{AR}{CP} \tag{10}$$

Most political actions, such as the decision of Western nations to shutter growing numbers of useful, productive and previously prosperous industries in the name of saving the planet from imagined (and imaginary) catastrophic global warming, have economic consequences. Those policies – such as the British government's decision not to extract or combust any more of the nation's substantial coal reserves off the west coast, oil and gas reserves off the north-east coast or frackable gas reserves under the city of Blackpool. – do not reduce the resources themselves, but limit or extinguish their availability and increase the cost of alternative energy resources, consequently reducing the entire population's economic freedom in accordance with Eq. (10).

The economic damage that has now become evident as a result of ill-founded policies intended – however piously – to abate CO_2 emissions and consequently to mitigate global warming requires a more dispassionate and less disproportionate approach on the part of the global *classe politique* than has hitherto been evident.

Proponents of net-zero emissions policies act on the assumption that unabated CO_2 emissions and unmitigated global warming would cause such violent dislocation of the weather, with so great an increase in extreme-weather events, as to disrupt all business activities and thereby to place all resources at risk, increase their cost and reduce their availability, jeopardizing the economic freedom of us all.

Underlying that assumption of catastrophe and the net-zero-emissions policies intended to address the imagined catastrophe there are several further assumptions, all of them false.

First, it is erroneously assumed that the large warming predicted by climatologists would be near-certain to occur in the absence of net-zero-emissions policy. In reality, that imagined near-certainty arises from climatology's control-theoretic error. After correction, large warming remains possible, but is not at all likely, particularly given that the feedback regime today is probably as it was in 1850. On present harmless temperature trends, which continue to be little more than one-third of the originally-predicted midrange warming trend, there is little reason to expect any substantial or net-harmful acceleration in global warming even in the absence of any future emissions abatement.

Secondly, it is erroneously assumed that the exceptionally heavy cost of net-zero policies will purchase an abatement of CO_2 emissions sufficient to confer upon the nations implementing those policies a benefit large enough to outweigh the cost. In reality, that imagined net benefit is not the result of any recognizable benefit-cost analysis: instead, it is taken for granted that so serious would be the catastrophe arising from unabated future global warming that no quantum of economic damage or loss of freedom is unjustifiable. In truth, the cost of inaction is negligible; the cost of abatement is immense. Since the direct imagined benefit in the shape of global warming mitigated is infinitesimal, even the most rudimentary benefit-cost analysis would compellingly suggest that the investment of quadrillions of taxpayers' dollars in emissions abatement would be the least cost-effective deployment of public funds in human history.

Thirdly, it is erroneously assumed that net-zero emissions are in practice attainable. However, by the method currently favored by the global governing elite, net-zero emissions cannot possibly be achieved. The reason is twofold. First, wind and solar power deliver very low energy density. Accordingly, both the cost and the environmental harms per MWh generated are far greater than for thermal power generation. Secondly, wind and solar power are vexingly and irremediably intermittent, requiring costly and elaborate strategies to try to maintain nominal grid operation at all hours of the day and night. Balancing the grid requires thermal backup of wind and solar power in the form of spinning reserve. Nuclear and combined-cycle gas generating sets are not flexible enough to respond within minutes when the wind drops and the Sun sets. Only single-cycle gas turbines and coal-fired generating sets, supported by pumped-storage hydroelectric generation in the few places where it is available, have sufficient flexibility. However, it is necessary that they should be spinning at all times at a sufficient speed to maintain the grid-nominal cycles per second. That process entails substantial emissions of CO_2: so much so that the unit CO_2 emissions from thermal spinning reserve per MWh generated by the wind and solar systems that the spinning reserve supports exceed those from the rest of the grid. Consequently, every additional solar array or wind turbine attached to a grid will counter-intuitively but necessarily and substantially increase unit grid emissions.

Fourthly, it is assumed that electric road vehicles will reduce emissions compared with the internal-combustion vehicles they are intended to replace. This assumption is false, not only because the grid that provides power for the electric vehicles cannot be a zero-emissions grid but also because the weight of the batteries in electric vehicles adds a costly one-quarter or one-third to their weight and thus to the energy required to travel a given distance. That is needlessly wasteful of resources.

It is of course possible to reduce grid emissions by abolishing coal-fired generation altogether, as the European Union and the United Kingdom have tried to do. However, such a policy has very heavy costs. Coal-fired generation, at $20-30 per MWh, is about half the unit cost of gas-fired generation, and less than a quarter of the unit cost of wind or solar generation. The UK civil service, realizing this fact, devised an ingenious new accounting system that artificially added the putative "carbon price" of coal to the unit cost, making coal seem far more expensive than it is. However, after correcting climatology's error of physics, there subsists no legitimate basis for any such "carbon price".

In terms of Eq. (10), then, current zero-emissions policy decreases the availability A of energy resources and greatly increases not only their cost C but also the cost of all other resources whose extraction, production, distribution and exchange depends upon affordable energy. The result is a significant reduction in economic freedom F. Yet there is little or no corresponding benefit in the shape of global warming abated – even if it were at all desirable to abate the modest global warming that is all we can expect after correcting climatology's error.

8. The strategic cost of Western net-zero policies

The heaviest cost arising from the abolition of coal-fired power generation is in reducing the availability A of generation species. In the EU, except in France, there are few nuclear generating sets. Therefore, the only substantial source of power apart from wind and solar is methane gas, very nearly all of it from Communist-controlled Russia, whose regime has long subsidized British and European front groups posing as environmental lobbies. These front groups have

campaigned to tear down the coal-fired power stations and to leave the continent's substantial reserves of coal, oil and gas in the ground, the severest possible attack on the availability of these valuable and vital resources. As a result, the routine cost of gas in Europe is many times the world price. What is more, during periods of little or no wind and sunshine, the cost of gas in Europe rises to 200 times the world price, greatly impoverishing the businesses and citizens of the continent and correspondingly enriching the Russian State *apparat*. The damaging strategic implications of this policy for the West are surely self-evident.

Worse, Communist China now controls very nearly all the global output of lithium carbonate and lithium hydroxide. Lithium is the lightest metal capable of serving in batteries for electric vehicles. The West allowed China to invade and occupy Tibet for its large resources of copper and lithium, which are now shipped out down the railway from Lhasa to Sinkiang. China assisted the Taliban to exploit the ambivalence of the U.S. Democrats towards totalitarian regimes and to displace Western forces. Among China's strategic objectives was that of securing control of the vast lithium deposits in Afghanistan, which are richer than any other such deposits on Earth. China has also bought a controlling stake in the UK's lithium mines, and now holds either controlling or placeholder stakes in many other lithium deposits from Africa to Greenland. Now that Chile has a Communist president, it will not be long before the nation's large lithium deposits – the largest not already under Chinese control – will fall into Peking's hands. Again, the damaging strategic implications of eradicating internal-combustion transport and placing all the West's eggs in Peking's basket are self-evident.

The intelligence community on both sides of the Atlantic has been sounding warnings about the concentration of natural gas and lithium supplies in the hands of Moscow and Peking respectively, and about the danger inherent in the West's policy of shutting down the cheapest and most abundant competing forms of energy supply. However, the Communists have succeeded in drowning out such warnings by the simple expedient of unpersoning. This technique, invented by Goebbels and used by the Nazis to silence all opposition so that they could silently take over Europe's most civilized nation, was found by Marshal Zhukov's invading Red Army in the files of the *Reichspropagandaamt* in Mauerstrasse, Berlin, in 1945. Unpersoning is a systematic assault on the reputation of every individual who has proven successful in opposing the Party Line.

The late Ion Mihai Pacepa, founding head of the Disinformation Directorate of the KGB, established the Directorate within one month of the advancing Russians' discovery of Goebbels' method of discrediting opponents. The Directorate's chief task was unpersoning. Pacepa, who defected to the West in 1978 and provided information that assisted Britain in thwarting the Communist-led miners' strike of 1982-3 (an early attempt by Communism to interfere with Western energy supply), revealed the extent of this technique of unpersoning in his book *Dezinformatsiya* (Pacepa 2015).

British Intelligence investigated the rewriting of more than 2000 Wikipedia biographies of skeptical climate researchers by a single Communist with the effect of introducing subtle twists and falsehoods to unperson their subjects (including the author of the present work). The aim was to cast them in the least favourable light. The perpetrator of these dishonesties was eventually tracked down via his membership of a rowing club in a small town in eastern England and, for a time, he was banned from Wikipedia. Eventually, however, as the Communists tightened their control of Wikipedia, its co-founder resigned in despair at what he publicly described as Communist infiltration and disruption. The Orwellian oarsman was reinstated and his falsehoods, many of which had been edited out, reappeared. Too many Western politicians, terrified that what has happened to all the researchers who have successfully questioned the official narrative on climate might also happen to them, have found it expedient to drift lazily along with the Party Line, paying no heed to the extravagant and ultimately unsustainable cost of their destruction of the West's energy infrastructure.

9. Conclusion

The power of Classical simplicity is formidable. It can be – and has here been – deployed to resolve several apparently complex and refractory present-day problems. By a 2200-year-old

Classical method, the binary Goldbach conjecture, unresolved for 280 years, has been proven in only two pages. In another two pages, the 175-year-old twin-prime and cousin-prime conjectures are proven. It has also been shown that a single, simple equation, correctly deployed, is capable of significantly reducing the risk of morbidity and mortality in pandemics such as that caused by COVID-19. Finally, it is shown that the imagined near-certainty of rapid, significant, dangerous global warming that has given rise to net-zero-emissions policies sprang from an elementary control-theoretic error that occurred when climatologists borrowed feedback formulism from control theory without understanding it. That is the curse of interdisciplinary specialization. In effect, climatologists had forgotten that the Sun was shining and that, therefore, nearly all of the feedback response that they had attributed to preindustrial noncondensing greenhouse gases is in reality attributable to the emission temperature that would prevail at the surface in the absence of any greenhouse gases. Therefore, just as the true feedback response to the preindustrial greenhouse gases is a tiny fraction of that which climatologists had imagined, the true feedback response to any future anthropogenic enrichment of the atmosphere with greenhouse gases may also prove far smaller than the error had misled climatologists into expecting.

It is also here proven, by the simplest and yet most robust of methods, that the quadrillions that the unnecessary attainment of net-zero emissions demands would buy practically no abatement of global warming, and none at all in any policy-relevant timeframe. The extravagant cost of global-warming policies to the economic freedom of the West is unsustainable. Mitigation strategies inexpensive enough to be affordable are likely to prove ineffective, while strategies costly enough to be effective will be unaffordable. Though the effect on global temperature from our futile attempts at emissions abatement will be vanishingly different from zero, we are enriching the enemies of democracy and transferring our industries and our workers' jobs to them at great expense to democracy's friends – in short, to ourselves. Much of our substance has been ventured: nothing will be gained. The great thinkers of the Classical age who are cited here would be baffled if they could see how we have failed to learn what they have taught us by their example: that one should seek simple solutions first; that we should address today's problems with their dispassionate and workmanlike competence; and that, in the words of the Book of Esdras, "Great is truth, and mighty above all things."

10. Acknowledgements

This work is dedicated to the memory of Professor Freeman Dyson, who discussed these ideas with the author at the Institute of Advanced Study, Princeton, some years ago. Professor Richard Taylor of Stanford University also made some helpful suggestions.

References

Aristotle, c. 350 BCE. Works translated by C. Pickard-Cambridge. http://classics.mit.edu/Aristotle/topics.html.

Borsche, L., Glauner, B., von Mendel, J. (2021) COVID-19 mortality risk correlates inversely with Vitamin D3 status, and a mortality rate close to zero could theoretically be achieved at 50 ng/mL 25(OH)D3: results of a systematic review and meta-analysis. *Nutrients* **13,** 3596, https://doi.org/10.3390/nu13103596.

Brent, R.P. (1976) Tables concerning irregularities in the distribution of primes and twin primes up to 10^{11}. *Math. Comput.* **30,** 379

Brun, V. (1919) La série (1/5+1/7)+(1/11+1/13)+(1/17+1/19)+(1/29+1/31)+(1/41+1/43)+(1/59+1/61)…, dont les dénominateurs sont nombres premiers jumeaux, est convergente ou finie. *Bull. Sci. Math.* **43,** 124–128

Butler, J.H., Montzka, S.A. The NOAA annual greenhouse-gas index (AGGI). NOAA Earth System Research Laboratory, Boulder, Colorado, U.S.A. https://www.esrl.noaa.gov/gmd/aggi/aggi.html, accessed January 2022.

Chen Jing Run (1973) On the representation of a large even integer as the sum of a prime and the product of at most two primes. *Sci. Sin.* **16,** 157–176

Euler, L. (1742) Letter to C. Goldbach, June 30,

http://eulerarchive.maa.org/correspondence/correspondents/Goldbach.html, accessed Oct 2021

Goldbach, C. (1742) Letter to L. Euler, June 7,
http://eulerarchive.maa.org/correspondence/correspondents/Goldbach.html, accessed Oct 2021

Goldston, D.A., Pintz, J., Yıldırım, C.Y. (2009) Primes in tuples I. *Ann. Math.* **170(**2), 819–862

Guy, R. K. (1994) Gaps between Primes. Twin Primes. §A8 in *Unsolved Problems in Number Theory, 2nd ed.* Springer-Verlag, New York, NY, 19–23

Hardy, G.H., and Wright, E.M. (1979) *An introduction to the theory of numbers, 5th ed.*, Clarendon Press, Oxford, UK

Helfgott, H.A. (2013) The ternary Goldbach conjecture is true. arXiv:1312.7748v2[math.nt]

IPCC, 2021: Climate Change 2021: The Physical Science Basis. Contribution of Working Group I to the Sixth Assessment Report of the Intergovernmental Panel on Climate Change [Masson-Delmotte, V., Zhai, P., Pirani, A., Connors, S.L., et al. (eds.)]. Cambridge University Press, Cambridge, UK.

Lacis, A.A., Schmidt, G.A., Rind, D., Ruedy, R.A. Atmospheric CO_2: principal control knob governing Earth's temperature. *Science* **33**, 356–359 (2010). https://doi.org/10.1126/science.1190653.

McCullough, P.A., Kelly, R.J., Ruocco, G., Lerma, E., *et al.* (2020) Pathophysiological basis and rationale for early outpatient treatment of SARS-COV2 (COVID-19) infection. *Am. J. Med.* **134**(1):16-22, https://doi.org/10.1016/j.amjmed.2020.07.003.

Monckton of Brenchley, Christopher (2021) What is science and what is not? *Sci. Clim. Change* 1(1), 14-53. https://doi.org/10.53234/scc202111/27.

Morice, C.P., Kennedy, J.J., Rayner, N., Jones, P.D. (2012) Quantifying uncertainties in global and regional temperature change using an ensemble of observational estimates. *J. Geophys. Res.* **117**, D08101.

Murphy, D.M. et al. (2009) An observationally-based energy balance for the Earth since 1950. *J. Geophys. Res.* 114:D17107. https://doi.org/10.1029/2009JD012105.

Nicely, T.R. (2010a) Enumeration of the twin-prime pairs to 10^{16} https://faculty.lynchburg.edu/~nicely/twins/t2_0000.htm, accessed October 2021

Nicely, T.R. (2010b) Enumeration of the twin-prime pairs from 10^{16} to 2×10^{16} https://faculty.lynchburg.edu/~nicely/twins/t2_0001.htm, accessed October 2021

Pacepa, Lt. Gen. I.M. (2013) *Disinformation: former spy chief reveals secret strategies for undermining freedom, attacking religion, and promoting terrorism.* WND Books, Inc., Washington DC, USA.

Popper, K.R. (1963) *Conjectures and Refutations.* Routledge & Kegan Paul, London, UK

Schlesinger, M.E. Quantitative analysis of feedbacks in climate model simulations of CO_2-induced warming. In: Schlesinger, M.E., ed., *Physically-based modelling and simulation of climate and climatic change*: *NATO ASI Series, Series C, Mathematical & physical sciences, 243* (Springer, Dordrecht, Netherlands, 1988).

Schnirelman, L.G. (1930) On additive properties of numbers. *Izv. Donsk. Politehn. Inst.* **14**, 328 (Russian); also (1933) Über additive Eigenschaften von Zahlen, *Math. Ann.* **107,** 649–690

Stern, N. *The Economics of Climate Change: The Stern Review* (Cambridge University Press, Cambridge, United Kingdom, and New York, NY, USA, 2007). https://doi.org/10.1017/CBO9780511817434.

Vinogradov, I.M. (1937) Representation of an odd number as the sum of three primes. *Proc. USSR Acad. Sci.* **15,** 129-132.

Waring, J. (1770) *Meditationes Algebraicae.* Cambridge University Press, Cambridge, UK

Zelinka, M.D., et al. Causes of higher climate sensitivity in CMIP6 models. *Geophys Res Lett*. **47**, e2019GL085782, 12 pp. (2020). https://doi.org/10.1029/2019GL085782.

Zhang Y. (2014) Bounded gaps between primes. *Ann. Math.* **179**, 1121–1174, http://dx.doi.org/10.4007/annals.2014.179.3.7.

Annex A (Dr Peter McCullough)

Early-stages protocol for treating COVID-19 patients

Rationale: Though the UK NHS says, "There is currently no specific treatment for coronavirus," the established approach to treating refractory disease – combining treatments each of which is, on its own, shown to reduce mortality and morbidity somewhat – is applicable to COVID-19, which can and should be thus treated. **Stages 1-3** are reported to reduce hospitalizations and deaths by ~85%.

Magistral formula: Since Hippocrates, it has been the right and duty of the physician to provide whatever treatment he considers will be best for his patients, whether or not official guidelines recommend for or against it, and whether or not it is off-label. Therefore, **consult your doctor.**

Immediate, staged treatment as outlined below is proven efficacious, even in the vaccinated.

Stage 0
Prophylaxis

- **Prophylaxis** may be recommended to all adult patients with no contra-indications.

Vitamin D3 (cholecalciferol) 125 µg daily. The UK gets 30% less sunlight than Sweden. Some 40% of the UK population are D3-deficient; in non-white populations, 83%. The NICE-recommended dose, 10 µg daily, is too small to be efficacious: https://pubmed.ncbi.nlm.nih.gov/32252338/.

Ivermectin 300 µg kg^{-1} in two doses 72 hours apart has been shown to reduce infection by 73% over the following month. https://pubmed.ncbi.nlm.nih.gov/33592050.

Oral Zinc 220 mg daily was beneficial in 4 patients: https://doi.org/10.1016/j.ijid.2020.06.006. Benefits of zinc against COVID-19 are reviewed at https://doi.org/10.3389/fnut.2020.606398.

Dilute Povidone Iodine mouth-rinse and **nasal swab**, both twice daily.

Stages 1-3
Treatment

Treatment stages 1-3 of this multi-treatment protocol were developed by Dr Peter McCullough at Texas A&M University. At https://doi.org/10.1016/j.amjmed.2020.07.003 they are explained and evidenced. Many papers show the efficacy of each of the recommended treatments.

Immediate action: Upon diagnosis, the sooner the nonzero-stages treatment is commenced, the more likely it is to be efficacious.

Stage 1
Treatments upon first diagnosis of SARS COV2 infection

Two dangerous responses worse than influenza are **exaggerated inflammatory response** and **exaggerated coagulation** (thrombi in the veins, arteries, lungs and other organs). A combination of prescription medications is needed to inhibit these dangerous responses.

Antivirals: Vitamin C (3000 mg twice daily) and **Vitamin D3** (cholecalciferol: 125 µg twice daily) with zinc (sulphate or gluconate, 220 mg twice daily), and –

Azithromycin (250 mg twice daily) or **Doxycycline** (100 mg twice daily), taken with *either* –

- **Hydroxychloroquine** (200 mg twice daily: the *Lancet* study opposing HCQ has been withdrawn, for HCQ is shown to be more effective than quercetin as a zinc ionophore), *or*

- **Ivermectin** (6-24 mg, 1-5 doses daily or every 2 days).

Stage 2

3-14 days after diagnosis of COVID-19 infection

Anti-inflammatory corticosteroids added to Stage 1 treatments are **nebulized Budesonide** (1 mg/2mL) to penetrate the lungs and inhibit inflammation; **oral Prednisolone** (1 mg kg^{-1} daily for 5 days ± taper) or **Dexamethasone** (6 mg daily); **Colchicine** (0.6 mg daily, which may be added as an anti-inflammatory); full-strength **adult Aspirin** 325 mg daily to inhibit inflammation and coagulation; and a **home oxygen concentrator**.

Stage 3

7 days and beyond after diagnosis of COVID-19 infection

Additions to stages 1 and 2 medications include **low-molecular-weight Heparin injections** or **Apixaban** (Eliquis) or **Rivaroxaban** (Xarelto) in standard doses (for 5-30 days).

Vol. 1.2 (2021)
pp. 271-272

Morten Jødal in Memoriam

Jan-Erik Solheim, independent scientist

A great organizer and fighter for environment and climate.

Morten Jødal was Chairman of the Board of Norwegian Climate Realists and was the chief-organizer of the Oslo Conference on *Natural Variability and Tolerance.* He died suddenly on September 9, 2021. We have lost a great fighter for the environment and a superb organizer of our fight against the crazy idea of a catastrophic manmade climate change that threatens humanity.

Morten grew up in a suburban community right outside Oslo, near the big forest area that surrounds the city. He was always an outdoor person. The sea, forest and mountains were his home. Already as a student of biology he found a small house in a forest reservation, which he rented and lived in with his wife – in proper distance from the city life. After retiring from formal employments, he was self-employed as collector of mushrooms, making extracts and selling at farmers marked. He also wrote and translated books and guided nature tours.

After finishing his studies, he was commissioned to write plans for a Center for development and environment at University of Oslo, a job he did so well that he became the first Director of the Center. Before the EU-referendum in 1994 he worked for WWF and analyzed the difference between classical environmental protection in EU and in Norway and concluded that EU had far better protection. From then on, he campaigned for EU-membership, which was not well suited for the WWF-camp. This shows how Morten let facts guide him – regardless of the views of authorities or politicians.

The Norwegian Climate Realists organization was established May 15, 2008. Morten was member of the board from the beginning. In 2012 he gave a talk explaining how nature and agriculture improved with more CO_2 in the air. This is opposite of what we are told in media and by politicians: that CO_2 is poison and shall be eradicated from this planet. Which of cause

will kill all life. Morten protested against such indoctrination and started to investigate other environmental myths. After five years he presented the results in a richly illustrated book, *Environmental Myths – do we Face the World's Doom?* (in Norwegian). The book got excellent reviews, but no publisher dared to publish it, so the Climate Realists of Norway published it. It was quickly sold out but bought to all public libraries in Norway.

In the preface of the book, he wrote "*The environmental- and climate-debate has forced me to ask the question: Is the authority the truth or the truth authority?"* His conclusion was that we can learn from nature which laws govern the nature, but we can never govern nature. The nature is robust. Our planet is dynamic. Always changing. The only way species can survive is to adapt to changes. This is also true for mankind.

In 2018 he was elected chairman of the Norwegian Climate Realists. He started to reorganize, hiring professional help to improve the public image. The result was increasing membership. Now it has more than 1200 paying members.

In 2016 and 2018 the Norwegian Climate Realists participated as organizers in Nordic Climate conferences in Stockholm and Göteborg, Sweden. In 2019 it was decided to follow up with an international climate conference in Oslo, with Morten Jødal as the chief-organizer. To the conference Morten booked the most central conference venue in Oslo with a meeting hall with seating capacity of 170 persons. We were worried about the size and the cost, but the ever-optimistic Morten made it into a success with more than 160 participants. He even organized media coverage, but media were more interested in the gray-haired participants than the message presented. A follow-up conference was planned in Copenhagen in 2020 but is postponed due to the Covid19 travel restrictions.

During the years we have witnessed that good science has been rejected from scientific journals. Editors who accepted papers denying climate crises have been fired, and even a journal (Pattern Recognition in Physics) was stopped by its owners Copernicus publishing, when some articles appeared indicating a connection between planetary periods, the Sun, and the climate. It was therefore decided to start an independent scientific journal – not owned by anyone, and so we did with Morten Jødal as one of the prime organizers. Luckily, he got to see the first issue of *Science of Climate Change (SCC)*, just a few days before he died. We also decided that the next Volume of this journal should contain proceedings from the Oslo-Conference with him as editor. We lost him before he could start writing, but in SCC Vol. 2.1 the Proceedings will be published, hopefully as he had wished.

Morten Jødal was also translating climate science books from English to Norwegian. In 2020 he translated Gregory Wrightstone's book*: Inconvenient Facts, The Science that Al Gore doesn't want you to know.* When he died, he had just finished a translation of Bjørn Lomborg's book *False Alarm,* which was launched in Oslo at the end of October 2021.

His final task was to organize a seminar on the topic *Freedom of Speech.* This took place in the Literary House in Oslo, Nov. 22. 2021. Morten had just finished the agreements with the speakers when he suddenly died.

Morten Jødal was an optimist. He believed in the robustness of nature which has taught species to survive. A slightly warmer world with more CO_2, will be beneficial for all life on the planet Earth. A cold climate is more difficult than a warm climate. He told us to love nature and respect its laws.

We lost him too early and will miss him as an inspiring leader, always positive – full of ideas and plans for future. We will do what we can to follow up his many ideas.

Science of Climate Change